




Review

Permeability Models of Hydrate-Bearing Sediments: A Comprehensive Review with Focus on Normalized Permeability

Jianchun Xu ^{1,2}, Ziwei Bu ^{1,2}, Hangyu Li ^{1,2,*}, Xiaopu Wang ^{1,2} and Shuyang Liu ^{1,2}

¹ School of Petroleum Engineering, China University of Petroleum (East China), Qingdao 266580, China; xujianchun@upc.edu.cn (J.X.); 1602030122@s.upc.edu.cn (Z.B.); wxp@upc.edu.cn (X.W.); shuyang_liu@126.com (S.L.)

² Key Laboratory of Unconventional Oil & Gas Development, Ministry of Education, China University of Petroleum (East China), Qingdao 266580, China

* Correspondence: lihangyu@upc.edu.cn

Abstract: Natural gas hydrates (NGHs) are regarded as a new energy resource with great potential and wide application prospects due to their tremendous reserves and low CO₂ emission. Permeability, which governs the fluid flow and transport through hydrate-bearing sediments (HBSs), directly affects the fluid production from hydrate deposits. Therefore, permeability models play a significant role in the prediction and optimization of gas production from NGH reservoirs via numerical simulators. To quantitatively analyze and predict the long-term gas production performance of hydrate deposits under distinct hydrate phase behavior and saturation, it is essential to well-establish the permeability model, which can accurately capture the characteristics of permeability change during production. Recently, a wide variety of permeability models for single-phase fluid flowing sediment have been established. They typically consider the influences of hydrate saturation, hydrate pore habits, sediment pore structure, and other related factors on the hydraulic properties of hydrate sediments. However, the choice of permeability prediction models leads to substantially different predictions of gas production in numerical modeling. In this work, the most available and widely used permeability models proposed by researchers worldwide were firstly reviewed in detail. We divide them into four categories, namely the classical permeability models, reservoir simulator used models, modified permeability models, and novel permeability models, based on their theoretical basis and derivation method. In addition, the advantages and limitations of each model were discussed with suggestions provided. Finally, the challenges existing in the current research were discussed and the potential future investigation directions were proposed. This review can provide insightful guidance for understanding the modeling of fluid flow in HBSs and can be useful for developing more advanced models for accurately predicting the permeability change during hydrate resources exploitation.

Keywords: natural gas hydrates (NGHs); hydrate-bearing sediments (HBSs); numerical simulators; permeability models; gas production performance; hydrate resources exploitation



Citation: Xu, J.; Bu, Z.; Li, H.; Wang, X.; Liu, S. Permeability Models of Hydrate-Bearing Sediments: A Comprehensive Review with Focus on Normalized Permeability. *Energies* **2022**, *15*, 4524. <https://doi.org/10.3390/en15134524>

Academic Editors: Reza Rezaee, Zhenyuan Yin and Shuxia Li

Received: 19 May 2022

Accepted: 18 June 2022

Published: 21 June 2022

Publisher's Note: MDPI stays neutral with regard to jurisdictional claims in published maps and institutional affiliations.



Copyright: © 2022 by the authors. Licensee MDPI, Basel, Switzerland. This article is an open access article distributed under the terms and conditions of the Creative Commons Attribution (CC BY) license (<https://creativecommons.org/licenses/by/4.0/>).

1. Introduction

Natural gas hydrates (NGHs) are ice-like crystalline compounds composed of water molecules and gas molecules [1]. Gas molecules, such as methane (CH₄), carbon dioxide (CO₂), and so on, are known as “guest” and are trapped in cages of hydrogen-bonded water molecules [2]. Global NGH resources are mainly found to be widely distributed in high-altitude permafrost and deep-sea marine sediments, where low-temperature and high-pressure conditions are favorable for nucleation and formation of NGH, and enough supply of methane gas is available [3].

NGH has been treated as a crucial future energy source in the 21st century due to its massive reserve in nature [4] and high energy density [5]. In recent years, NGHs have received more attention from several countries (USA, China, Japan, Canada, India, etc.)

and drawn tremendous interest in commercial production developments [6]. Additionally, numerous researchers have begun to investigate the evolution of the physical properties of hydrate-bearing sediments (HBSs) for the safe and effective exploitation of NGH resources [7,8]. HBSs are naturally occurring multiphase composite geomaterials, which are composed of the soil skeleton, solid hydrates, and pore fluids (gas and water) [9]. Methane gas can be extracted from HBSs by using commonly-adopted NGH production methods, such as depressurization, thermal stimulation, chemical inhibitor injection, carbon dioxide replacement, or their combinations [4]. In the process of NGH exploitation, the HBS permeability is one of the most crucial determinants of gas-water transport and fluid flow performance, which directly affects mass transfer, hydrate formation/dissociation, solid migration, sediments deformation, gas production efficiency, etc. [10].

In the past few decades, limited field tests [11–14] or laboratory experiments [15–17] have been carried out to explore the fluid production performance at the field or core scale. In addition, the fluid production efficiency of hydrate reservoirs under different NGH dissociation methods is also normally evaluated by a variety of numerical simulators [18,19]. As the basic inputs to all numerical simulators, the evolution of hydraulic properties of HBSs before, during, and after hydrate dissociation is crucial for gas production modeling [20]. Permeability (K), as a significant hydraulic parameter, is one of the key parameters for quantifying fluid flux and determining the economic feasibility of gas recovery from NGH deposits [21]. Therefore, the development and establishment of theoretical permeability models can make up for the shortcomings of physical experiments and numerical simulations, which is not only important but also necessary and urgent for scientific research and engineering practice related to hydrate resource exploitation.

The permeability controlling gas-water flow within pores of coarse-grained HBSs has been extensively investigated, as they are considered to be most beneficial for gas production in the future [22]. Previous experimental and numerical investigations have shown that the HBS permeability is affected by a series of factors, including hydrate growth habits [23–25], hydrate saturation [26,27], sediment particle size [28,29], effective stress [30,31], anisotropy and heterogeneity of sediments [32–34], hydrate dissociation and reformation [35,36], wettability [37], interfacial tension [38], etc. Consequently, the study of the HBS permeability is more complicated than that of other types of sediments. Among the above factors, hydrate saturation and growth habits are generally considered to be the two most critical factors determining the pore structure of HBSs [10]. The pore space available for gas-water flow in sediments shrinks with the formation and growth of hydrate. Furthermore, the pore characteristics (pore geometry, pore connectivity, and pore size distribution) can be dramatically changed by hydrate saturation and occurrence morphology, leading to different phenomena of increasing or decreasing fluid permeability caused by hydrate formation or reformation (i.e., a wide-range variation in the permeability under the same hydrate saturation) [39]. NGHs usually occur in the pores of coarse-grained sediments in the form of grain-coating, pore-filling, load-bearing, cementing, and patchy [10]. Pore-filling (PF) hydrates reduce permeability much more than grain-coating (GC) hydrates under the same hydrate saturation due to the larger surface area [40]. Consequently, the existing theoretical models for predicting HBS permeability are mostly established based on the function of hydrate saturation (S_H), combined with the characteristics of sediment pore space (e.g., parallel capillary tube model (PCTM) and Kozeny grain model (KGM)) and the occurrence position of hydrate in the pore space (e.g., grain coating (GC) and pore-filling (PF)) [23]. However, few efforts have been reported to incorporate other influencing factors into the theoretical investigation and establishment of the permeability model.

Due to the difficulties, the time-consuming nature, and the high cost of laboratory experiments study and field tests, theoretical analysis is widely used to investigate the permeability variation characteristics of HBSs. To characterize the HBS permeability change during theoretical analysis, the normalized permeability (K_n) is commonly used, which is defined as the ratio of the effective permeability ($K(S_H)$) for single-phase fluid through a porous media with a certain hydrate saturation to the absolute/intrinsic permeability (K_0)

for single-phase fluid through a porous media without hydrates [10]. At present, several permeability models have already been proposed to predict the dynamic permeability evolution of HBSs based on different methods (e.g., theoretical derivation or empirical fitting) or assumptions (e.g., idealized hydrate pore habits, morphology, and distribution) [10,23,40]. Appropriate selections of permeability prediction models and values of embedding parameters are required by macroscopic numerical modeling on gas production from hydrate deposits. In the gas hydrate community, empirical and semiempirical models are widely used [10]. However, these models vary greatly in expressions and contain many empirical constants or fitting parameters whose physical meaning is rather not clear, and even the values obtained by different researchers and methods are often quite different. Particularly, these empirical constants or fitting parameters often appear at the power exponential position in the expression of the analytical model, thus making small differences in values lead to large prediction errors [41]. From the above discussions, it is clear that there are still many problems and challenges in the study and establishment of the HBS permeability model due to the complex influence mechanism of the seepage characteristics of hydrate reservoirs. Therefore, there is an urgent need to establish an HBS permeability prediction model, which is elegant and simple in form, reasonable in physical parameters, and can be easily implemented for numerical simulations and practical applications. Therefore, a comprehensive review and summary of existing permeability models of HBSs are very important and necessary for future work.

In the past 20 years, great progress has been made in the study and development of the HBS normalized permeability model based on two classical theoretical models, the PCTM and the KGM [23]. For instance, Masuda et al. [42,43] proposed a fully empirical model (i.e., Tokyo model), which is based on the PCTM and uses the reduction exponent N to relate the permeability and the hydrate saturation. However, the exponent N lacks a clear physical meaning, and its value is difficult to determine, ranging from 2.6–14 for different hydrate formation methods [44] and from 1.25–25 for different hydrate pore habits [40]. Therefore, there is still much controversy here regarding the determination of the value of exponent N . Compared to the widely used Tokyo model, the LBNL model [45], the CMG built-in model [46], and the Civan model [47] were less adopted but have also been written into some special simulators for gas production from hydrate reservoirs during NGH exploitation. For example, the LBNL model was incorporated into EOSHYDR/Tough2 [48,49] and the CMG built-in model was employed by CMG STARS. In addition to the models mentioned above, Sakamoto et al. [50] proposed a new permeability model with a piecewise form based on the Tokyo model. In different hydrate saturation ranges, the exponent N value is different due to the different assumptions of hydrate growth habits. These models also utilize various fitting parameters without specific physical meaning, which could result in a wide range of prediction results.

The HBS permeability model proposed based on the Kozeny–Carman (KC) equation [51,52] and its equivalent form [23] is called the KC-based or modified KC model. As numerical methods develop, some modified models were further proposed [40,53]. Some modified model was also established through geometric analyses to enhance the understanding of the relationship between the pore structure characteristics and the normalized permeability in ideal porous media containing hydrates [54–57]. However, some of the built parameters in these modified models either have unclear physical meaning or are difficult to accurately measure through experiments [58]. Moreover, different values of exponents in these models are suggested for different hydrate saturation ranges [56] due to there being no strict correlation with characteristics of the pore structure of HBSs [59,60].

Recently, to overcome the inherent shortcomings of the permeability models proposed in previous literature, the influence of other hydrate- or sediment-related factors on fluid flow and permeability changes has been studied based on new theories and research methods, and many new HBS permeability prediction models have been developed. As known, where and how a hydrate forms in pores significantly influence the microscopic pore structure characteristics of sediments and thus affect the permeability evolution [7]. Therefore, it

is generally believed that the empirical parameter values of normalized permeability models are mostly determined by the microscopic pore structure of sediments [61]. However, the pore structure becomes more complex due to the presence of hydrates, which makes it difficult to select values of empirical parameters. Hence, the fractal geometry method was adopted to study the relationship between permeability evolution and pore structure change in HBSs induced by hydrate phase transition [60–62] by fractal dimensions, which can quantify how inner microstructures evolve. In addition, Hou et al. [63] studied the influence of hydrate pore habits and morphology on the size and tortuosity evolution of controlling seepage channels through 2D lattice Boltzmann micro-flow simulation. Based on the simulation results, a permeability model with a new form and easily determined parameters associated with physical concepts was proposed. Guo et al. [58] proposed an innovative permeability model based on Poiseuille's law and the concept of the three-dimensional hydraulic radius. A key advantage of this model is that the unique embedded parameter has a clear physical meaning and is easy to determine, and illustrates the contribution of hydrate. Considering the effect of hydrate-related interface evolution on the NMR transverse surface relaxivity, Zhang et al. [64] modified the SDR model. However, this model may be only acceptable for engineering applications but not suitable for modeling gas production from hydrate reservoirs. Chen et al. [65] and Liu et al. [66] modified the Corey model by considering the effect of hydrate growth habits on the exponent of the Corey model. Due to the coexisting hydrate pore habits in HBSs, Delli and Grozic [67] and Wang et al. [68] proposed hybrid models in the form of a weighted combination. Two fitting parameters need to be determined for these two hybrid models respectively and the parameter uncertainty is a challenge to numerical simulation and application.

These permeability models based on new theories and methods proposed in recent years can capture the general characteristics of the dynamic evolution of permeability with hydrate saturation, but they still ignore some potential and non-negligible factors affecting fluid flow and pore structure in HBSs. The influence of wettability of hydrate-bearing mix systems on fluid flow, which had been commonly neglected by previous permeability model studies, was first considered by Lv et al. [69]. In a significant step forward for the investigation of the HBS permeability model, the Tokyo model widely used in numerical simulation studies was modified by adding a wettability term. In addition, the permeability stress sensitivity of fine-grained sediments is higher than that of coarse-grained sediments, and its permeability changes are very sensitive to pore structure changes caused by effective stress [70]. Based on the unique mechanical characteristics of fine-grained HBSs, Lei et al. [71] and Zhang et al. [20] developed novel stress-dependent permeability models to predict the fine-grain HBS permeability behavior under stress conditions by theoretical derivation based on fractal theory and modification of KC equation based on experimental results, respectively. Moreover, Lei et al. [72] innovatively introduced the cubic-fracture permeability model commonly used in coalbed methane (CBM) reservoir [73] into the NGH reservoir and established a new semi-theoretical permeability model, which is quite different from the assumptions of previous theoretical models on pore space characteristics and hydrate pore morphology.

In summary, much research on permeability models for HBSs has been carried out recently. However, data from different researchers are widely distributed. The data tend to deviate from the predictions of permeability models, sometimes falling outside the bounds. These findings indicate that our understanding of how the presence of hydrates affects HBS permeability is still limited [10,27,39]. In addition, due to the various form and lack of a unified understanding of their applicability, how to choose the appropriate one from various permeability models for numerical modeling is still a problem. It is generally believed that uncertainties in permeability models have become one of the main error sources in the numerical analysis of gas production behavior during NGH exploitation [41]. Therefore, establishing a comprehensive permeability model is necessary to improve the reliability of the modeling and analysis of NGH resource extraction from different hydrate

reservoirs. To the best of our knowledge, no literature review has been published in recent years on the permeability model of HBSs.

The primary goal of this study is to review the efforts that have been made to establish permeability models of HBSs. To realize this objective, the existing normalized permeability models of HBSs are primarily divided into the four groups based on their theoretical basis and derivation method: classical permeability models derived from classical theories (Section 2), reservoir simulator used models (Section 3), modified permeability models based on the KC equation (Section 4), and novel permeability models based on new theories and research methods (Section 5). We review the various permeability models in detail and summarize the advantages, limitations, and characteristics of each model. Then in Section 6, the conclusions of existing work are given. We also provide suggestions for establishing new permeability models. Research challenges and prospects for this subject are comprehensively discussed in Section 7.

2. Classical Permeability Models Derived from Classical Theories

2.1. SDR Model

In the petroleum industry, an NMR-based permeability model based on the Kenyon relationship [74], known as Schlumberger-Doll Research (SDR) model, is widely recognized in oilfield NMR logging as follows:

$$K = C(\phi_{NMR})^4(T_{2LM})^2 \quad (1)$$

where K is the absolute permeability; C is a mineralogy-dependent constant; T_{2LM} is the logarithmic mean value of the distribution of transverse relaxation time T_2 . Physically, T_{2LM} is conceptually related to the ratio of surface area to volume of pore space, A_{pore}/V_{pore} . In addition, ϕ_{NMR} was the porosity measured by NMR and C is expected to be proportional to the square of the surface relaxivity ρ_2 .

Kleinberg et al. [23] assumed that hydrates are located in pore centers based on the evidence of T_2 distribution. The NMR-determined permeability of hydrate sediments was proposed by Kleinberg et al. [23] as follows:

$$K_n = (1 - S_h)^4 \left(\frac{T_{2LM}(S_h)}{T_{2LM}(S_h = 0)} \right)^2 \quad (2)$$

The predicted results of this model can be used for engineering applications. However, the pore structure changes during hydrate formation and dissociation are mainly reflected by the logarithmic average value of the T_2 characteristic spectrum, which inevitably leads to oversimplification of the influence of pore structure factors on permeability in the SDR model.

2.2. Classical Conceptual Models

The study of the permeability of hydrate sediments is more complicated but more attractive and interesting than other types of sediments due to the existence of hydrate in the pore. Kleinberg et al. [23] provided two porous media conceptual models simulating different microscopic pore geometry and pore space characteristics of porous media and considering two idealized pore habits of hydrate in pore space, to quantify the relationship between normalized permeability (K_n) and hydrate saturation (S_h). A schematic diagram of the pore geometry of HBSs with different hydrate pore habits is shown in Figure 1.

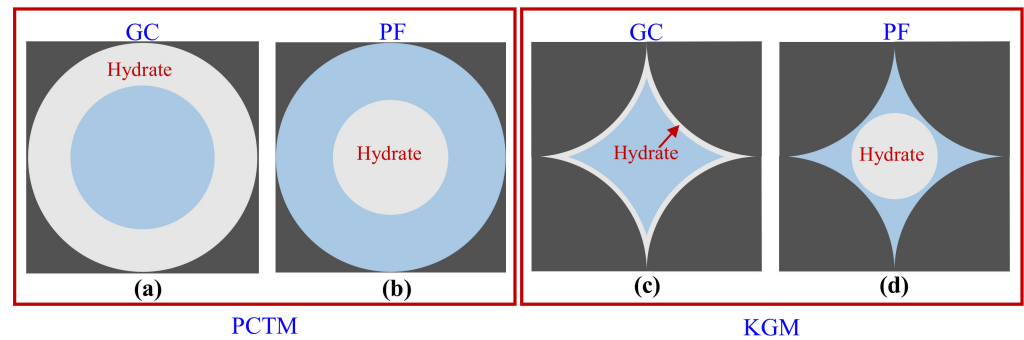


Figure 1. Idealized pore space characteristics and hydrate pore habits in porous media for permeability conceptual models. (a,b) refer to tube-wall coating and tube-center occupying hydrates within a cylindrical tube; (c,d) refer to grain-coating and pore-filling hydrates within an intergranular pore.

2.2.1. Parallel Capillary Tube Model

The first one, the Parallel capillary tube model (PCTM) [10,23], is derived based on the Hagen–Poiseuille equation and the assumption of pore spaces in sediment as a bundle of the equal-diameter parallel capillary. There are two types of hydrate pore habits in capillary (i.e., capillary wall coating hydrates and capillary center occupying hydrates) to explain the relationship between normalized permeability and hydrate saturation.

It is assumed that the pore space of a porous media consists of a bundle of the straight and equal-diameter parallel capillary with length L and inner radius a . The total volume flow rate of fluid through a unit cross-sectional area containing n such capillaries is:

$$q = \frac{n\pi a^4 \Delta p}{8\mu L} \quad (3)$$

where μ is the dynamic viscosity of fluid and $\Delta p/L$ is the pressure gradient. Considering the relationship between porosity ϕ and capillary number n per unit cross-sectional area ($\phi = n\pi a^2$), the absolute permeability of a porous media without hydrate is:

$$K_0 = \frac{\phi a^2}{8} \quad (4)$$

If hydrates uniformly coat the walls of each cylindrical capillary tube wall, the relationship between normalized permeability and hydrate saturation of sediments is given by:

$$K_{n_GC} = (1 - S_h)^2 \quad (5)$$

When the formed hydrate occupies the center of the cylindrical capillary, leaving the annular pore space for fluid flow, the radius of the hydrate cylinder in pore space is b , and the volume flow rate of fluid in a single capillary tube is:

$$q = \frac{\pi \Delta p}{8\mu L} \left[a^4 - b^4 - \frac{(a^2 - b^2)^2}{\ln\left(\frac{a}{b}\right)} \right] \quad (6)$$

Considering the relationship between hydrate saturation, pore radius, and hydrate radius ($S_h = (b/a)^2$), the relationship between normalized permeability and hydrate saturation of sediments is given by:

$$K_{n_PF} = 1 - S_h^2 + \frac{2(1 - S_h)^2}{\ln S_h} \quad (7)$$

2.2.2. Kozeny Grain Model

The second one, the Kozeny grain model (KGM) [10,23], is derived based the on Kozeny–Carman (KC) equation and the assumption of simulating pore spaces as cylindrical

tubes between packed spherical grains in sediment. The following assumptions are made in the model: (1) the electrical tortuosity of sediment can replace the hydraulic tortuosity; (2) the shape factor does not change with varying hydrate saturation; (3) sediment pores can be regarded as capillaries. Based on the above assumptions, there are also two hydrate pore habits in pores (i.e., grain surface coating hydrates and pore center occupying hydrates) to explain the relationships between normalized permeability K_n and hydrate saturation S_h for hydrate-bearing sediments.

It is well known that the skeleton of actual sediments is composed of matrix particles/grains. Due to the irregularity of pore space, in this case, the actual fluid flow path l_a in the pore space is longer than the straight-line distance l along the direction of the pressure gradient. Therefore, permeability estimation of granular media is significantly more difficult than that of simple capillary tube media. A widely used starting point is the KC equation. KC equation is widely used in liquid permeability calculation [75,76]:

$$K = \frac{\phi}{v\tau(A_{pore}/V_{pore})^2} \quad (8)$$

where v is the shape factor of skeleton grains in sediments; A_{pore} is the internal surface area of the pore space; V_{pore} is the volume of the pore space; τ is the tortuosity of the seepage channel, $\tau = (l_a/l)^2$. Hearst et al. [77,78] pointed out that the relationship between the tortuosity τ , the electrical formation factor F , and the porosity ϕ is $\tau = F\phi$. Spangenberg [79] discusses the electrical conduction problem for various hydrate growth habits. Then the relationship between $F(S_h)$ and F_0 is:

$$\frac{F(S_h)}{F_0} = (1 - S_h)^{-n} \quad (9)$$

where n is the Archie saturation exponent. Therefore, the normalized permeability of hydrate-bearing sediments with a certain hydrate saturation is given by the KC permeability model:

$$K_n = (1 - S_h)^{n+2} \left(\frac{A_0}{A(S_h)} \right)^2 \quad (10)$$

When hydrates coat the grain surface, if the sediment pores are cylindrical tubes, the pore surface area initially filled with water decreases with increasing hydrate saturation. Therefore, the relationship between normalized permeability and hydrate saturation of sediments is given by:

$$K_{n_GC} = (1 - S_h)^{n+1} \quad (11)$$

where the saturation exponent n equals 1.5 [79].

If the generated hydrates occupy the pore center, the internal pore surface area increases with the increase of hydrate saturation. Then the normalized permeability of sediments is given by:

$$K_{n_PF} = \frac{(1 - S_h)^{n+2}}{(1 + \sqrt{S_h})^2} \quad (12)$$

where the saturation exponent n equals $0.7 S_h + 0.3$ [79].

The permeability reduction curves for PCTM and KGM are shown in Figure 2. Generally, pore-filling hydrate reduces the normalized permeability more significantly than grain-coating hydrate. The K_n - S_h relationships predicted by PCTM and KGM change dramatically, with results too broad to be useful in field application. In addition, it should be noted that the permeability prediction area of KGM is smaller than that of PCTM due to the main difference in the assumption of pore space characteristics. For example, as shown in Figure 2b, to reduce the normalized permeability to one-tenth of that in hydrate-free sediments (i.e., $K_n = 0.1$), the PCTM and KGM for pore-filling hydrate require $S_h = \sim 0.3$ and $S_h = \sim 0.4$, respectively; while the PCTM and KGM for grain-coating hydrate require

$S_h = \sim 0.7$ and $S_h = \sim 0.6$, respectively. These two models also do not consider the pore-scale heterogeneity of hydrate distribution in natural sediments. In addition, pore geometry plays a key role in the dependence between normalized permeability on hydrate saturation (Figures 1 and 2).

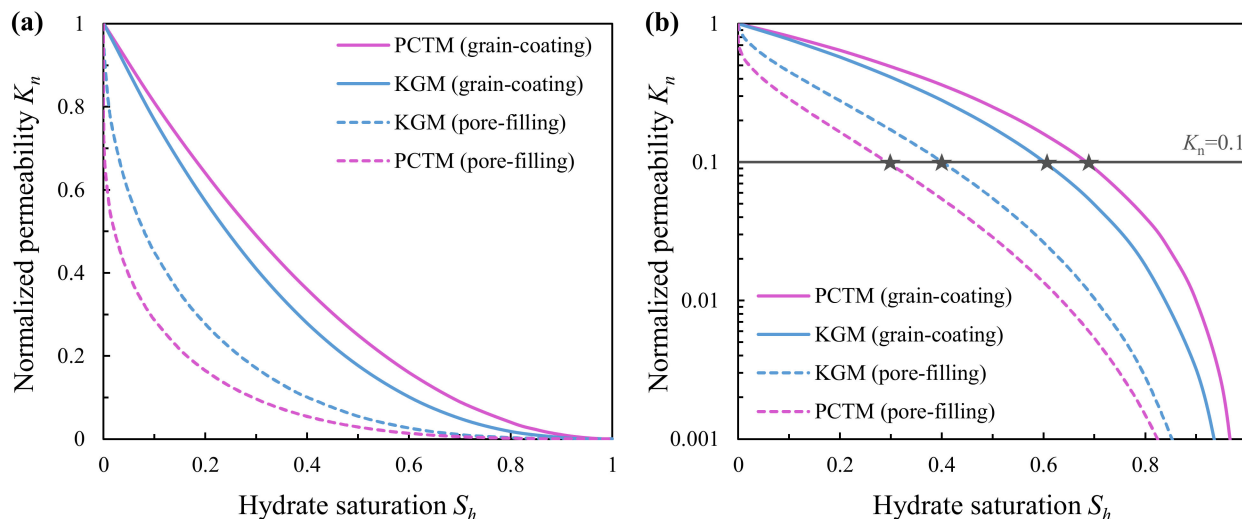


Figure 2. The K_n - S_h relationships of PCTM and KGM. (a) A description in the general coordinate system; (b) A description in the semilog coordinate system.

2.3. Summary

- (1) The SDR model can be used for engineering applications to predict the field permeability data of hydrate reservoirs in the presence of NMR data. However, the SDR model described in this section is not well established due to the lack of consideration for the effects of hydrate formation and dissociation characteristics on the transverse surface relaxation. In addition, it is not recommended to use this model for modeling the gas production behavior of hydrate reservoirs due to the difficulty of obtaining NMR data for natural hydrate sediments.
- (2) PCTM and KGM are introduced into the study of HBS permeability, and their application to numerical modeling of gas production has been widely accepted due to their simplicity and ability to capture the main pore structure characteristic of sediments and two typical hydrate pore habits. Both models show that pore-filling hydrates decrease normalized permeability more significantly than grain-coating hydrates. They provided a theoretical fundamental basis for other permeability models considering the effect of saturation of hydrate with these two typical pore habits on permeability.
- (3) The prediction results of PCTM and KGM can well describe the general reduction trend of the permeability with increased hydrate saturation. However, due to the assumptions of the idealized inner structure of pore space and growth habits and morphology of hydrate, their analytical expressions are oversimplified.
- (4) The research methods, the advantages and limitations, the using parameters and their physical meaning of various models, and the factors that models consider are also provided. Table 1 lists the research methods, advantages, and limitations of classical models of HBSs, while Table 2 summarizes the characteristics of various classical models of HBSs.

Table 1. Research methods, advantages, and limitations of classical models for permeability prediction of HBSs.

Model	Research Methods	Advantages and Limitations
SDR model [23,74]	Derived based on Kenyon relationship	Simple form and generally known; but neglecting the effect of hydrate-related surface evolution on mineralogy constant C
PCTM [23]	Derived based on capillary tube assumption	Simple form and generally known; but a little idealistic about assumption on pore structure
KGM [23]	Derived based on the KC equation	Simple form and generally known; but containing empirical parameters n

Table 2. Characteristics of classical models for permeability prediction of HBSs.

Model	Parameters	Physical Meaning	Influencing Factors
SDR model [23,74]	T_{2LM}	✓	Hydrate saturation
PCTM [23]	\	\	Hydrate saturation, pore habits, morphology, and distribution; the pore structure of sediment
KGM [23]	n	×	Hydrate saturation, pore habits, morphology, and distribution; the pore structure of sediment

3. Reservoir Simulator Used Models

Numerical simulations of gas production from HBSs are derived from theoretical models and extensive data from various laboratory-scale and field-scale tests, which are used to assess the gas production potential of NGH reservoirs and predict gas production performance with the help of numerical simulators [80]. As the key input parameter for laboratory-scale numerical simulation of the hydrate exploitation process, permeability is the most important for controlling hydrate decomposition kinetics and the productivity of hydrate reservoirs [10]. To date, multiple types of permeability reduction models without considering specific hydrate pore habits have been proposed and implemented into the numerical simulators for simulating gas production from reservoirs containing hydrates.

3.1. Tokyo Model

Among the models used in the numerical simulators, the Tokyo model (also known as the Masuda model) is the most widely and frequently adopted model. Masuda et al. [42,43] generalized the PCTM in which hydrate grows on the capillary tube walls and proposed an exponential relationship model between the permeability of HBSs and the saturation of hydrate. The K_n is given by:

$$K_n = (1 - S_h)^N \quad (13)$$

In this purely empirical model with the simplest form, an adjustable permeability reduction exponent N was proposed, which makes the model capable of agreeing well with experimental data and suitable for permeability variation trends for different hydrate pore habits. The effect of the hydrates on the permeability is reflected in the exponent N . However, the determination of N lacks a reliable physical basis and its value varies with the nature of hydrate formation. Considering the growth of hydrate in the throat, the value of N should be appropriately increased. For different hydrate reservoirs, the corresponding N value is different, which needs to be obtained by fitting data from the

seepage experiment. Various N values in the Tokyo model, such as 10 or 15 [43], 2.6 to 14 [44,81], 3 to 5 [82], 4.4 [83], 7.7 to 9.4 [84], and 1.25 to 25 [40], have been suggested or used for certain sediment and/or specific pore habits under different research method. By adjusting the value of exponential parameter N ($N = 3, 5, 10, 15, 25$), the Tokyo model with the simplest form provides a wide normalized permeability prediction range that can cover the predictions of all other numerical models (Figure 3a), which make it as the most popular permeability model used in field-scale modeling gas production from NGH reservoirs. Figure 3b summarizes the dependence of normalized permeability on hydrate saturation from PCTM and KGM, together with the Tokyo model using three N values (i.e., 1.25, 5, and 25).

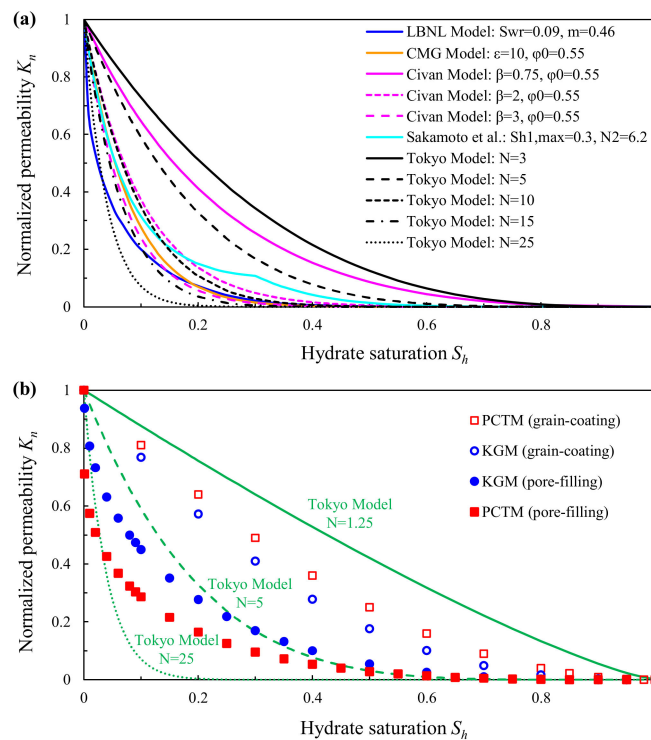


Figure 3. (a) The K_n - S_h relationships of various permeability models (i.e., reservoir simulator used models called in this paper); (b) changes in normalized permeability vs. hydrate saturation of PCTM and KGM, together with results of the Tokyo model assuming $N = 1.25, 5,$ and 25 (green lines).

3.2. Lawrence Berkeley National Laboratory (LBNL) Model

In the EOSHYDR/TOUGH2 simulator developed by Lawrence Berkeley National Laboratory, Moridis et al. [48,49] proposed the LBNL model based on the van Genuchten (vG) model [45,85] since HBSs are partially saturated with hydrate. The K_n is given by:

$$K_n = S_{nw}^{0.5} \left[1 - \left(1 - S_{nw}^{1/m} \right)^m \right]^2 \tag{14}$$

$$S_{nw} = \frac{S_w - S_{wr}}{1 - S_{wr}} \tag{15}$$

where S_w is the water saturation. This model employs two parameters. One is the irreducible water saturation S_{wr} , which depends on the pore structure of sediment ($S_{wr} = 0.09$ for Berea sandstone [23]), whereas the other is an empirical fitting parameter m , which is 0.46 for sands, silts, and sandstones [86]. It is worth noting that there is no direct hydrate saturation term in this model.

3.3. CMG Built-In Model

CMG-STARS [46], mature software widely used in the oil and gas industry, offers the option to determine the reservoir's effective permeability using a Carman–Kozeny type formula, which regards permeability as a function of fluid porosity:

$$K_n = \left(\frac{\phi_e}{\phi_0} \right)^\varepsilon \left[\frac{1 - \phi_0}{1 - \phi_e} \right]^2 \quad (16)$$

where ϕ_e is the effective porosity, ϕ_0 is the initial porosity, and ε is an empirical parameter ($\varepsilon = 10$ [41]) that determines the decreasing rate of normalized permeability with effective porosity. During the hydrate dissociation process, the hydrate-occupied pore space is freed, thus increasing sediment porosity and permeability, which favors fluid transport through the reservoir. The effective porosity may be reduced with the increasing hydrate saturation as represented by Equation (17), and a new form of normalized permeability model is given by Equation (18):

$$\phi_e = \phi_0(1 - S_h) \quad (17)$$

$$K_n = (1 - S_h)^\varepsilon \left[\frac{(1 - \phi_0)}{1 - \phi_0(1 - S_h)} \right]^2 \quad (18)$$

3.4. Civan Model

Phirani, Pitchumani, and Mohanty [87] studied the transport characteristics of HBSs through pore-scale modeling. Additionally, the seepage theory proposed by Helba et al. [88] was adopted to simulate fluid migration through the sediments. The above authors have considered the relationship between the porosity and permeability, presented by Equation (19), which is a power law model proposed by Civan [47]:

$$K_n = \frac{\phi_e}{\phi_0} \left[\frac{\phi_e(1 - \phi_0)}{\phi_0(1 - \phi_e)} \right]^{2\beta} \quad (19)$$

where β is Civan's correlation ($\beta = 0.75$ [87], 2 or 3 [41]), which determines the decreasing rate of normalized permeability with effective porosity. This model accurate representation of the effect of porosity on permeability by a simpler lumped-parameter model. The effective porosity reduces with an increase in S_h , as represented by the relationship in Equation (17). Thus, a new form of the Civan model for normalized permeability K_n prediction) is given by Equation (20):

$$K_n = (1 - S_h) \left[\frac{(1 - S_h)(1 - \phi_0)}{1 - \phi_0(1 - S_h)} \right]^{2\beta} \quad (20)$$

3.5. Sakamoto et al. Model

Sakamoto et al. [50] proposed a permeability model in the form of a piecewise function with different N values based on the Tokyo model according to the definition of a two-component system of hydrate, as illustrated in Figure 4a, in pore space, and this function was introduced into the developed numerical simulator by themselves. In the two-component system of hydrate, one component that coats the sediment grain surface is derived from irreducible water and the other component that forms inside the pore space is derived from free water. The K_n in the hydrate two-component system is expressed as follows:

$$K_n = (1 - S_h)^{N_1}; S_h \leq S_{h1,max} \quad (21)$$

$$K_n = (1 - S_{h1,max})^{N_1} \left(\frac{1 - S_h}{1 - S_{h1,max}} \right)^{N_2}; S_h \leq S_{h1,max} \quad (22)$$

where $S_{h1,max}$ is the maximum value of saturation of hydrate derived from irreducible water, and N_1 and N_2 are permeability reduction exponents for different hydrate saturation condi-

tions. In this model, setting the value of N_2 to be smaller than N_1 , it is possible to reproduce the extreme permeability reduction observed in the experiments of Sakamoto et al. [50] (Figure 4b).

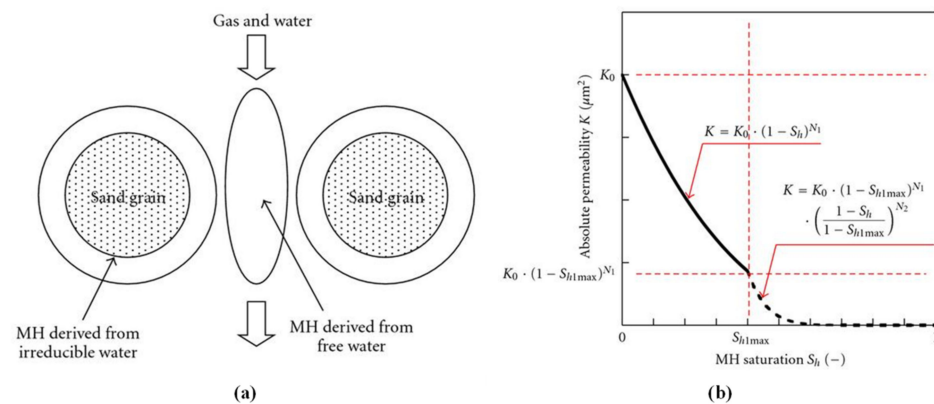


Figure 4. (a) Schematic diagram of hydrate two-component system; (b) formulation of permeability as a function of hydrate saturation in the two-component system. All rights reserved [50].

3.6. Summary

- (1) The reservoir simulator used models for permeability prediction of HBSs directly used for the numerical study on gas production from NGH reservoirs or embedded in simulators only taking into hydrate saturation account. Moreover, the determination of empirical parameters (N , m , ε , β) lacks a reliable physical basis, and their values vary with the properties of HBSs.
- (2) One special parameter in the LBNL model is the irreducible water saturation S_{wr} measured by the lab experiment and it is difficult to determine in numerical simulation, as well as $S_{h1,max}$ in the Sakamoto et al. model.
- (3) The inherent power law fitting characteristic of the Tokyo model makes it possible to match the experimental data well by adjusting the N value. However, the determination of the N value still lacks a sound physical foundation and cannot be estimated based on lithology or other remotely detectable reservoir parameters. Since the Tokyo model is widely adopted in many modeling studies to estimate gas production from NGH reservoirs, the influence of hydrate (considering the effects of hydrate pore habits, hydrate heterogeneous distribution) and pore structure on the value of the exponent N will be a new research hotspot for the permeability model of HBSs.
- (4) Figure 3 shows the permeability reduction curves with varying hydrate saturation depicted by these mentioned above reservoir simulator used models. The research methods, the advantages and limitations, the using parameters and their physical meaning of various reservoir simulator used models, and the factors that models consider are also provided. Table 3 lists the methods, advantages, and limitations of these reservoir simulator used models of HBSs, while Table 4 summarizes the characteristics of these reservoir simulator used models for permeability prediction of HBSs.

Table 3. Research methods, advantages, and limitations of reservoir simulator used models for permeability prediction of HBSs.

Model	Research Methods	Advantages and Limitations
Tokyo model [42,43]	Generalized form based on PCTM	Simplest form and widely used but containing empirical parameter N

Table 3. Cont.

Model	Research Methods	Advantages and Limitations
LBNL model [45,48,49]	Derived based on the vG model for unsaturated soils	Simple form and generally known; but containing empirical parameters m and irreducible water saturation S_{wr}
CMG built-in model [46]	Derived based on KC equation	Simple form and generally known; but neglecting the effect of hydrate pore habits and pore structure and containing empirical parameter ε
Civan model [47]	Derived based on KC equation	Simple form and generally known; but neglecting the effect of hydrate pore habits and pore structure and containing empirical parameter β
Sakamoto et al. [50]	A piecewise function based on the Tokyo model	Considering two hydrate formation mechanisms; but containing empirical parameters N_1 and N_2

Table 4. Characteristics of reservoir simulator used models for permeability prediction of HBSs.

Model	Parameters	Physical Meaning	Influencing Factors
Tokyo model [42,43]	N	×	Hydrate saturation and the assumed tube-wall coating hydrate; the pore structure of sediment
LBNL model [45,48,49]	m S_w S_{wr}	× ✓ ✓	Water and irreducible water saturation
CMG built-in model [46]	ε ϕ_0	× ✓	Hydrate saturation; intrinsic porosity of sediment
Civan model [47]	β ϕ_0	× ✓	Hydrate saturation; intrinsic porosity of sediment
Sakamoto et al. [50]	N_1, N_2 $S_{h1, \max}$	× ✓	Hydrate saturation and growth patterns; irreducible water and free water

4. Modified Permeability Models Based on KC Equation

Many various modified permeability models have been proposed by different research methods for accurately describing and predicting the permeability variations of HBSs based on the classical Kozeny–Carman (KC) equation and some related assumptions. At present, the transformed form of the KC equation (i.e., Equation (10) called KC permeability model in this paper) was generally accepted, and this model was widely used as the starting point for other equivalent forms [10,23]. Hence, these modified models were also known as modified KC models or KC-based models in the permeability research field of the hydrate community.

4.1. Dai and Seol Model

To a large extent, the fluid flow through a porous media depends on relationships between permeability and porosity K - ϕ . Kozeny defined this relationship as K proportional to ϕ^3 [51]. Later, Carman realized that streamlines in the pore space are far from being

straight and parallel, and fluid flows faster in a porous media with less flow path tortuosity τ [52], as described by the Kozeny-Carman equation:

$$K = c \frac{\phi^3}{\tau^2 S_s^2} \quad (23)$$

where c is a constant and the S_s is the specific surface of the pore space in porous media. Dai and Seol [40] first attempted to study the τ - ϕ relationship in HBSs. For a given pore network, τ and S_h would be related directly.

Dai and Seol [40] investigated the relationship between water permeability and hydrate saturation using a pore network modeling method, considering hydrate saturation, hydrate growth habits, and heterogeneity. Their modeling results showed that accumulating hydrates within pore space reduces the porosity and increases the tortuosity to slow the fluid flow. They further proposed a modified Kozeny-Carman model based on the various linear relationships between hydrate saturation and multiplying of tortuosity and specific surface (Figure 5a) to characterize the reduction of water permeability with increasing hydrate saturation in HBSs. The K_n - S_h relationship is given by:

$$K_n = \frac{(1 - S_h)^3}{(1 + BS_h)^2} \quad (24)$$

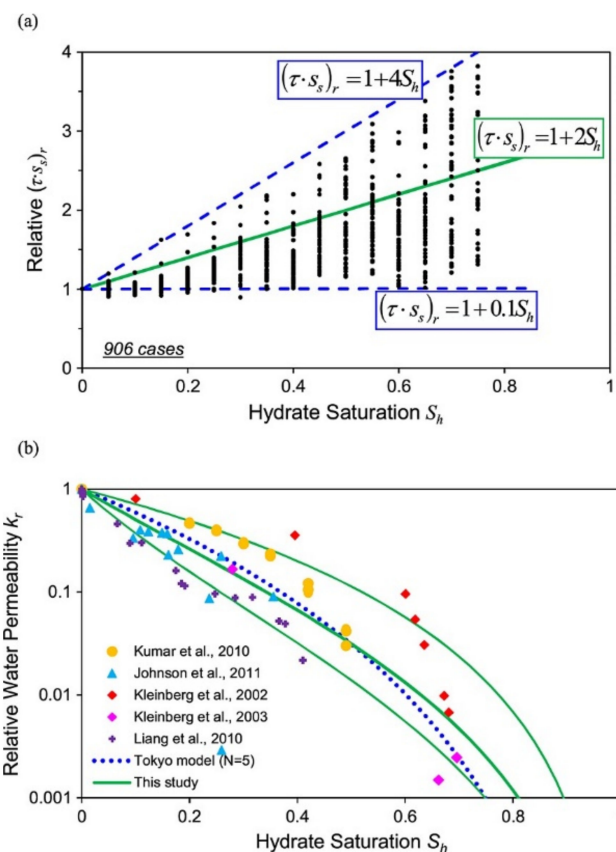


Figure 5. (a) Changes in tortuosity and specific surface in sediments due to hydrate formation; (b) relative water permeability as a function of hydrate saturation: comparison of models and experimental data [23,42,43,82,89–91]. Reprinted with permission from Ref. [40]. Copyright 2014 American Geophysical Union.

According to their modeling results, the upper and lower limits of the empirical parameter B value are 0.1 and 4, respectively. They also recommended $B = 2$ as an average value in simulations (the middle solid green line in Figure 5b). This model uses no extra

empirical variables other than B , to describe the permeability reduction trend during the hydrate formation process, but still captures the basic flow characteristics and can be easily incorporated into reservoir numerical simulators to investigate the seepage characteristics of HBSs. In this model, parameter B reflects the relationships among tortuosity, specific surface, and hydrate saturation. As shown in Figure 5b, this model agrees well with the measurement data of both laboratory-synthesized samples and field-recovered samples.

4.2. Kang et al. Model

The experimental permeability values shown in Figure 6 show that in excess-gas condition or excess-water condition, data scatter widely due to the difference in measurement methods and the uncertainty in hydrate formation. It is worth mentioning that some measured permeability values fall outside the predicted ranges of two analytical models (i.e., PCTM and KGM). In addition, the PCTM [23], KGM [23], and Dai and Seol's model [40], shown in Figure 6, does not take into account the effect of capillarity on nucleation patterns.

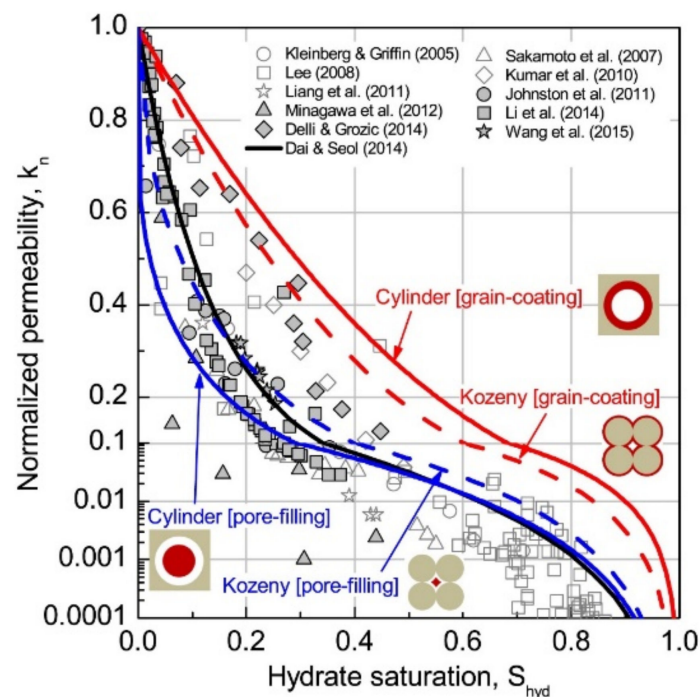


Figure 6. Comparison of experimental data [24,82,89,92–98] and prediction results [23,40] due to hydrate growth. Reprinted with permission from Ref. [53]. Copyright 2022 American Geophysical Union.

Kang et al. [53] conducted LBM flow simulations considering the capillary effect during hydrate formation and growth and different shape of pore channels due to the different hydrate pore habits to study the evolution of water permeability. A salient observation from flow simulation results (Figure 7) is that for both grain-coating and pore-filling cases, the normalized permeability is higher when the capillarity is considered than when it is not considered.

The Kozeny–Carman equation (Equation (23) in this paper), a semi-empirical and semi-theoretical model, is transformed into various other forms based on the relationships among tortuosity, specific surface area, and porosity. Normalized permeability can be further derived as follows [53]:

$$K_n = \frac{K(S_h)}{K_0} = c_r \frac{(1 - S_h)^3}{(\tau S_s)_r^2} = \frac{(1 - S_h)^3}{\left(\frac{\tau S_s}{\sqrt{c}}\right)_r^2} \quad (25)$$

Previous studies have commonly set $c_r = 1$ for permeability studies [23,40]. However, there exists a difference in the micromorphologies between GC and PF hydrate, resulting in different shapes of flow channels in porous media. This means that the geometrical parameter c should be varied with increased hydrate saturation. Hence, Kang et al. [53] conserved the geometrical parameter c in Equation (25) as $\tau S_s / \sqrt{c}$, which is called the effective pore area.

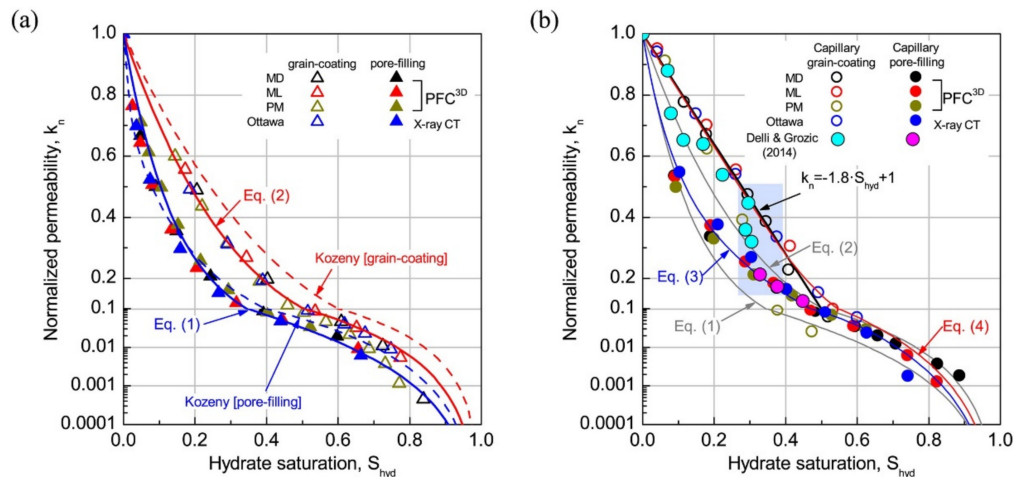


Figure 7. Normalized permeability calculated by lattice Boltzmann flow simulation that (a) ignores capillary effects and (b) considers capillary effects. Reprinted with permission from Ref. [53]. Copyright 2022 American Geophysical Union. Note: Please refer to the original literature for the experimental data points and equations shown in the figure.

As shown in Figure 8, relative effective pore area $(\tau S_s / \sqrt{c})_r$ increase with increasing hydrate saturation. In addition, polynomial regression is conducted for the curve fitting of relative effective pore area with hydrate saturation by Kang et al. using the formula:

$$\left(\frac{\tau S_s}{\sqrt{c}}\right)_r = 1 + \sum_i a_i S_h^i \tag{26}$$

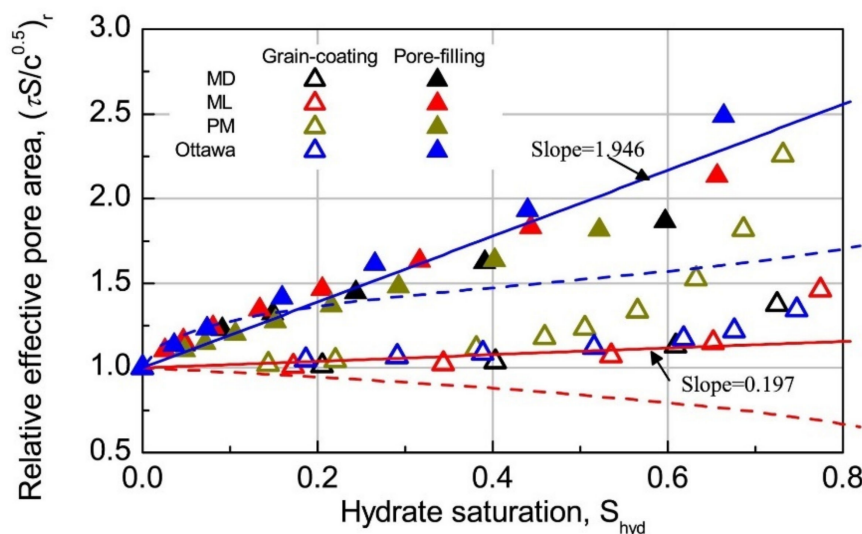


Figure 8. Relative effective pore area for the noncapillary effect. The dashed lines are obtained from KGM for the grain-coating (red color) and pore-filling (blue color) cases. Reprinted with permission from Ref. [53]. Copyright 2022 American Geophysical Union. Note: Please refer to the original literature for the experimental data points shown in the figure.

In the cases of noncapillary effect, simple linear regression was used. The values of a_1 are 0.197 and 1.946 for grain-coating and pore-filling cases, respectively (Figure 8). Therefore, based on the modification of the KC equation, Kang et al. [53] proposed a new normalized permeability model:

$$K_n = \frac{(1 - S_h)^3}{\left(1 + \sum_i a_i S_h^i\right)^2} \quad (27)$$

where i and a_i represent the order of polynomial and fitting parameters, respectively. For the capillary effect cases in the Kang et al. simulations [53], cubic polynomial equations (i.e., $i = 3$) are used for fitting the simulated results considering different hydrate pore habits. A polynomial-based model improves prediction accuracy by changing the value of the polynomial order. However, as the polynomial order increases, the number of parameters increases significantly. Many experiments are required to estimate multiple parameter values, which may result in overfitting.

4.3. Katagiri et al. Model

Based on the KC permeability model (i.e., Equation (10) in this paper), Katagiri et al. [54] assumed that the sediment grains were cubic packs for cylinders, cubic and random packs for spheres, and then formulated the KC-based permeability models when hydrates grow uniformly on the grain surface/cylindrical tube wall and pore center. In this paper, the model was only chosen from the premise of a random sphere pack. For a random sphere pack with GC hydrate, the K_n is:

$$K_{n_GC} = \frac{(1 - S_h)^{n+2}}{(1 + eS_h)^{\frac{4}{3}}} \quad (28)$$

where e is the void ratio, $e = \phi_0 / (1 - \phi_0)$. For a random sphere pack with PF hydrate, the K_n is given by:

$$K_{n_PF} = \frac{(1 - S_h)^{n+2}}{(1 + C_p e S_h)^2} \quad (29)$$

where C_p is the ratio of the sediment grain radius to the hydrate's radius. More over, C_p has a certain physical significance, that is, it can be used to represent the average size of small PF hydrate clusters in pores. Hence, the value of C_p indicates whether the main hydrate is GC or PF, and C_p increases as PF hydrate dominates. This also indicates that the morphology of hydrate in pores can be predicted by the relationship between S_h and K_n in this model.

In addition, the K_n obtained by pore-scale CFD modeling was compared with that from their analytical models and with reported experimental results (Figure 9a). Finally, they compared the prediction accuracy of their model with reported permeability reduction models (Figure 9b,c). Their proposed model showed reasonable prediction accuracy.

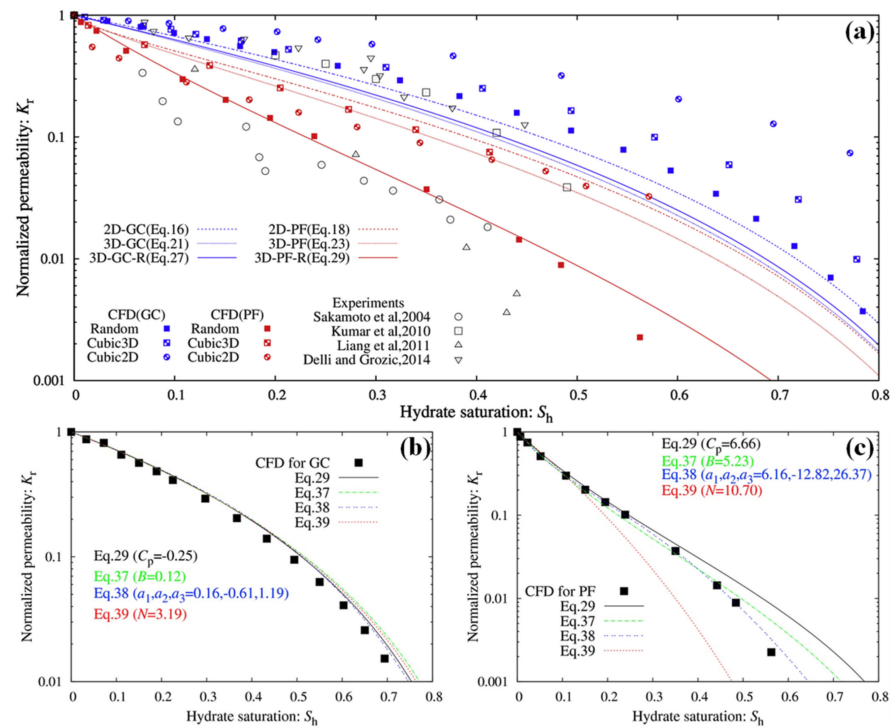


Figure 9. Relation between hydrate saturation and the normalized permeability [54]. (a) Comparison between simulated K_n from Katagiri et al. CFD simulations, calculated K_n from Katagiri et al. analytical models, and experimental results from previous studies [24,82,95,99]. (b,c) Prediction performances of the Katagiri et al. analytical models and other existing permeability reduction models [40,42,53]. Reprinted from Journal of Natural Gas Science and Engineering, Vol. 45/pages 537–551, Katagiri et al. Pore-scale modeling of flow in particle packs containing grain-coating and pore-filling hydrates: Verification of a Kozeny–Carman-based permeability reduction model, Copyright (2017), with permission from Elsevier.

4.4. Li et al. Model

In 2017, Li et al. [55] investigated the permeability of HBSs in the two aspects of experimental and theoretical research. The different K_n - S_h relationships were obtained with the verification and fitting of experimental data from the permeability test in coarse quartz sands under different hydrate saturations. For S_h lower than 0.1, the K_n - S_h relationship was proposed based on the KGM for hydrate occupying the pore centers (i.e., Equation (12) in this paper). For the case of S_h higher than 0.1, the K_n - S_h relationship was mathematically derived based on the 3D model of a simple cubic sphere pack for quartz sands with the assumptions of uniform sphere sediment grain and homogeneous hydrate distribution. Additionally, pore water was considered to be an ideal spherical shell surrounding the grain surface (i.e., the three-dimensional shape of hydrate particle, which occupies pore centers is not a regular ideal sphere), as shown in Figure 10. Based on the KC permeability model (i.e., Equation (10) in this paper), the K_n is expressed as a function of r/L and the saturation exponent n :

$$K_n = \left\{ \left[-2\pi \left(\frac{r}{L} \right)^3 + 4.5\pi \left(\frac{r}{L} \right)^2 - 2.5\pi \right] / (6 - \pi) \right\}^{n+2} \left[\frac{3\sqrt{2} - 4}{3 \left(\frac{r}{L} \right) - 2 \left(\frac{r}{L} \right)^2} \right]^2; 1 \leq \frac{r}{L} \leq \sqrt{2} \quad (30)$$

where r is the radius of pore fluid and L is the radius of sediment grain.

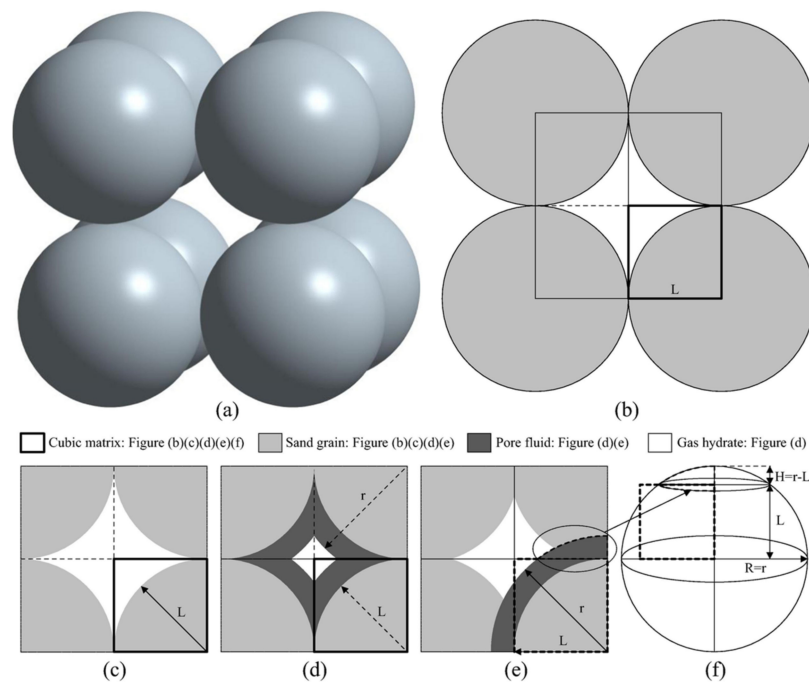


Figure 10. A model of a simple cubic sphere pack for unconsolidated quartz sands reprinted from [55] with permission from Elsevier. (a) Simple cubic sphere pack for unconsolidated quartz sands; (b) front view of simple cubic sphere pack model; (c) the sand grain and the pore space without hydrate; (d) the sand grain and the pore space filled with gas hydrate and the water shell around the grains; (e,f) the calculation process of the volume of the water shell within the matrix.

The Kozeny–Carman equation [51,52] is a widely used model, which successfully relates the permeability of porous media with the parameters that describe the properties of the pore structure. It is important to note that in a previous study [23,55], the shape factor ν in the Kozeny–Carman equation was assumed to be a constant, which did not change with hydrate saturation. However, the pore-specific surface area would increase because of the presence of hydrates, which would cause a decrease in the shape factor. Additionally, the shape factor ν was significantly sensitive to the characteristics of the porous media with wide particle size ranges, complex grain shapes, surface roughnesses, and packing patterns. Therefore, in 2019, Li et al. [26] further proposed new piecewise K_n - S_h relationships for S_h lower and higher than 0.1 based on Equations (8), (12), and (30) and the relationship between shape factor ν and S_h (i.e., $\nu(S_h) = \nu_0(1 - S_h)^2$) in HBSs. The new piecewise K_n - S_h relationships are:

$$K_n = \frac{(1 - S_h)^n}{(1 + \sqrt{S_h})^2}; 0 \leq S_h \leq 0.1 \quad (31)$$

$$K_n = \left\{ \left[-2\pi \left(\frac{r}{L} \right)^3 + 4.5\pi \left(\frac{r}{L} \right)^2 - 2.5\pi \right] / (6 - \pi) \right\}^n \left[\frac{3\sqrt{2} - 4}{3 \left(\frac{r}{L} \right) - 2 \left(\frac{r}{L} \right)^2} \right]^2; 1 \leq \frac{r}{L} \leq \sqrt{2}; S_h \geq 0.1 \quad (32)$$

4.5. Shen et al. Model

Shen et al. [56] conducted permeability measurements in fine quartz sands with various grain sizes and further derived the normalized permeability model based on the KC permeability model (i.e., Equation (10) in this paper) and the 3D simple cubic model with regular ideal sphere hydrate occupying pore centers (Figure 11). The K_n was given by:

$$K_n = \left[1 - \frac{\pi}{6 - \pi} \left(\frac{r}{L} \right)^3 \right]^{n+2} \left(\frac{L^2}{r^2 + L^2} \right)^2; 0 \leq \frac{r}{L} \leq \sqrt{3} - 1; S_h \leq 0.43 \quad (33)$$

where r is the radius of hydrate particle and L is the radius of sediment grain. The effect of grain size on K_n was eliminated and the saturation exponent n was recommended between 20 and 30 in their experiments [56]. It is worth mentioning that n tended to increase with increased hydrate saturation. Due to the complexity of the formula, the expressions of K_n for higher S_h were not given.

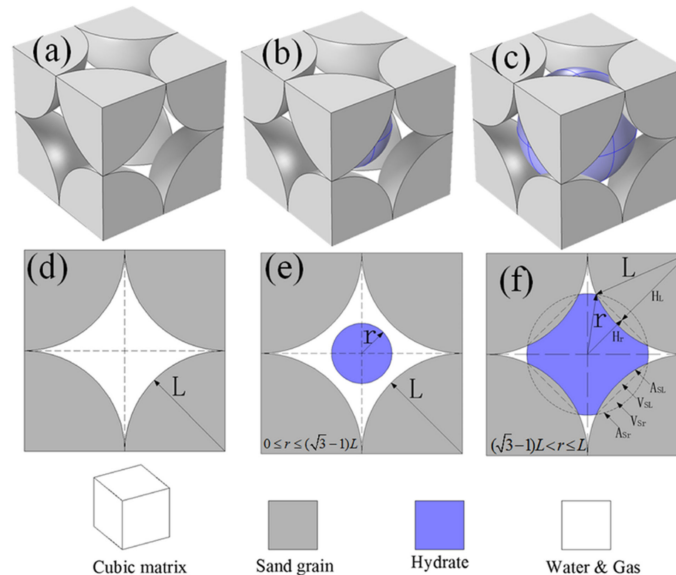


Figure 11. The simple cubic sphere pack model unit of hydrate occupying pore centers reprinted from [56] with permission from Elsevier. (a) The simple cubic sphere pack model; (b,c) the simple cubic sphere pack model with hydrate growth; (d) the front view of the sand grain and the pore space without hydrate; (e) the front view of hydrate occupying pore center; (f) the front view of the cubic matrix when the grains intersect with hydrates.

Shen et al. [100] investigated permeability variation in fine quartz sands with different initial porosities of porous media and further derived the new permeability reduction models based on the KC permeability model (i.e., Equation (10) in this paper) and different particle stacking structures (the simple cubic model and the oblique cubic model considering sphere hydrate, which occupies pore centers, as shown in Figure 12). The unification model of K_n for different stacking structures could be simplified as:

$$K_n = \frac{(1 - S_h)^{n+2}}{\left(1 + S_h^{\frac{2}{3}}\right)^2} \quad (34)$$

In this unification model, the normalized permeability could be expressed by S_h and n . The effect of the initial porosity of porous media on K_n could be eliminated.

According to the KC permeability model, it was found that the K_n of HBSs was closely related to S_h , n , A_0 , and $A(S_h)$. However, the calculation of the A_0 and $A(S_h)$ was extremely difficult, and many researchers ignored the effect of the ratio of A_0 and $A(S_h)$ on the K_n , or simply replaced it with S_h . Hence, in the work by Shen et al. [101], the water permeability of glass beads with S_h from 0 to 0.42 was determined, and a single matrix unit considering GC and PF hydrate was constructed based on the hypothesis of wedge tetrahedral filling of glass beads (Figure 13). Moreover, the hydrate occupying pores and the hydrate coating particle surfaces were two completely different modes in this unit. Therefore, it was assumed that the diameter of the glass bead was the same in the wedge tetrahedral model so that the internal surface area of the pore space could be expressed by a mathematical formula, which provided an ideal method to evaluate the influence of the evolution of internal surface area caused by hydrate growth on the permeability.

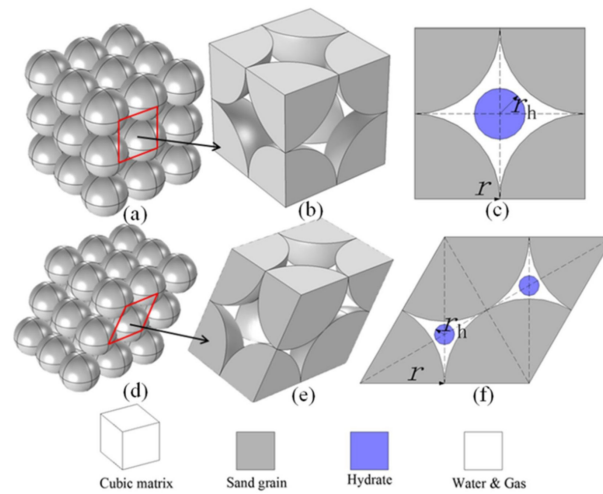


Figure 12. Simple cubic model and oblique cubic model of hydrate occupying pore centers reprinted from [100] with permission from Elsevier. (a) The simple cubic stacking structure; (b) the minimum cubic matrix of the simple cubic model; (c) a side view of the minimum cubic matrix of the simple cubic model with hydrate; (d) the oblique cubic stacking structure; (e) the minimum cubic matrix of the oblique cubic model; (f) a side view of the minimum cubic matrix the oblique cubic model with hydrate.

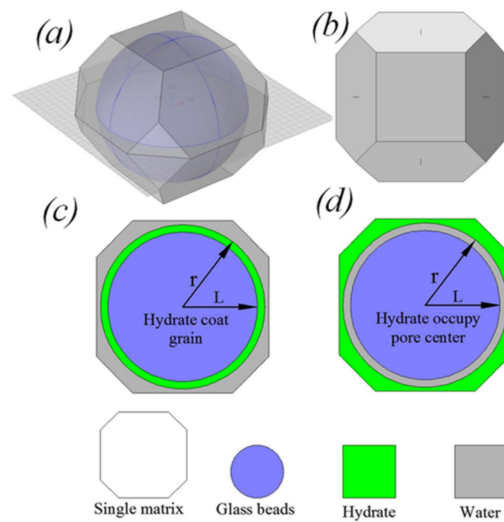


Figure 13. The models of hydrate coating grain and hydrate occupying pore center reprinted from [101] with permission from Elsevier. (a) A minimum repeatable matrix unit with purple glass bead in the center of a wedge tetrahedral; (b) the top view of the A minimum repeatable matrix unit; (c) the model of hydrate coating grain; (d) the model of hydrate occupying pore center.

It was found in Figure 14a,b that the evolution of the internal surface area of pore space under two hydrate occurrence modes was completely different. When hydrate coats the grain surface, the $A_0/A(S_h)$ decreased with increased S_h ; however, when hydrate occupies the pore center, the $A_0/A(S_h)$ increased with increasing S_h . This difference made a completely different influence on the sediment permeability. In other words, this difference can be used to find out whether the hydrate coats the grain surface or hydrate occupies the pore center. Only normalized permeability model for GC hydrate based on a new expression of S_h and the ratio of internal surface area $A_0/A(S_h)$ was given:

$$K_n = \left\{ \frac{(9 + 5\pi) - 15\pi\left(\frac{r}{L}\right)^2 + 8\pi\left(\frac{r}{L}\right)^3}{9 - 2\pi} \right\}^{n+2} \left[\frac{L^2}{5rL - 4r^2} \right]^2; 1 \leq \frac{r}{L} \leq 2\sqrt{3}/3; S_h \leq 0.79 \quad (35)$$

where r is the radius of hydrate and L is the radius of the glass bead. As shown in Figure 14c, it was found that the model of hydrate coating grain surface was similar to the model of Masuda et al., and the only difference was the value of n . Therefore, the Equation (35) could be simplified as follows:

$$K_n = (1 - S_h)^{n+1} \tag{36}$$

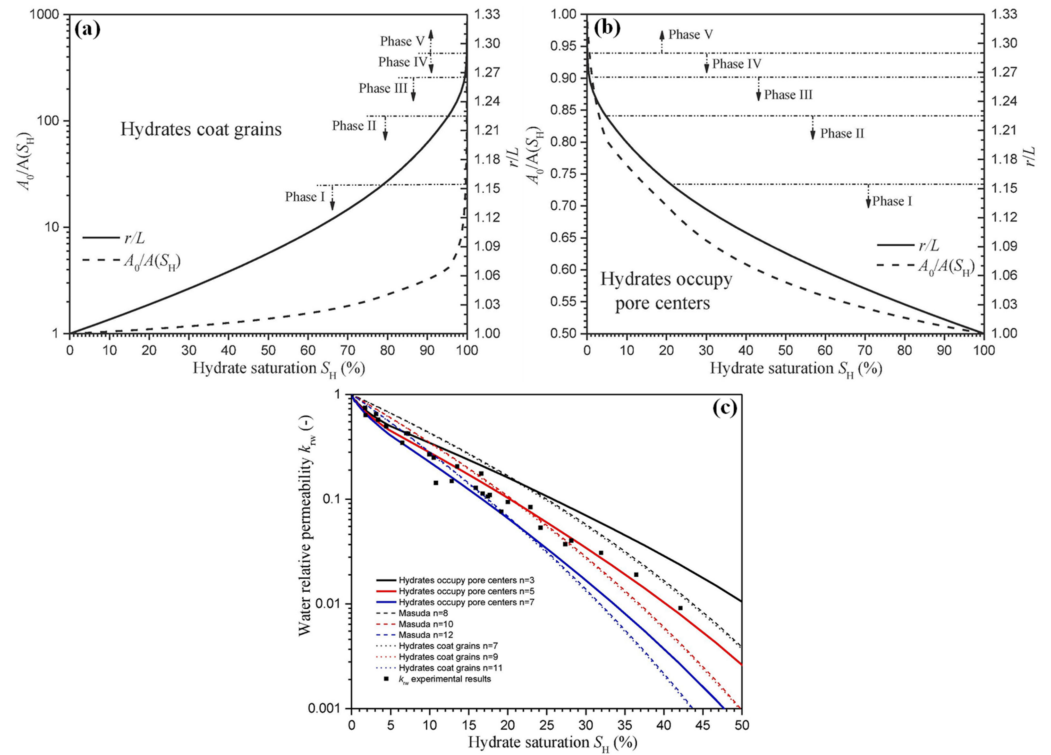


Figure 14. The relationship between S_h , $A_0/A(S_h)$, and r/L in the model of (a) hydrates coating grain surfaces and (b) hydrates occupying pore centers; (c) experimental data and the K_n-S_h relationship reprinted from [101] with permission from Elsevier.

4.6. Xiao et al. Model

In a study by Xiao et al. [57], methane hydrate was synthesized in porous media with glass beads as the skeleton structure and the water permeability were obtained. The distribution of hydrate at the pore scale appeared as irregular hydrate clusters in the sediments [10]. Hence, a clustered equal diameter particle (CEDP) model was proposed that hydrate was clustered as equal diameter spheres and occupied the center of pore space of the oblique cubic model, as shown in Figure 15. The internal surface area of pore space with and without hydrate was simplified and a new mathematical model of the hydrate saturation and the normalized permeability was proposed:

$$K_n = \frac{(1 - S_h)^{n+2}}{\left[1 + \frac{(3\sqrt{3}-\pi)}{\pi} \cdot \frac{r_s}{r_h} \cdot S_h \right]^2} \tag{37}$$

where r_s is the radius of glass beads, μm ; r_h is the radius of hydrate particle, μm . In the Xiao et al. study, the radius of hydrate particles adopted the measured results of Clarke’s work [102] and was defined as $r_h = 8.0/2 = 4.0 \mu\text{m}$.

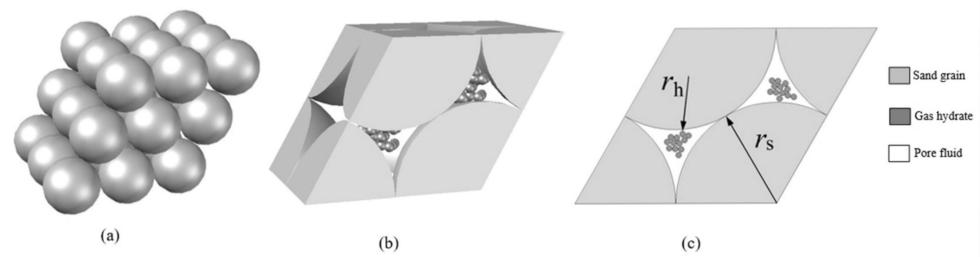


Figure 15. The oblique cubic model of hydrate particles occupying pore centers reprinted from [57] with permission from Elsevier. (a) The schematic diagram of a three-dimensional oblique accumulation structure; (b) a minimum unit of the oblique cubic model; (c) a side view.

4.7. Kou et al. Model

Kou et al. [103] used X-ray CT to identify the pore structure characteristics of porous media containing hydrates with different growth habits. It was found that the formation and growth of hydrates in the pore led to the occurrence of non-interconnected pores (Figure 16), which further limits the validity of pore structure analysis and the accuracy of permeability estimation. Hence, they proposed a permeability model based on the KC equation according to the linear correlation of hydrate saturation with interconnectivity degree m with a definite physical meaning.

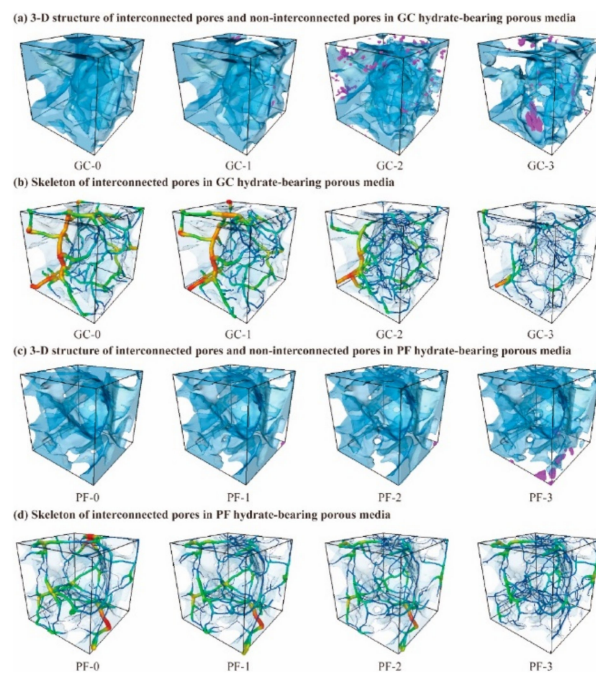


Figure 16. The pore structure of hydrate-bearing porous media reprinted from [103] with permission from Elsevier. (a,c) the 3-D structure of effective pores in blue and non-interconnected pores in purple; (b,d) the skeleton of effective pores.

In previous studies, the premises of establishing permeability models included that all pores are interconnected and the pore size is reasonable and uniform [10,23,54–57,100,101]. However, in the work by Kou et al. [103], it was found that the hydrate in pore space strongly affects the effective pore diameter distribution, as well as the pore interconnectivity. Therefore, the interconnectivity degree (m) of the porous media was proposed by Kou et al. to clarify the effects of hydrate formation and growth on pore interconnectivity and to

modify the KC permeability model. The interconnectivity degree (m) denoted the ratio between the mean diameter of overall pores (D_{All}) and interconnected pores (D_{Eff}):

$$m = \frac{D_{All}}{D_{Eff}} \quad (38)$$

The dependence of m on S_h was shown in Figure 17a. It was evident that m linearly reduces with increasing S_h , either for GC hydrate or PF hydrate. This indicated that the difference between the overall pore size and effective pore size increases significantly with the further increased hydrate saturation. The linear correlation between m and S_h has been given by:

$$m = 1 - S_h \quad (39)$$

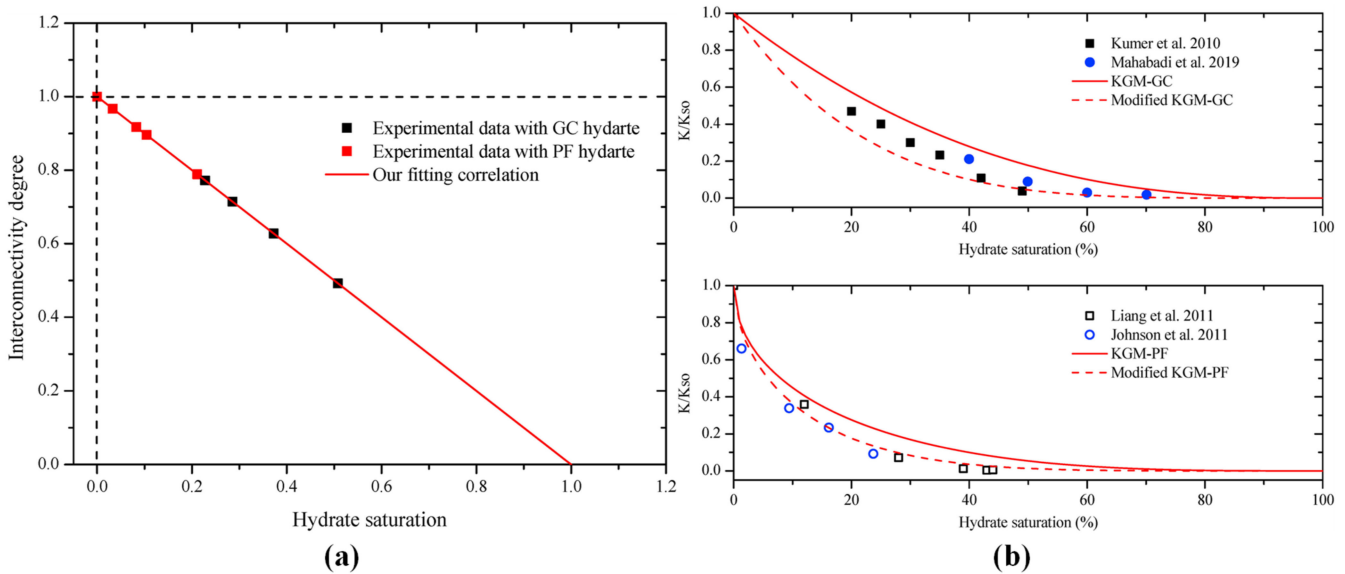


Figure 17. Dependence of interconnectivity degree and normalized permeability on hydrate saturation reprinted from [103] with permission from Elsevier. (a) Interconnectivity degree; (b) normalized permeability with experimental data [27,82,89,95] and analytical results [23]. Note: Please refer to the original literature for the experimental data points shown in the figure.

Based on the above, considering the effect of hydrate with different growth habits on pore interconnectivity in sediments, the modified models of permeability estimation were given by:

$$K_{n_GC} = (1 - S_h)^{n+3}; n = 1.5 \quad (40)$$

$$K_{n_PF} = \frac{(1 - S_h)^{n+4}}{(1 + \sqrt{S_h})^2}; n = 0.7 \times S_h + 0.3 \quad (41)$$

Figure 17b shows the relationship between normalized permeability and hydrate saturation from previous experiments and reported permeability models. It can be concluded that the modified model proposed by Kou et al. [103] performs better with higher accuracy in permeability prediction.

4.8. Summary

- (1) The modified KC model for permeability prediction of HBSs can be established by adding the fitting parameter or the polynomial, which comprehensively considers the relationship between hydrate saturation and shape factor, porosity, tortuosity, pore surface area, and pore volume based on numerical simulation results. The prediction accuracy of models could be improved by changing the value of the fitting parameters or the order of the polynomial.

- (2) The modified permeability model of HBSs based on the KC equation can be established by strict mathematical deduction of new expressions of S_h and the ratio of internal surface area $A_0/A(S_h)$ based on assumptions of particle stacking structures, hydrate pore habits, and 3D microscopic growth morphology. Moreover, there are only parameters in part of the modified models that represent the radius of sediment particles and hydrate to show the effect of related factors on the permeability of HBSs.
- (3) The KC-based modified permeability models consisted of parameters with specific physical meaning to better explain the effect of hydrate on the pore structure characteristic and permeability variation. The influences of hydrates (considering the effect factors such as the hydrate saturation and hydrate growth habits) on the pore structure characteristics (e.g., porosity, pore-throat size, tortuosity, pore connectivity) of hydrate sediments will be a new research hotspot for the permeability prediction model of HBSs.
- (4) The research methods, the advantages and limitations, the using parameters and their physical meaning of various modified permeability models, and the factors that models consider are also provided. Table 5 lists the methods, advantages, and limitations of these modified permeability models of HBSs, while Table 6 summarizes the characteristics of these modified permeability models for permeability prediction of HBSs.

Table 5. Research methods, advantages, and limitations of modified permeability models for permeability prediction of HBSs.

Model	Research Methods	Advantages and Limitations
Dai and Seol [40]	Modified KC model based on PNM simulation	Simple form based on simulation results; but may not apply to all the actual sediments and containing empirical parameter B
Kang et al. [53]	Modified KC model based on fitting by LBM simulation	A polynomial-based model with high prediction accuracy but overfitting may arise with the increased value of the polynomial order
Katagiri et al. [54]	Derived based on the KC permeability model	Simple form based on geometric analyses and strict mathematical derivation but containing empirical parameter n
Li et al. [26,55]	Derived based on the KC permeability model	Piecewise function based on experiment results strict mathematical derivation but complicated form and based on the assumption of sediment particle and hydrate
Shen et al. [56,100,101]	Derived based on the KC permeability model	Analytical formula based on experimental results and strict mathematical derivation but complicated form with limited prediction range and based on the assumption of sediment particle and hydrate

Table 5. Cont.

Model	Research Methods	Advantages and Limitations
Xiao et al. [57]	Derived based on the KC permeability model	Analytical formula based on experimental results and strict mathematical derivation but complicated form and based on the assumption of sediment particle and hydrate
Kou et al. [103]	Derived based on the KC permeability model and experimental results	Simple form based on pore structure analysis but aiming at specific experimental conditions and containing empirical parameters n

Table 6. Characteristics of modified permeability models for permeability prediction of HBSs.

Model	Parameters	Physical Meaning	Influencing Factors
Dai and Seol [40]	B	×	Hydrate saturation and heterogeneity; tortuosity and specific surface
Kang et al. [53]	$a_i S_h^i$	×	Hydrate saturation; tortuosity, specific surface, and shape factor
Katagiri et al. [54]	e	✓	Hydrate saturation and pore habits; 3D sediment particles packing patterns
	C_p	✓	
	n	×	
Li et al. [26,55]	r_1	✓	Hydrate saturation, 3D shape, and assumed the pore-filling habit; 3D simple cubic sphere pack, the radius of pore fluid and sediment grain, shape factor
	L	✓	
	n	✓	
Shen et al. [56,100,101]	r_2	✓	Hydrate saturation, 3D shape, and pore habits; 3D packing patterns and radius of sediment particle
	L	✓	
	n	×	
Xiao et al. [57]	r_s	✓	Hydrate saturation and radius of clustered hydrate particle in pore center; 3D packing patterns and radius of sediment particle
	r_h	✓	
	n	×	
Kou et al. [103]	n	×	Hydrate saturation and pore habits; Pore structure and pore connectivity of sediments

5. Novel Permeability Models Based on New Theories and Research Methods

Most existing models for permeability prediction in the existence of hydrate are either empirical based on data fitting of simulated results or theoretically based on simplistic representations of the pore structure and hydrate morphology. Multiple models are usually required to interpret widely distributed permeability data observed in the laboratory experiment over different hydrate saturation ranges. To assess the long-term gas production capacities of HBSs over a time scale of decades, it is necessary to establish a comprehensive permeability model that can accurately capture the complex seepage characteristics of HBSs during NGH exploitation and to introduce the model into a numerical simulator for the prediction and optimization of gas production performance of marine hydrate deposits. Recently, many novel normalized permeability prediction models of HBSs have

been developed based on new theories and research methods investigating the effect of other hydrate- or sediment-related factors on the fluid flow and the permeability variation.

5.1. New SDR Model Considering the Effect of Hydrate-Related Interface Evolution

The decomposition of hydrate results in the variations in the multiphase saturation and the evolution of the interfaces between fluid (i.e., water and gas), hydrate, and sediment particles. In HBSs, the working principles of NMR measurement are based on the nuclear magnetic relaxation response of target nuclei residing in the various phases are different [104,105]. Recently, several studies have been conducted to study the hydrate formation and dissociation characteristics of, pore size distribution (PSD), and hydraulic permeability of hydrate sediments estimated by explaining the transverse relaxation time (T_2) spectrum obtained from NMR measurements [106–108]. In the surface-limited regime, the transverse relaxation time T_2 can be estimated by:

$$T_2 = \frac{1}{\rho_2} \frac{V_{pore}}{A_{pore}} \quad (42)$$

where V_{pore}/A_{pore} is the ratio of pore volume over pore surface area; ρ_2 is the transverse surface relaxivity and the value of ρ_2 is highly dependent on the mineralogy of the solid surface. Even though the surface mineralogy of minerals is different in most cases in a porous media, an equivalent ρ_2 -value (i.e., a uniform value throughout the sample measured volume) is commonly used. However, if the mineralogy and morphology of the fluid-solid interface vary in a porous media the equivalent ρ_2 -value is expected to change as well [92], which suggests that further deep investigation is required to understand the influences of the spatially variable ρ_2 in the petro-physical properties predictions based on NMR data [64].

In these researches [106–108], the ρ_2 -value of HBSs is assumed to be constant during hydrate phase transition. However, during the actual phase transitions process, the ρ_2 value in hydrate sediments will change due to variations in the mineralogy and morphology of the fluid-solid interface. It should be noted that the SDR model expressed as Equation (2) ignores the effect of hydrate-related interface evolution on the NMR transverse surface relaxivity.

In NMR measurements, to quantitatively evaluate the effect of hydrate-related surface evolution on ρ_2 , Zhang et al. [64] proposed a normalized transverse surface relaxivity ρ_2^* , which was defined as a ratio between the transverse surface relaxivity of hydrate-bearing media to that of hydrate-free media. The value of ρ_2 depends independently on the relaxation characteristics of different solid surfaces in the porous media [92]. Next, considering the two main controlling factors (i.e., the influencing weight and surface proportion of hydrate phase and quartzitic sand phase) influencing ρ_2^* in the HBSs, a prediction model for ρ_2^* is also proposed:

$$\rho_2^* = \alpha(S_h) \Pi + \beta(S_h) \quad (43)$$

where $\alpha(S_h)$ and $\beta(S_h)$ are the proportion of the hydrate-brine interface area and the sand-brine interface area over the total solid-brine interface area, respectively, which follows $\alpha(S_h) + \beta(S_h) = 1$; Π is a dimensionless coefficient defined as a ratio of the transverse magnetic relaxivity of the hydrate-brine interface to that of the sand-brine interface.

Considering the effect of hydrate-related interface evolution during the hydrate dissociation process on the NMR transverse surface relaxivity [64], the normalized permeability K_n can be calculated by:

$$K_n = \rho_2^*(1 - S_h)^4 \left[\frac{T_{2LM}(S_h)}{T_{2LM}(S_h = 0)} \right]^2 \quad (44)$$

5.2. Fractal Theory-Based Permeability Prediction Model

Prediction of permeability in HBSs has been a challenge because there are many different models based on simple pore characteristics and grain geometries [10,23,40]. Most of these models do not consider the interaction between hydrate and pore structure of the host sediment. However, the key to accurately predicting the permeability of HBSs is to extract effective parameters that can reflect the microscopic pore structure characteristics of sediments and establish a quantitative relationship between these parameters and permeability [60,61].

To date, the fractal geometry method is introduced by many scholars to investigate the effects of pore structure change caused by hydrate formation and dissociation on permeability [109]. Many permeability prediction models based on fractal characterization of HBSs have been proposed recently [60,61]. The most important aspect of using these models to predict HBS permeability is that microscopic pore structure information (e.g., the maximal pore diameter and related fractal dimensions) can be properly and precisely characterized [61].

5.2.1. Daigles Model

Most existing permeability models contain several empirical constants that are not strictly related to the pore characteristics of HBSs. In addition, a common issue faced by all these permeability models is that the permeability does not fall to 0 until the hydrate saturation is 100%. This is not consistent with the concepts of percolation threshold or irreducible saturation.

Daigle [60] first proposed a theoretical permeability model of HBSs based on the combination of pore-solid-fractal (PSF) geometry and the critical path analysis (CPA) method. Critical path analysis (CPA) provides a framework for permeability prediction based on the properties of the pore system, including the percolation threshold and width of the pore size distribution (PSD). Regardless of hydrate growth habits, permeability variation estimated by this model considers the presence of hydrate in the largest pores (Figure 18). This work has made significant progress in linking pore structure and transport properties of HBSs. The permeability model is given by:

$$K_n = \left[\frac{\beta - \phi_0 + \phi_0(1 - S_h - p_c)}{\beta - \phi_0 p_c} \right]^{\frac{D}{3-D}}; S_h < 1 - S_x \quad (45)$$

$$K_n = \left[\frac{\beta - \phi_0 + \phi_0(S_x - p_c)}{\beta - \phi_0 p_c} \right]^{\frac{D}{3-D}} \left[\frac{S_w - p_c}{S_x - p_c} \right]^2; S_h > 1 - S_x \quad (46)$$

$$S_x = p_c + \frac{2\left(\frac{\beta}{\phi_0} - 1\right)}{\frac{D}{3-D} - 2} \quad (47)$$

where β is a scaling factor in the PSF model; p_c is the percolation threshold that depends on the connectivity degree of the pore system, and the flow of the given phase occurs only when the saturation of that phase exceeds p_c ; D is the fractal dimension; S_x is crossover saturation determined as the saturation at which the derivatives of Equations (45) and (46) with respect to S_w equal.

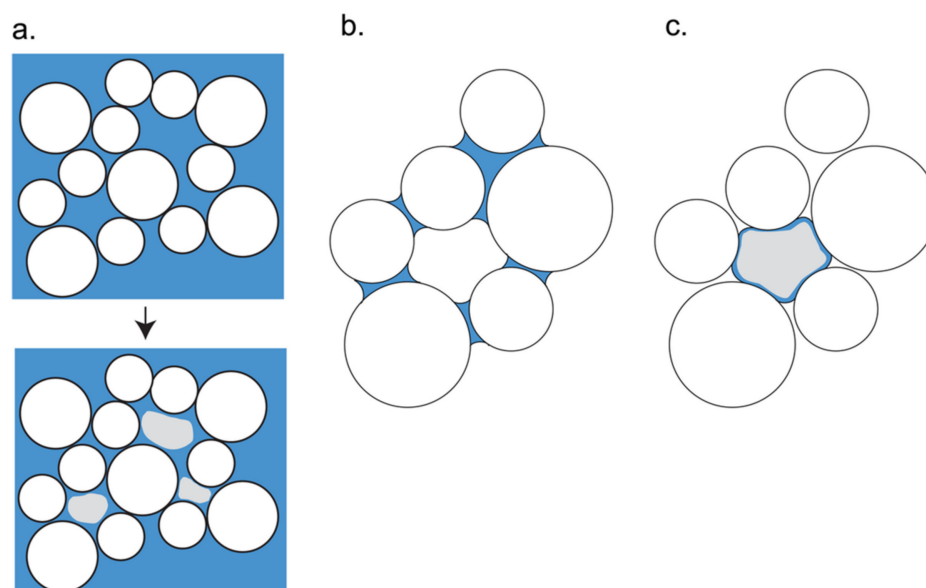


Figure 18. Conceptual illustration of hydrate formation reprinted from [60] with permission from Elsevier. (a) Hydrate formation from dissolved gas; (b) hydrate formation from the partial water saturation method; (c) when hydrate forms it occupies the larger pores due to redistribution of phases.

5.2.2. Zhang et al. Model

In a Zhang et al. study [61], the area and volume pore-size fractal dimensions, tortuosity fractal dimension, and the area maximal pore diameter for the pore space occupied by fluids were extracted by X-ray computed tomography scans of methane hydrate sands. Then, a permeability prediction model of HBSs based on fractal theory is established by extending the extracted parameters. After a series of simplifications, the normalized permeability of HBSs can be expressed as follows:

$$K_n = [\lambda_{\max 2}^*]^{3+D_{T,0}} \quad (48)$$

$$\lambda_{\max 2}^* = 1 - (1 - a)\sqrt{S_h} - aS_h^b \quad (49)$$

where a and b are fitting parameters. $D_{T,0}$ is the tortuosity fractal dimension and $1 \leq D_{T,0} \leq 2$ for a two-dimensional space while $1 \leq D_{T,0} \leq 3$ for three-dimensional space. It is obvious in Equation (48) that the normalized maximal pore diameter $\lambda_{\max 2}^*$ is the main parameter to determine the normalized permeability of HBSs. Moreover, Equation (49) is an alternative form for the weighted average of theoretical models $\lambda_{\max 2}^* = 1 - S_h^{0.5}$ for PF hydrates and $\lambda_{\max 2}^* = (1 - S_h)^{0.5}$ for GC hydrates [109,110].

Figure 19 shows normalized permeability curves determined by Equation (48) and available experimental data. The results show that the proposed permeability model has good feasibility and can reflect the basic physics of permeability evolution in artificial hydrate samples. It is inferred from this model that the variation of the normalized permeability is largely determined by the uncertainty of the maximal pore diameter value. Moreover, some fine-grained sediments contain a large number of dead pores that are occupied by pore fluids but do not contribute to fluid flow. Therefore, this fractal theory-based normalized permeability prediction model can only be applied for coarse-grained sediments.

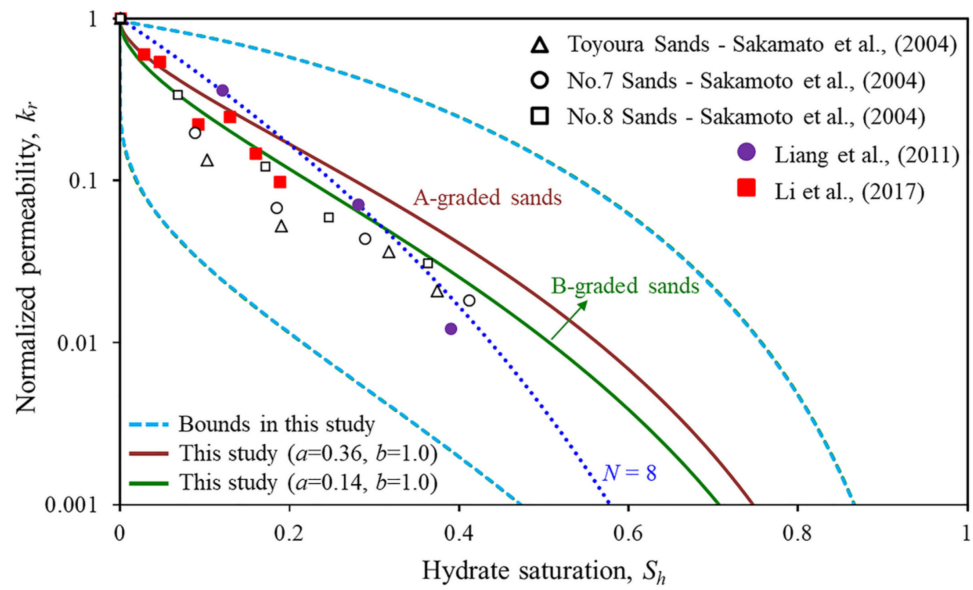


Figure 19. Comparison of prediction results from fractal-based models and reported experimental data [55,95,99]. Reprinted with permission from Ref. [61]. Copyright 2022 American Geophysical Union.

5.2.3. Du et al. Model

Du et al. [62] established a permeability prediction model for hydrate-bearing porous media with the coexistence of pore-filling and grain-coating hydrate (Figure 20) based on the fractal theory. This model is a function of some parameters with specific physical meaning, such as the pore area fractal dimension, tortuous dimension, porosity, hydrate saturation, and maximum pore diameter. Here, the pore area fractal dimension reflects the size distribution of the particles and the complexity of the pore space at the micro scale. The tortuous dimension describes the tortuosity of the capillary tube and streamlines and porosity characterizes the pore space size in porous media.

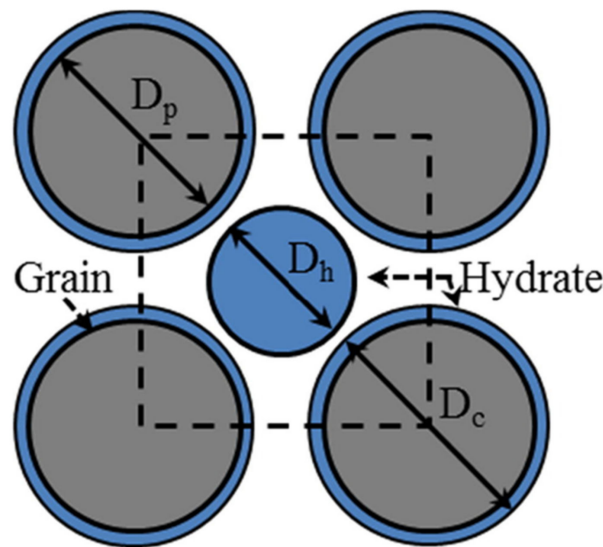


Figure 20. Representative elementary volume (REV) of hydrate-bearing porous media with the coexistence of pore-filling and grain-coating hydrate reprinted from [62] with permission from Elsevier.

Combined with Darcy's law and modified Hagen–Poiseuille equation, the fractal normalized permeability can be written as:

$$K_n = \frac{C_{f,h}}{C_{f,0}} \frac{(1 - \phi_0)^{(1+D_t)/2} \phi_0^{(D_{t,h}-D_t)/2}}{(1 - \phi)^{(1+D_{t,h})/2}} (1 - S_h)^{(7+D_{t,h})/2} \quad (50)$$

$$C_{f,h} = \frac{(\pi D_{f,h})^{(1-D_{t,h})/2} [4(2 - D_{f,h})]^{(1+D_{t,h})/2}}{128(3 + D_{t,h} - D_{f,h})} \quad (51)$$

$$C_{f,0} = \frac{(\pi D_f)^{(1-D_t)/2} [4(2 - D_f)]^{(1+D_t)/2}}{128(3 + D_t - D_f)} \quad (52)$$

where D_t and $D_{t,h}$ are the water phase tortuous dimension of hydrate-free and hydrate-bearing porous media, respectively; D_f and $D_{f,h}$ are the pore area fractal dimension of hydrate-free and hydrate-bearing porous media, respectively.

To further verify the reliability of the proposed fractal permeability model, relevant parameters in the above equation were calculated as follows:

$$D_f = D_E - \frac{\ln \phi_0}{\ln(\lambda_{\min,0}/\lambda_{\max,0})} \quad (53)$$

$$D_t \approx (D_E - D_f + 1) + (D_E - D_f) \frac{\log [D_f / (D_f - 1)]}{\log \phi_0} \quad (54)$$

$$D_{f,h} = D_f - \frac{\ln(1 - S_h)}{\ln(\lambda_{\min,0}/\lambda_{\max,0})} \quad (55)$$

$$D_{t,h} \approx (D_E - D_{f,h} + 1) + (D_E - D_{f,h}) \frac{\log [D_{f,h} / (D_{f,h} - 1)]}{\log \phi} \quad (56)$$

where D_E is the Euler dimension; $\lambda_{\max,0}$ and $\lambda_{\min,0}$ are the maximum and minimum pore diameters of porous media in the absence of hydrate. It can be seen clearly from Equations (50)–(56) that the normalized permeability is expressed as the function of structural parameters of porous media and fluid properties. The K_n is not only closely related to the macrostructure parameters (the porosity ϕ_0/ϕ , the fractal dimension D_f , and the tortuous dimension D_t) but also to the microstructure parameters (the maximum pore size $\lambda_{\max,0}$, and the particle diameter D_p) of porous media.

From Figure 21, it can be seen that the prediction results of this proposed fractal permeability model agree well with the experimental data than other reported empirical models. It is clear that almost all experimental data points fall around the black solid line. Additionally, Du et al. [62] also found that the permeability reduction index (N) and the saturation index (n) are nonlinear functions related to porosity, hydrate saturation, and pore size ratio, rather than empirical constants without physical significance. However, this discovery is not well reflected in the traditional permeability models. Thus, traditional permeability prediction models cannot capture the underlying physical mechanism that determines the permeability variation of HBSs.

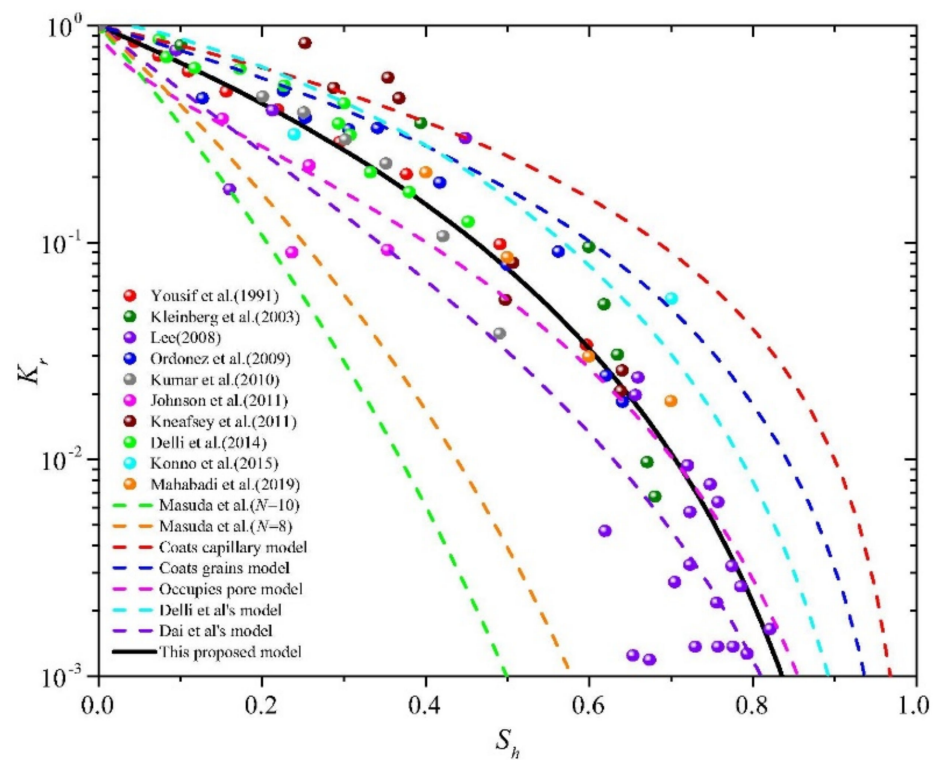


Figure 21. Relationships between relative water permeability and hydrate saturation from reported experiment data [23,24,27,82,89,94,111–114] and analytical prediction results [23,24,40,42] reprinted from [62] with permission from Elsevier.

5.3. Chen et al. Model

Chen et al. [65] used the LBM flow simulation to calculate the pore-scale gas permeability in the pore structure of the experimental HBSs retrieved from μ CT data. Based on their simulation results, the expression of the proposed modified Corey model that multiplies a linear Corey model (i.e., $K_n = 1 - S_h$) with an exponential function of S_h is:

$$K_n = (1 - S_h) \cdot \exp(-C \cdot S_h) \quad (57)$$

where C is a fitting parameter. The linear Corey term ($1 - S_h$) makes endpoint permeability in its simplest form, and the exponential function helps this new model fit the simulation data.

The solid black line in Figure 22 is Equation (57) and fully represents the permeability data across the entire range of hydrate saturation with only one fitting parameter C ($C = 4.95$ for best fit of LBM simulation results [65]). Chen et al. further suggested that C indicates the degree of crystal coarsening and patch size in general for a multiphase system. For example, a small value of C means strong coarsening, crystal coalescence, and long correlation length between patches that make permeability slowly decrease with increasing hydrate saturation. On the other hand, a large value of C means little coarsening, dispersed crystal, and short correlation length that make permeability quickly decrease with increased S_h .

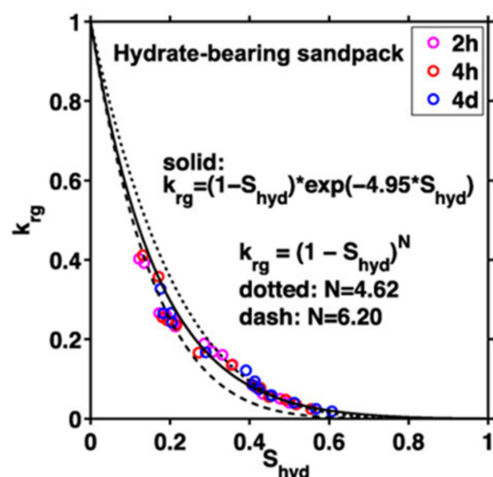


Figure 22. Gas relative permeability versus hydrate saturation, Corey-type fits, and new model fits. Reprinted with permission from Ref. [65]. Copyright 2022 American Geophysical Union.

5.4. Liu et al. Model

Liu et al. [66] proposed a new permeability prediction model based on a simple Corey model and permeability data for HBSs obtained from LBM simulation with X-ray micro-CT imaging information of xenon hydrate pore-scale distribution in sand sediments, pointing out that exponent N in simple Corey model can be described by a function with S_h as an independent variable:

$$K_n = (1 - S_h)^N = (1 - S_h)^{f(S_h)} = (1 - S_h)^{a \cdot S_h} \tag{58}$$

where a is a fitting parameter without definite physical meaning. This modified functional form effectively quantifies the K_n - S_h relationship and enhances the applicability of the simple Corey model.

Gas relative permeability data for the xenon hydrate-bearing sediments of the Liu et al. experiment [58] is plotted in Figure 23. The experimental permeability data could be fitted with the simple Corey model (blue solid line in Figure 23a) with the Corey exponent of 4.42. However, the correlation coefficient for this fit was 0.74. While this fit was good for $S_h > 0.52$, it was very poor for $S_h < 0.52$. Thus, Liu et al. fitted the data with the new model (Equation (66)). A much better fit was obtained, with a significant improvement in the correlation coefficient ($R^2 = 0.98$), implying a very good correlation.

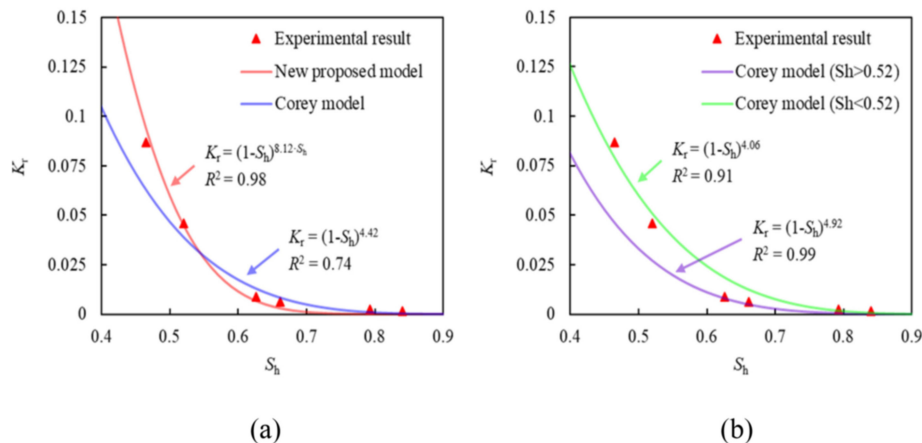


Figure 23. The relative permeability data for xenon hydrate-bearing sediments reprinted from [66] with permission from Elsevier. (a) Simple Corey model fit (blue solid line) and new proposed model fit (red solid line); (b) simple Corey model fit with different exponent N .

5.5. Hou et al. Model

Hou et al. [63] conducted micro-flow simulations using LBM to study the effects of mineral particle arrangement, hydrate saturation, hydrate pore habits, and distribution morphology in 2D porous media on permeability. Their simulation results showed that the effect of mineral particle arrangement on permeability evolution is not obvious in the 2D homogeneous porous media; however, the permeability variation is sensitive to the hydrate pore habits (i.e., GC hydrate or PF hydrate) and distribution morphology in the pore center (i.e., PF hydrate with a different shape), as shown in Figure 24. In addition, they proposed the control seepage channel between mineral particles and hydrates, which controls the dynamic permeability evolution characteristics by comparing and analyzing the pore-scale distribution difference in velocity field obtained by LBM flow simulation (Figure 24).

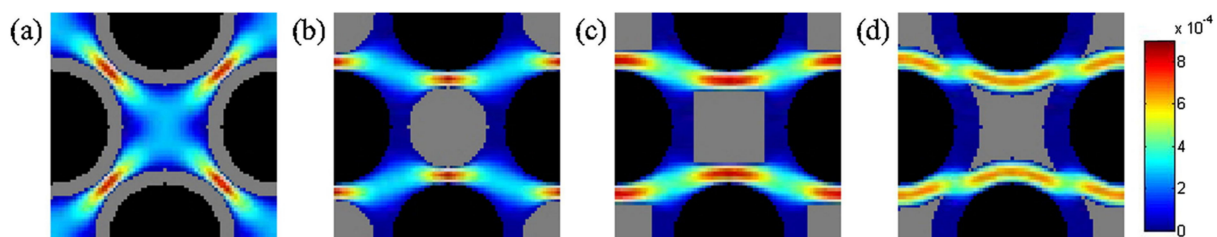


Figure 24. Distribution of hydrate and pore-scale velocity field in the porous media model reprinted from [63] with permission from Elsevier. (a) Hydrate coats grain surface; (b–d) hydrate occupies pore centers with different micromorphology. The gray is regarded as hydrate. The color fluid is regarded as a velocity field obtained by LBM.

Furthermore, they established a novel permeability prediction model based on the size and tortuosity of the control seepage channel according to the simulation results and the relationship between permeability and porosity (i.e., $K \propto \phi^3$ [52]). In considering two hydrate-formation habits (GC and PF), the relationships of K_n-S_h are as follows:

$$K_{n_GC} = (1 - bS_h)(1 - S_h)^3 \quad (59)$$

$$K_{n_PF} = \left(1 - d\sqrt{S_h}\right)(1 - S_h)^3 \quad (60)$$

where b and d are fitting parameters. Moreover, the value of b is related to the porosity of hydrate-free porous media and the value of d is relevant to the micromorphology of PF hydrate, which occupies the pore center.

This proposed model contains two parameters that can be easily obtained or set in practical applications, which describe the basic seepage characteristics and pore-scale influencing mechanism of permeability evolution of HBSs. Hence, they can be easily implemented in reservoir simulators for gas production behavior modeling. In addition, K_n-S_h relationships presented on the base of 2D homogeneous porous media are appropriate for 2D inhomogeneous porous media. Hence, it provides a reference for microscopic visualization experiments.

Compared to the models proposed by Kleinberg et al. [23] (i.e., PCTM and KGM) and Masuda et al. [42], the Hou et al. permeability model provided a better agreement with the reported experimental data, as shown in Figure 25. The results show that the permeability model for PF hydrate (Equation (60)) can better describe the evolution of experimental relative permeability than that of GC hydrate (Equation (59)), and this indicates that the hydrate mainly grows in the pore center as a pore-filling type under the experimental conditions.

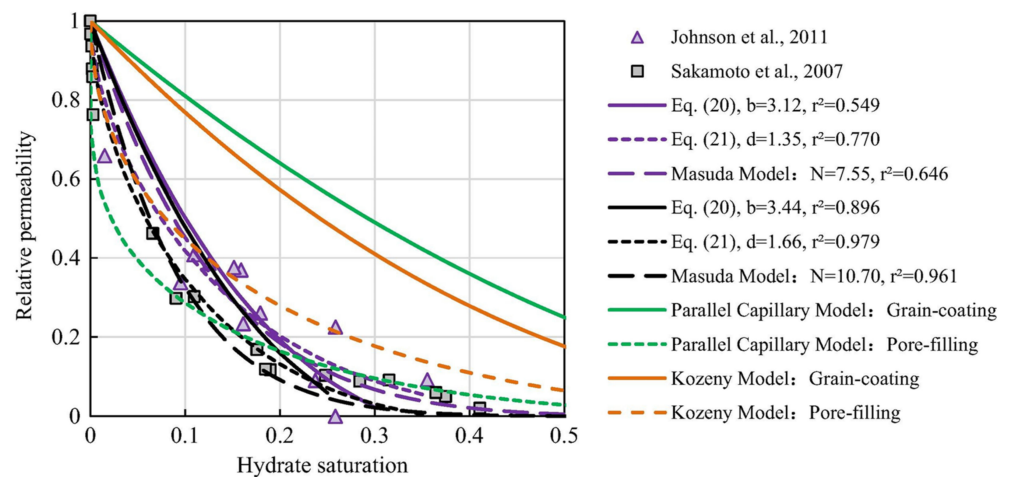


Figure 25. Comparison of experiment results [89,93] and calculation results from reported permeability models [23,42] reprinted from [63] with permission from Elsevier.

5.6. Guo et al. Model

In a study by Guo et al. [58], the space occupied by hydrate was assumed to be part of the pore volume and hydrate was thought to be an independent phase. Hence, for sediment with given hydrate saturation (as shown in Figure 26), there are three components: water, sediment particles, and solid hydrates. Then, Guo et al. [58] proposed two new concepts of hydrate void ratio e_h and effective void ratio e_e , which were defined as the ratio of the hydrate volume V_h and the water volume V_w to the volume of sediment particles V_s .

Based on Poiseuille's law and the concept of the three-dimension hydraulic radius (Figure 27), Guo et al. [58] proposed a novel permeability prediction model considering different hydrate pore habits in coarse-grained HBSs. Equations (61) and (62) show the permeability model for GC HBS and PF HBS, respectively.

$$K_{n_GC} = \frac{(1 - S_h)^3}{(1 + e_t S_h)^{\frac{4}{3}}} \quad (61)$$

$$K_{n_PF} = \frac{(1 - S_h)^3}{\left[1 + (e_t S_h)^{\frac{2}{3}}\right]^2} \quad (62)$$

where e_t is total void ratio, that is, the ratio of pores volume to sediment particles volume. The e_t in this Guo et al. study [58] was assumed to be the total void ratio of sediment without hydrate, that is, a constant parameter. Due to the assumption of e_t , the accuracy of this model is slightly lower, but it is easier to be applied in numerical simulation and practical applications. However, it is undeniable that the unique embedded parameter e_t has a clear physical meaning and is easy to determine, which is the main advantage of this novel model.

Figure 28 shows the comparison of the predicted results of the Guo et al. permeability model with the observed data taken from laboratory-synthesized coarse-grained sediment samples and with the predicted permeability of other widely used analytical models. The model for the GC case and PF case proposed by Guo et al. form the upper bound and lower bound of the prediction area in grey, respectively. In addition, compared with PCTM and KGM, this new model has a narrower prediction range of permeability, which means that a more accurate prediction of permeability can be obtained even hydrate pore habits are unclear (Figure 28a). However, the relative inconsistency (Figure 28b,c) or large deviation (Figure 28e,f) between the prediction results of the new model and experimental data compared to other KC-based models is due to the ideal assumption of

the embedding parameters in this model, i.e., the void ratio e_t without considering hydrate is used throughout the prediction range.

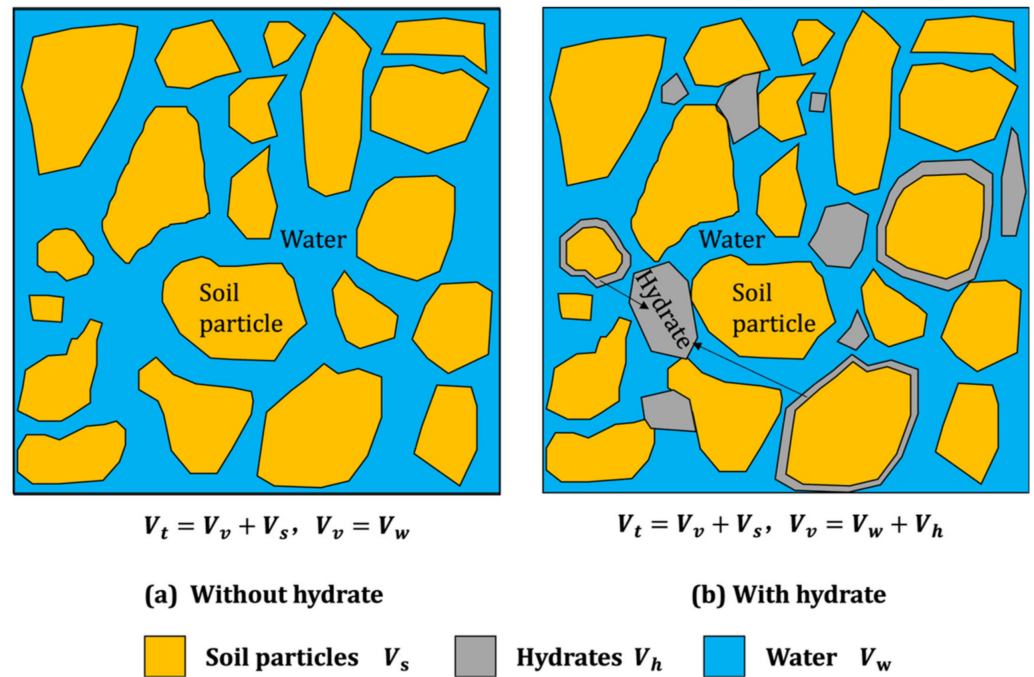


Figure 26. Schematic diagram of sediment (a) without hydrate and (b) with hydrate reprinted from [58] with permission from Elsevier.

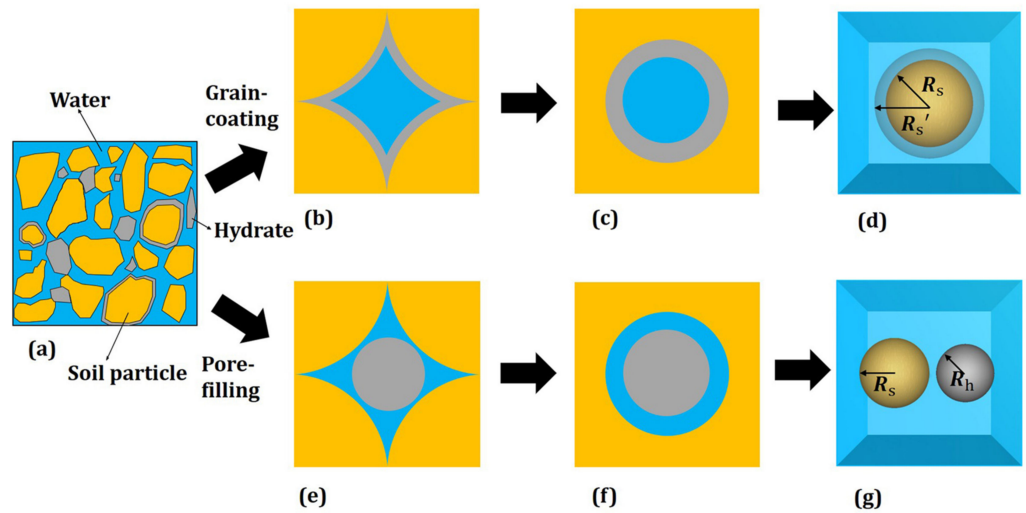


Figure 27. The schematic diagram of saturated sediment with hydrates reprinted from [58] with permission from Elsevier. (a) The real internal pore structure of HBSs; (b) grain-coating hydrates in HBSs; (c) capillary tube with grain-coating hydrates; (d) the 3D hydraulic radius of grain-coating hydrate; (e) pore-filling hydrates in HBSs; (f) capillary tube model with pore-filling hydrates; (g) the 3D hydraulic radius of the pore-filling hydrate.

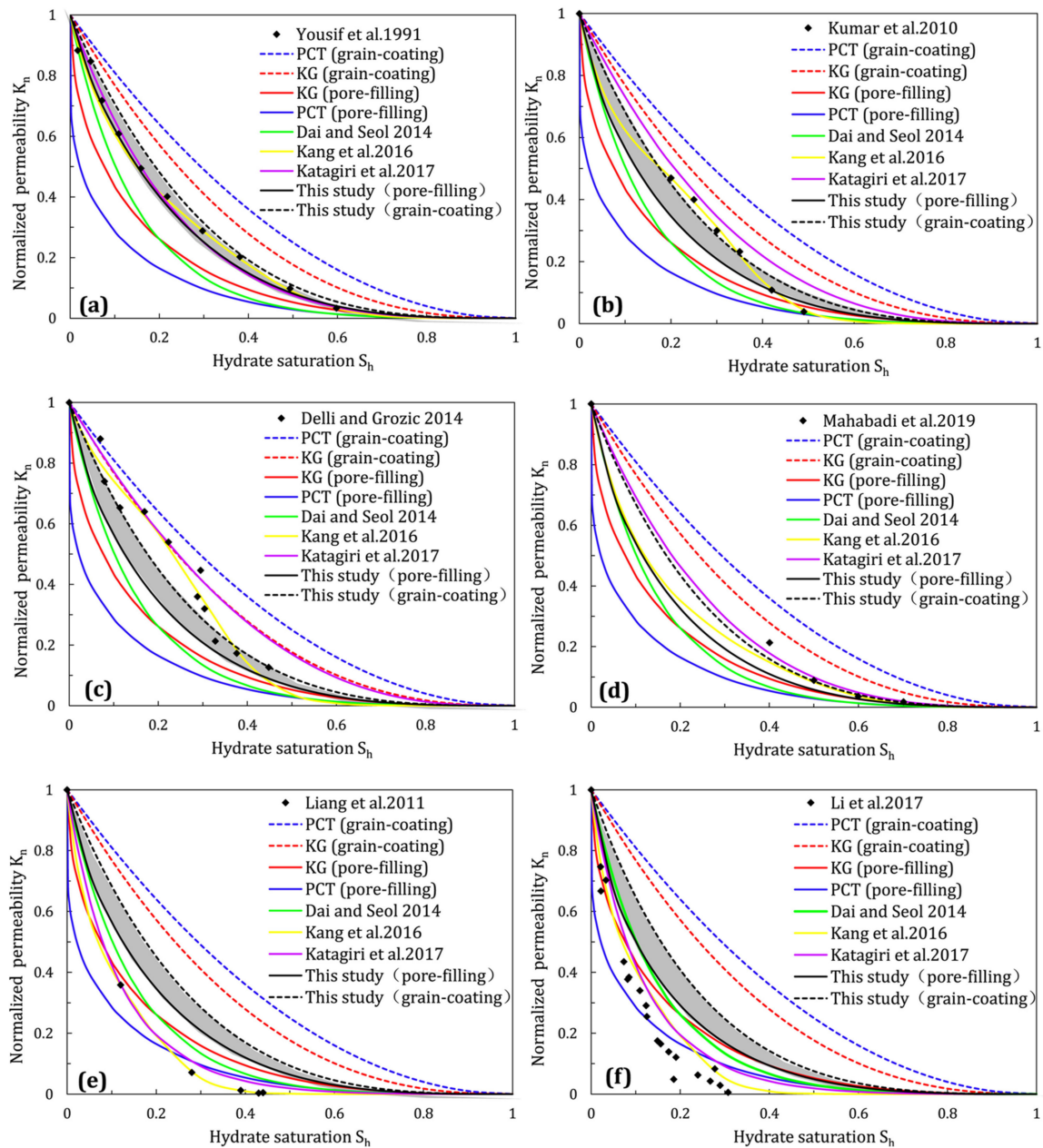


Figure 28. The verification of the new model reprinted from [58] with permission from Elsevier. The adopted existing KC-based models are from literatures [23,40,53,54]; experiment results: (a) Yousif et al. [111]; (b) Kumar et al. [82]; (c) Delli and Grozic [24]; (d) Mahabadi et al. [27]; (e) Liang et al. [95]; (f) Li et al. [55].

For a given natural or an artificial HBS sample, it is usually difficult to distinguish whether the hydrate pore habit is a single pore-filling type or a single grain-coating type. Hydrate pore habits vary depending on hydrate formation methods, hydrate saturation, and host sediment types [10,27], and can change from one type to another (e.g., Chen and Espinoza [115]). Additionally, there may be multiple types of hydrate pore habits coexisting in HBSs. Hence, Guo et al. [58] proposed that for a given sample with unknown pore habits of hydrate, the normalized permeability can be expressed as follows:

$$K_n = \alpha K_{n_GC} + \beta K_{n_PF} = \alpha \frac{(1 - S_h)^3}{(1 + e_t S_h)^{\frac{4}{3}}} + \beta \frac{(1 - S_h)^3}{\left[1 + (e_t S_h)^{\frac{2}{3}}\right]^2} \quad (63)$$

where α and β are weighting parameters for GC hydrate and PF hydrate, respectively.

5.7. Lei et al. Model

Lei et al. [72] introduced the cubic fracture-permeability model (simplified as the Cubic model) that is commonly used in coalbed methane reservoirs [73] into the gas hydrate reservoir and constructed a new semi-theoretical permeability model based on the pore space characteristics and hydrate pore morphology, which are completely different from those assumed by PCTM and KGM. As shown in Figure 29, in the physical model of their Cubic permeability model considering different hydrate growth habits, the cubes, and the platy pores are simulated as the sediment grains and pores of HBSs, respectively.

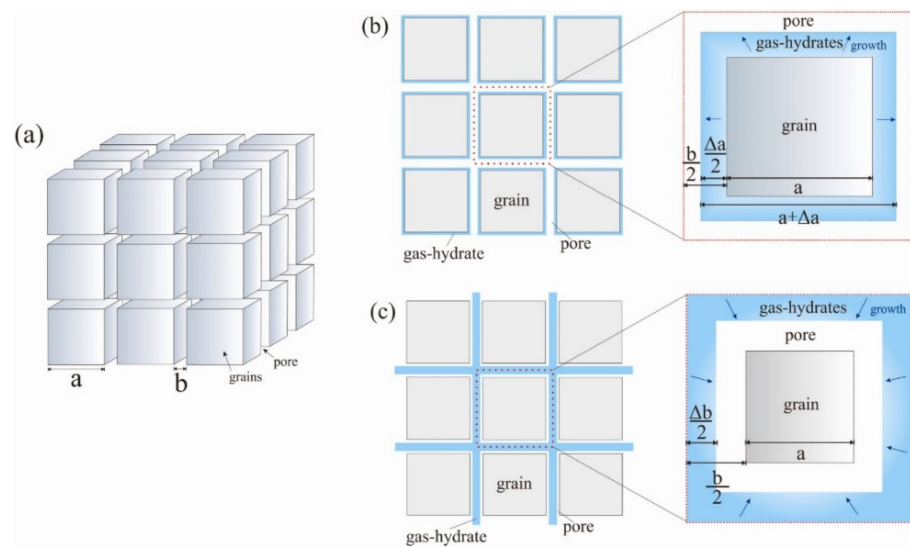


Figure 29. Geometry scheme of the Cubic model for GC and PF hydrate reprinted from [72] with permission from Elsevier. (a) Pore system and framework of the cubic model; (b) pore system changed by GC hydrate; (c) pore system changed by PF hydrate.

The cubic permeability model for GC hydrate and PF hydrate can be expressed as Equations (64) and (65), respectively:

$$K_{n_GC} = \frac{\left(1 - \frac{3S_h}{\phi_0(1-S_h)+3}\right)^3}{\left(1 + \frac{\phi_0 S_h}{\phi_0(1-S_h)+3}\right)} \quad (64)$$

$$K_{n_PF} = \begin{cases} (1 - S_h)^{13.157} \left(1 - \frac{\phi_0 S_h}{6 + \phi_0}\right) (1 - S_h)^3; & 0 < S_h < 0.1 \\ \frac{1}{4} \left(1 - \frac{\phi_0 S_h}{6 + \phi_0}\right) (1 - S_h)^3; & S_h \geq 0.1 \end{cases} \quad (65)$$

where ϕ_0 is the porosity of the hydrate-free sediment. The ϕ_0 has little effect on K_n , therefore, this model still works when the porosity of the reservoir cannot be accurately measured in permeability prediction.

Two sets of experimental data from Lei et al. work [72] were used to validate the Cubic permeability model. Results showed that most of the experimental permeability data points fall between two fitted line segments of the provided cubic models (pink area in Figure 30). When selecting the calibration models, most of the experimental data should plot between the curves of the GC and PF models, and the models should aim to provide the narrowest possible prediction range. The cubic model (pink area) covered more data than the Kozeny grain model (green lines in Figure 30) and covered a narrower area than the Parallel capillary tube model (blue lines in Figure 30) in the case that both models cover the same amount of data. This suggested that the Cubic model provides more accurate prediction results. These results also indicated that the behaviors of existing GC and PF

hydrates in the process of hydrate synthesis and thus a hybrid growth pattern (Figure 31) provide a better explanation for the experimental and simulated results in their study.

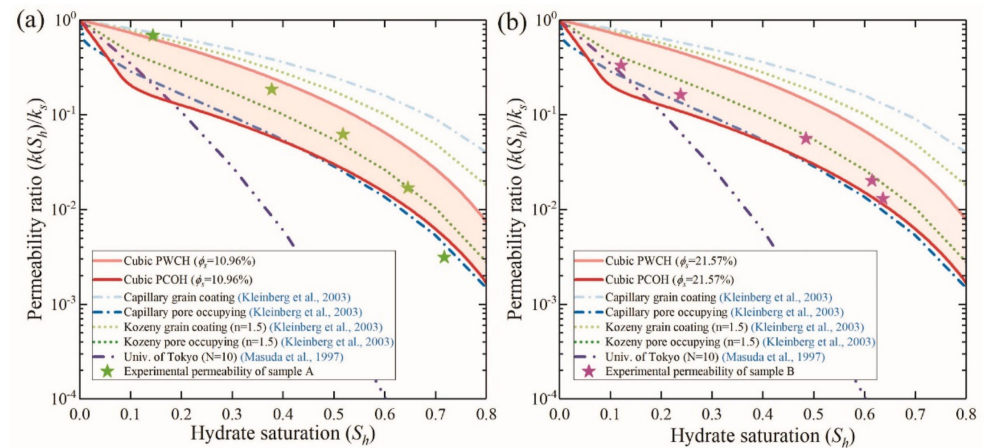


Figure 30. Model validation by the analytical model predictions [23,42] and experimental results from the work by Lei et al. reprinted from [72] with permission from Elsevier. (a) Sample A, initial porosity $\phi_0 = 10.96\%$; (b) sample B, $\phi_0 = 21.57\%$. Note: Please refer to the original literature for the experimental data points shown in the figure.

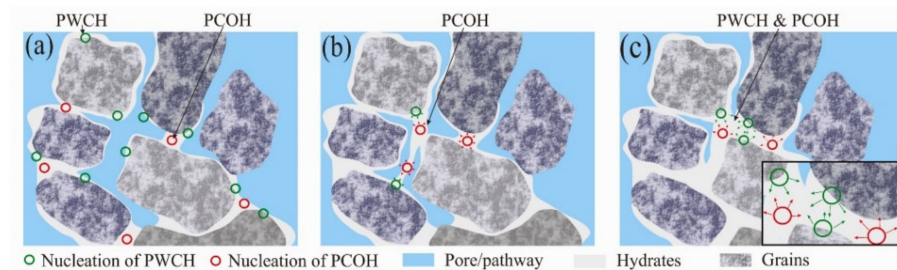


Figure 31. Hybrid growth habit of hydrate in pore spaces reprinted from [72] with permission from Elsevier. (a) Low hydrate saturation stage; (b) middle hydrate saturation stage; (c) high hydrate saturation stage.

5.8. Delli and Grozic Hybrid Model

Delli and Grozic introduced quantitative performance measurement methods, normalized mean squared error (NMSE) [67] and geometric mean variance (GMV) [24], to evaluate the effectiveness of a model in predicting permeability. Then, a hybrid modeling approach based on the weighted combination of the existing permeability model (i.e., KGM) is proposed.

Delli and Grozic [24,67] comprehensively considered the two growth patterns of hydrate in hydrate-bearing porous media and derived a hybrid permeability prediction model based on weights by modifying the KG model. The normalized permeability of the hybrid modeling can be expressed as:

$$K_n = \alpha K_{n_PF} + \beta K_{n_GC} \quad (66)$$

where K_{n_PF} and K_{n_GC} are the normalized permeabilities obtained from the KGM [23] of pore-filling and grain-coating hydrate as given in Equations (11) and (12), respectively; α and β are the corresponding weighting parameters that are functions of hydrate saturations.

The relation between weighting parameters α and β and hydrate saturation is as follows:

$$\begin{aligned} \alpha &= S_h^N \\ \beta &= (1 - S_h)^M \end{aligned} \quad (67)$$

where N and M are the exponents and empirical parameters controlling the change of α and β with hydrate saturation. Additionally, N and M determine the dominant role of single hydrate pore habits in porous media on permeability evolution. Figure 32 shows the variation of weighting parameters as a function of S_h for $N = M$, $N > M$, and $N < M$. Assuming $N = M = 1$, the pore-filling weight α increase and (grain-coating weight β reduces) linearly with increasing hydrate saturation with $\alpha = \beta$ at 50% of hydrate saturation. To determine the exponents N and M , Delli and Grozic adopted the NMSE and GMV measure as a performance criterion. The optimal N and M are expected to produce the least NMSE.

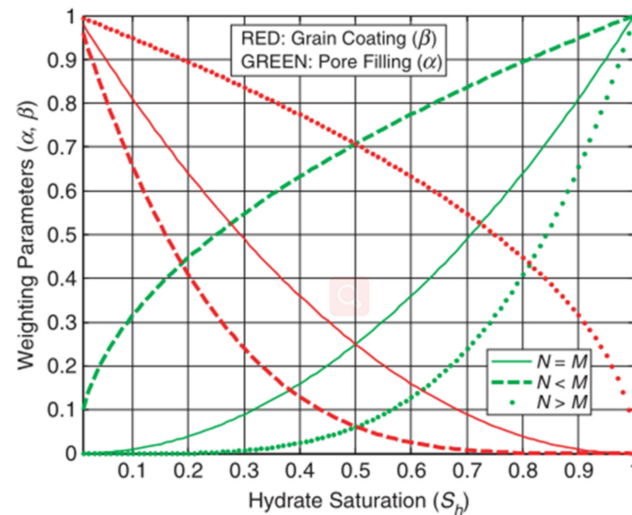


Figure 32. The change of weighting parameters as a function of hydrate saturation. Red lines: grain coating; green lines: pore-filling. Reprinted with permission from Ref. [67]. Copyright 2013 Society of Petroleum Engineers.

Figure 33 shows the measured relative permeability from Yousif et al. [111], the predicted results from KGM for GC and PF cases, and the predicted results of the hybrid modeling. The results show that the hybrid model can better predict the experimental results with $N = M = 1.6$. Thus, this model predicts the evolution of the GC hydrate at lower hydrate saturation to PF hydrate for higher hydrate saturation.

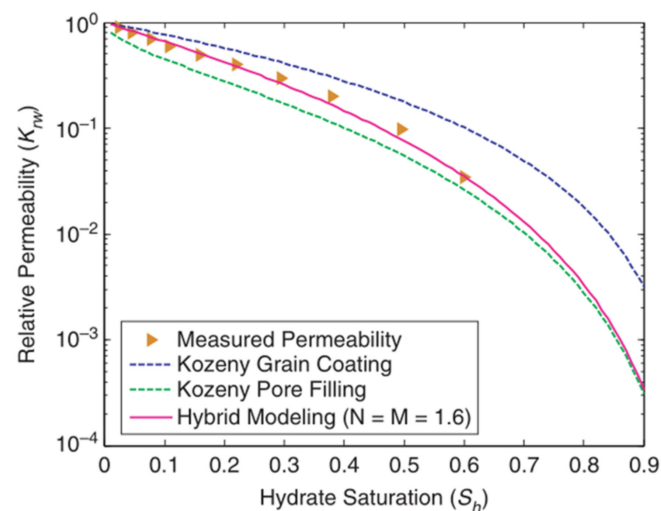


Figure 33. Relative permeability values varying with hydrate saturation from experiment [111] and theoretical models [23,67]. Reprinted with permission from Ref. [67]. Copyright 2013 Society of Petroleum Engineers.

5.9. Wang et al. Hybrid Model

Pore morphology of hydrate in sediment pore evolves from a single pore habit toward a complicated hybrid pore habit, which depends on hydrate formation conditions with increasing hydrate saturation, exerting diverse controls over permeability. However, almost all existing permeability prediction models assume single and simplified hydrate pore morphology in HBSs, thus they fail to capture the dynamic permeability evolution characteristics with varying hydrate saturation in sediments.

As can be seen from Figure 34, regardless of whether hydrate is formed by the excess-gas method, the excess-water method, or the dissolved-gas method, the pore habits of hydrate will be mainly characterized by the coexisting GC and PF hydrates with increased hydrate saturation. Therefore, in most cases, the hydrates in sediment exist in the existing pore habits, while hydrates with a single pore habit occur only in a few extreme cases.

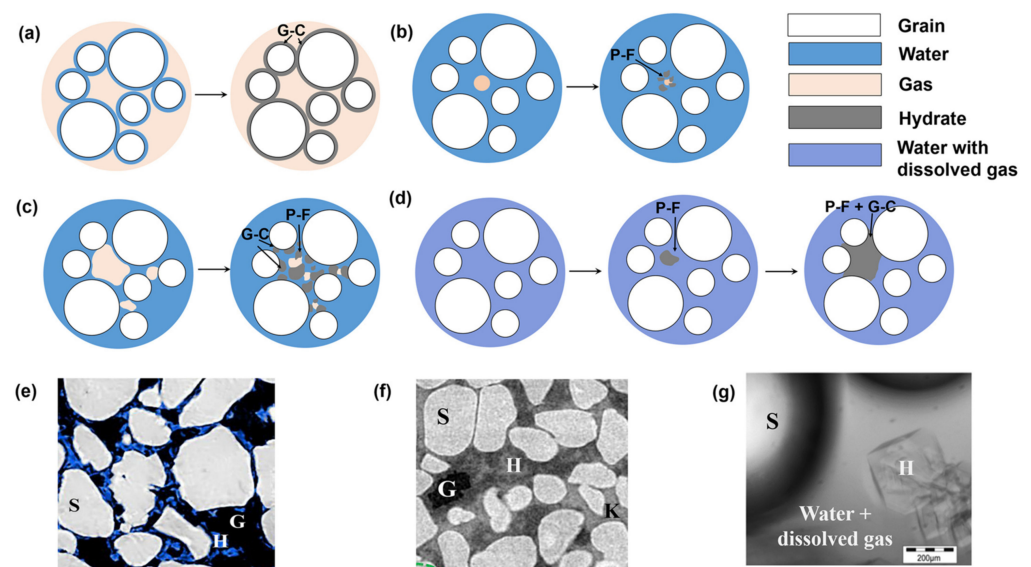


Figure 34. Diverse and complex morphology of hydrate in sediments. (a–d) Distribution characteristics of water, gas, and hydrate in systems with is abundant, scarce, moderate, and dissolved gas phase; (e) a micro-CT image of methane hydrate in the pore under excess-gas conditions; (f) a micro-CT image of methane hydrate in the pore under excess-water conditions; (g) a microscopic image of methane hydrate formed from dissolved methane in water. Reprinted with permission from Ref. [68]. Copyright 2022 American Geophysical Union.

Previous studies have shown that the change in pore habits of hydrate in the sediment pores varies with sediment types and hydrate formation conditions [115–117], leading to a significant difference in the reduction trend of permeability with the increase of hydrate saturation [24,27]. Based on the understanding of the dynamic evolution of hydrate pore habits in sediment pores shown in Figure 34, Wang et al. [68] established a new model called the pore-morphology-weighted permeability model by using a two-parameter logistic function [118,119] based on the logarithm form of the overall permeability considering coexistence of hydrate pore habits [120] to quantitatively relate microscopic hydrate pore habits evolution with macroscopic permeability change as hydrate saturation changes. The new permeability prediction model considering both grain-coating and pore-filling hydrate and their evolution with the increase of hydrate saturation is expressed as follows:

$$K_n = \left[(K_{n_GC})^{1/[1+(S_h/\alpha)^\beta]} \cdot (K_{n_PF})^{1-1/[1+(S_h/\alpha)^\beta]} \right] \quad (68)$$

where K_{n_PF} and K_{n_GC} are the normalized permeabilities obtained from the PCTM [23] of PF and GC hydrate as given in Equations (5) and (7), respectively. It can be seen

from Equation (68) that the weight in this model is the reciprocal function of hydrate saturation. In addition, two fitting parameters α and β with definite physical significance will be described in detail as follows. Here, α defines a transitional hydrate saturation, at which both the grain-coating and pore-filling hydrates contribute equally to sediment permeability, and the dominant pattern of permeability evolution begins to change from one pore habit to the other pore habit. Additionally, the parameter β indicates the evolutionary direction of hydrate pore habits and the sensitivity of permeability variation with increasing hydrate saturation: the pore habit of hydrate changes from PF to the coexisting habits with the increase of hydrate saturation when the value of β is negative, while a positive β value suggests that hydrate pore habit changes from GC to the coexisting habits. Moreover, the smaller α or bigger β makes the permeability reduction curve more easily changes from one type of hydrate pore habits to the other type.

To verify the applicability and robustness of the new model (i.e., Equation (68)), Wang et al. [68] used published permeability data of HBS samples with hydrate formed under excess-gas, excess-water, or dissolved-gas conditions, as shown in Figure 35. The comparison results show that this physics-based permeability model provides a mechanistic understanding of permeability variation and can capture well the dynamic permeability characteristics of sediments containing hydrates in the pore with complex pore habits. Moreover, due to the elegant form and solid theoretical basis of this new model, it can be implemented in reservoir simulators for field studies and field-scale gas production estimation.

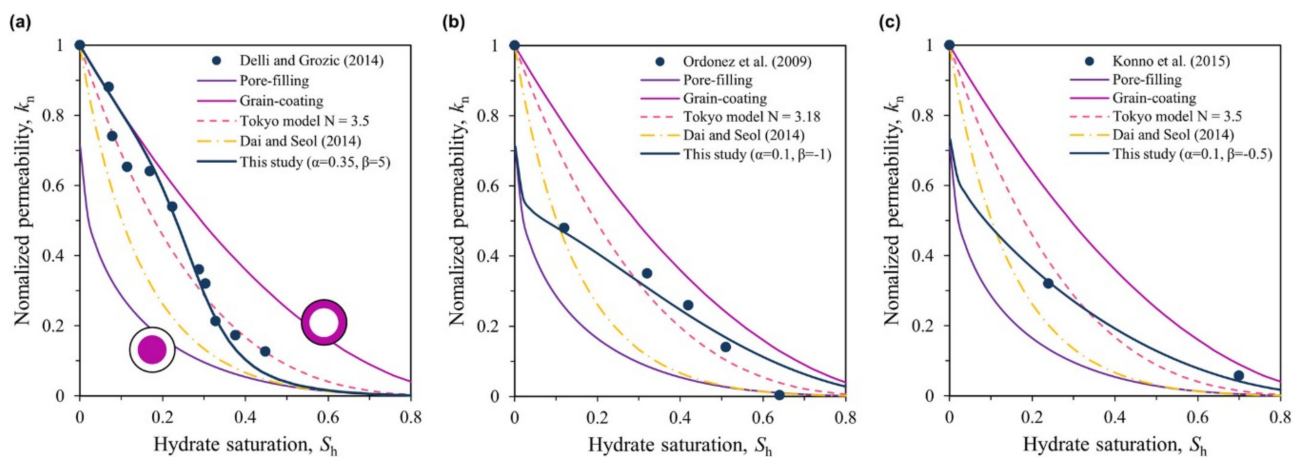


Figure 35. Permeability evolution in hydrate-bearing sediments with hydrate formed under different conditions. (a) Experimental results from excess-gas method [24]; (b) experimental results from excess-water method [112]; (c) experimental results from dissolved-gas method [114]. The adopted existing analytical models are from literatures [23,40,42]. Reprinted with permission from Ref. [68]. Copyright 2022 American Geophysical Union.

5.10. Lei et al. Stress-Dependent Permeability Model

In the process of methane gas exaction from the hydrate reservoir, the pore structure permeability will be strongly affected by the geomechanical conditions due to the change in pore pressure induced by hydrate phase transition, thus changing the seepage characteristics of HBSs. Therefore, due to insufficient research on the mechanical properties of hydrate sediments, the modeling and prediction of permeability behavior in HBSs under stress conditions are extremely difficult.

Lei et al. [71] established a new analytical model to predict the dynamic evolution behavior of stress-dependent permeability of HBSs based on the assumption that the pore structures of porous media containing hydrates are statistically self-similar fractals. This permeability model was derived by solving the steady-state Navier–Stokes equations for fluid flow in the capillary tube model with hydrate under stress conditions (Figure 36). Compared with the previous empirical and theoretical models, Lei et al. analytical model [71]

took the hydrate saturation, hydrate pore habits, retained water, and stresses (e.g., radial stress and axial stress) into account.

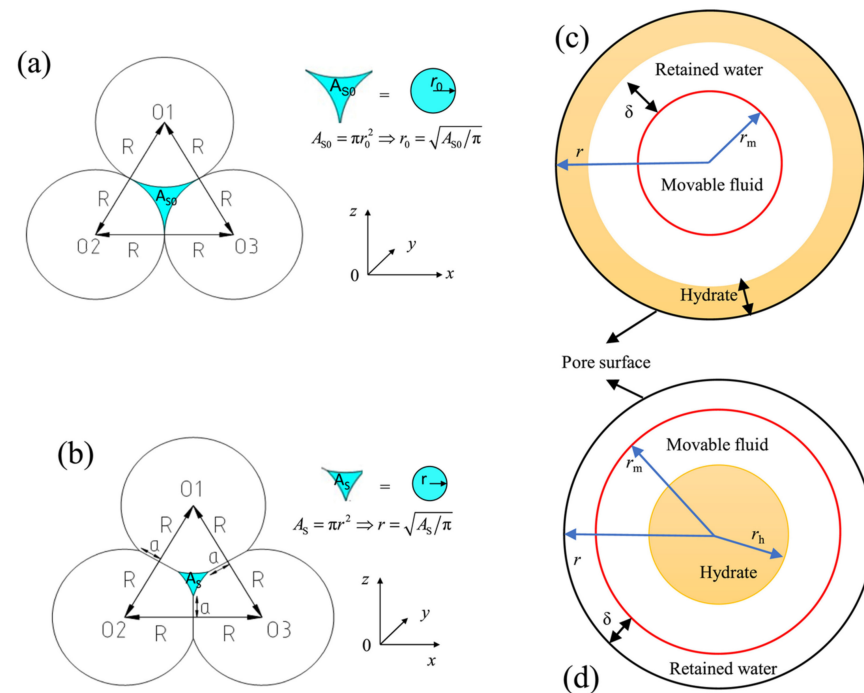


Figure 36. Schematic diagram of two hydrate pore habits in the pore under stress condition reprinted from [71] with permission from Elsevier. (a) Pore under zero stress condition; (b) pore deformation under normal stress; (c) wall-coating hydrates in the pore; (d) pore-filling hydrates in the pore.

Based on the total volumetric flow rates for hydrate-bearing porous media and Darcy's law, normalized permeability of fractal sediments with GC and PF hydrates under stress conditions are:

$$K_{n_GC} = \left\{ 1 - \frac{1 - \sqrt{1 - S_h}}{\psi} \right\}^4 \quad (69)$$

$$K_{n_PF} = 2 - \frac{2S_h}{\psi^2} - \left[1 - \frac{S_h}{\psi^2} \right]^2 \cdot \left[1 + \frac{1}{\ln\langle \psi / (\sqrt{S_h}) \rangle} \right] \quad (70)$$

$$\psi = 1 - 4 \left[\frac{3\pi(1 - \nu^2)p_{effr}}{4E} \right]^\beta \quad (71)$$

where petrophysical parameters of porous media ν are the Poisson's ratio independent S_h , while E is the elastic modulus (GPa), which is a linear function of S_h ; p_{effr} is the radius stress, MPa; β is the power law index related to the pore surface morphology.

Based on Equations (69) and (70), Lei et al. further proposed an average permeability model considering different hydrate pore habits by using the statistical average method, as shown in the following equation:

$$K_n = K_{n_PF}^\lambda K_{n_GC}^{1-\lambda} \quad (72)$$

where λ is the proportion of PF habits in all pore habits of hydrates. Figure 37 shows the relationship between dimensionless permeability (i.e., normalized permeability in this paper) and hydrate saturation of different experimental samples, as well as the stress-dependent permeability model of Lei et al. [71]. It can be seen from Figure 37 that with the increase of hydrate saturation, the parameter λ increases (i.e., the proportion of PF habit

in all pore habits of hydrate increases), that is, the pore habit of hydrate changes from GC habit to PF habit.

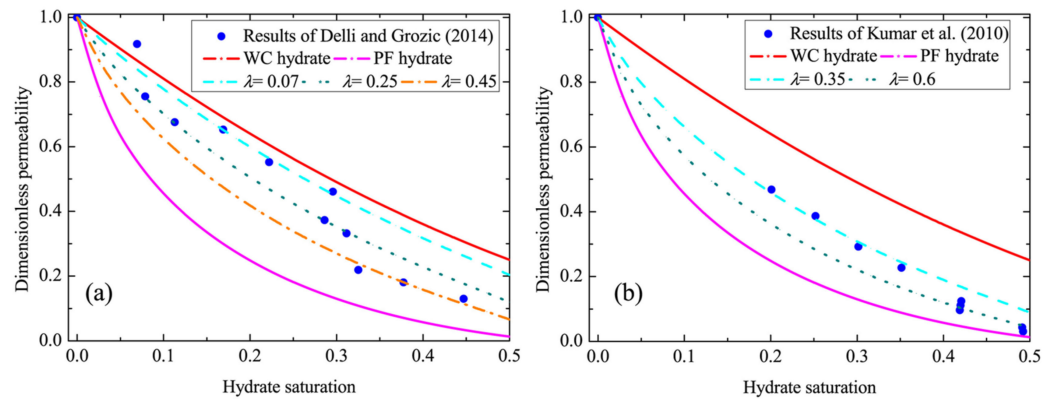


Figure 37. Dimensionless permeability varying with hydrate saturation reprinted from [71] with permission from Elsevier. (a) Experimental results of Delli and Grozic [24]; (b) experimental results from Kumar et al. [82].

5.11. Zhang et al. Stress-Dependent Permeability Model

It is well known that hydrate saturation and effective stress are the most significant factors controlling permeability evolution by changing the internal pore structure of hydrate sediments. As the permeability of fine-grained hydrate reservoirs is highly sensitive to stress [70], the permeability variations are very sensitive to the changes in pore structure available for fluid flow caused by effective stress.

In the experimental study by Zhang et al. [20], tetrahydrofuran (THF) hydrate-bearing sediments with $S_h = 0-0.6$ were synthesized using clay silty cores recovered from the Shenhu hydrate area in the South China Sea as the skeleton. Then, a series of stepwise loading and water permeability measurements were carried out on the permeability measurement system to quantitatively evaluate the effect of consolidation on the porosity and permeability of fine-grained HBSs. Furthermore, Zhang et al. proposed a modified KC equation to characterize the relationship between permeability, porosity, and effective stress in clay-silty sediments (Figure 38).

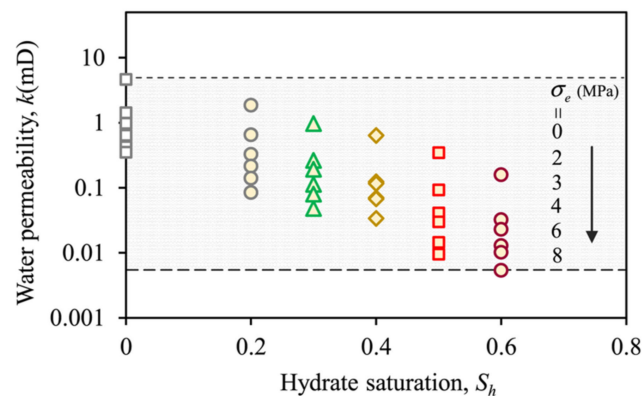


Figure 38. Measured water permeability with hydrate saturation of 0–0.6 at effective stress between 0 and 8 MPa reprinted from [20] with permission from Elsevier.

The experimental results-based empirical permeability model, describing the joint effect of effective stress and hydrate saturation on permeability, is given as follows:

$$K(S_h) = m \frac{\phi_e}{(1 - \phi_e)^{n-1}} = m \frac{\left[\phi_0(1 - S_h) - 0.05\sigma_e^{\alpha_0(1-3.12S_h^3)} \right]^n}{\left[1 - \phi_0(1 - S_h) + 0.05\sigma_e^{\alpha_0(1-3.12S_h^3)} \right]^{n-1}} \quad (73)$$

where m is the parameter characterizing the sensitivity of water permeability reduction to effective porosity reduction ($m = 5.2$ in the Zhang et al. study for clay silty sediments [20]); α_0 is the porosity stress sensitivity index of the sample without hydrate ($\alpha_0 = 0.57$ in Zhang et al. study for clay silty sediments [20]); n is an exponent that depends on the type of sediment ($n = 4$ in the Zhang et al. study for clay silty sediments [20]); σ_e is the effective stress, MPa.

The work by Zhang et al. [20] aimed to better understand the hydraulic properties of hydrate-bearing clay-silty sediments considering the effective stress and attempted to elucidate the combined effect of effective stress and hydrate saturation on permeability evolution [121]. Their findings provide a theoretical basis for the selection of permeability models during gas production modeling and accurate prediction of fluid production from fine-grained hydrate reservoirs.

5.12. Lv et al. Model

Lv et al. [69] studied the methane hydrate dissociation behaviors under different exploitation methods (depressurization, step-wise depressurization, and thermal stimulation), and analyzed the gas production behavior with the help of the NMR technique. Moreover, as shown in Figure 39, the current widely used permeability prediction models have limited accuracy because of lacking consideration of the effect of wettability of hydrate-bearing mix system on seepage behaviors (Figure 39). Compared with the other models, the Tokyo model ($N = 3$) had the best permeability prediction result for the experimental data, but the R^2 value is 0.8897, which is still not ideal.

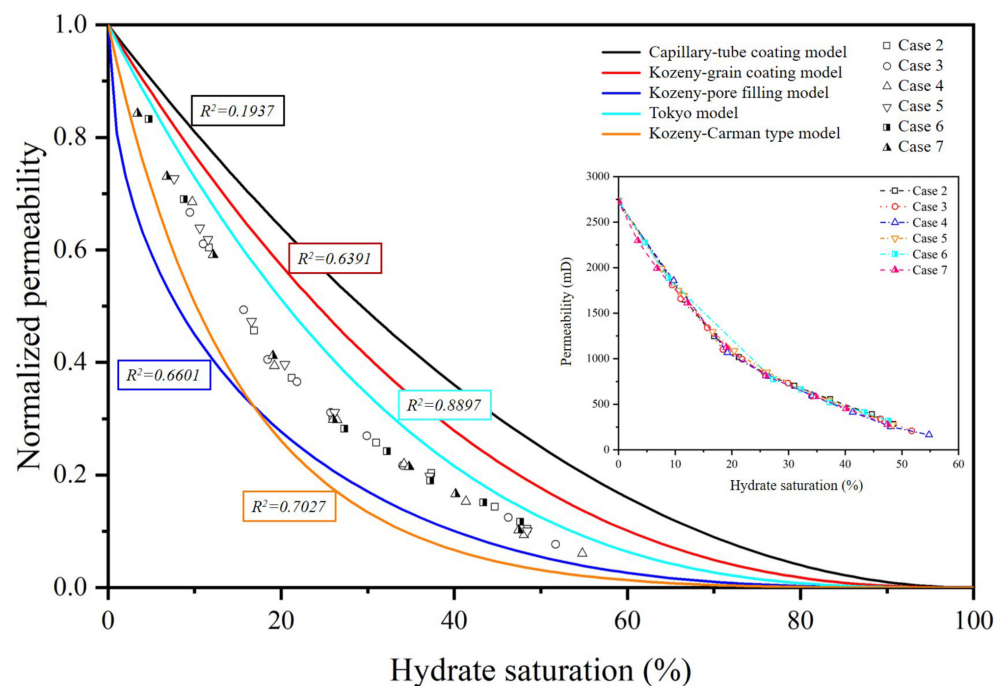


Figure 39. Comparison of normalized gas permeability between experimental results and permeability model predictions reprinted from [69] with permission from Elsevier. The adopted existing analytical models are from literatures [23,40,42].

An NMR-based approach for quantitatively characterizing the overall wettability of HBSs was proposed by Lv et al. [69] for the first time based on the theoretical basis that the average value of T_1/T_2 reflects the overall wettability of the sample [122]. In addition, a prediction model of normalized hydrophilicity (NH) of hydrate-bearing mix systems was proposed based on NMR experimental results. The equation of NH is shown as follows:

$$NH = 1 - \frac{1}{S_h^a} \quad (74)$$

where NH is the normalized hydrophilicity defined as the ratio between the average value of T_1/T_2 at a given hydrate saturation to intrinsic hydrophilicity value (average value of T_1/T_2 at initial condition $S_h = 0\%$), a is an adjustable parameter. The calculation using the NH prediction model requires the hydrate saturation to be larger than 0, while the default value of NH at $S_h = 0\%$ is 1.

As shown in Figure 40, the value of NH increases gradually with decreased hydrate saturation during the hydrate dissociation process. It should be noted that this NH prediction model assumed that the original sediment grains in hydrate-bearing porous media are more hydrophilic compared with the hydrate surface [123–125]. Therefore, the inner pore surface changes from hydrate dominant to quartz dominant, resulting in the increasing hydrophilicity of hydrate-bearing sediments with decreasing hydrate saturation.

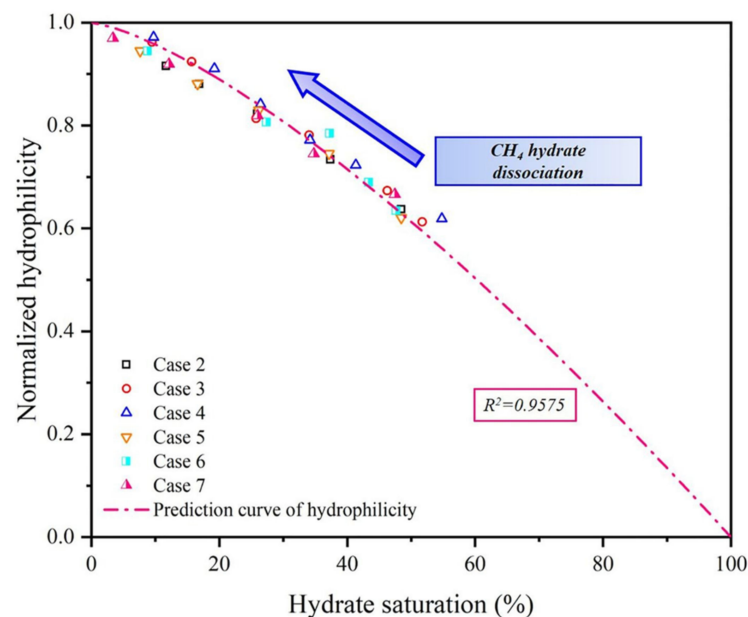


Figure 40. Normalized hydrophilicity versus hydrate saturation for different cases and prediction curve of hydrophilicity proposed in the study by Lv et al. reprinted from [69] with permission from Elsevier.

Next, based on the comparison of the goodness of fit for widely used permeability prediction models, Lv et al. further established a modified Tokyo model coupled with a wettability term for the prediction of permeability in HBSs. The equation of K_n is shown as follows:

$$K_n = (1 - S_h)^3 \times NH^b \quad (75)$$

where b is an adjustable parameter. Figure 41 presents the comparison between experimental normalized permeability data and permeability model prediction results. The results clearly showed that the prediction accuracy of the modified Tokyo model was improved significantly. Compared with the original Tokyo model, the prediction accuracy was improved by 9.75%.

The results also implied that the evolution of wettability in HBSs is crucial to the gas–water multiphase flow. Lv et al. [69] also pointed out that the fluid seepage behavior in the pore was not only governed by the hydrate pore habits but also by the wettability evolution, as shown in Figure 42.

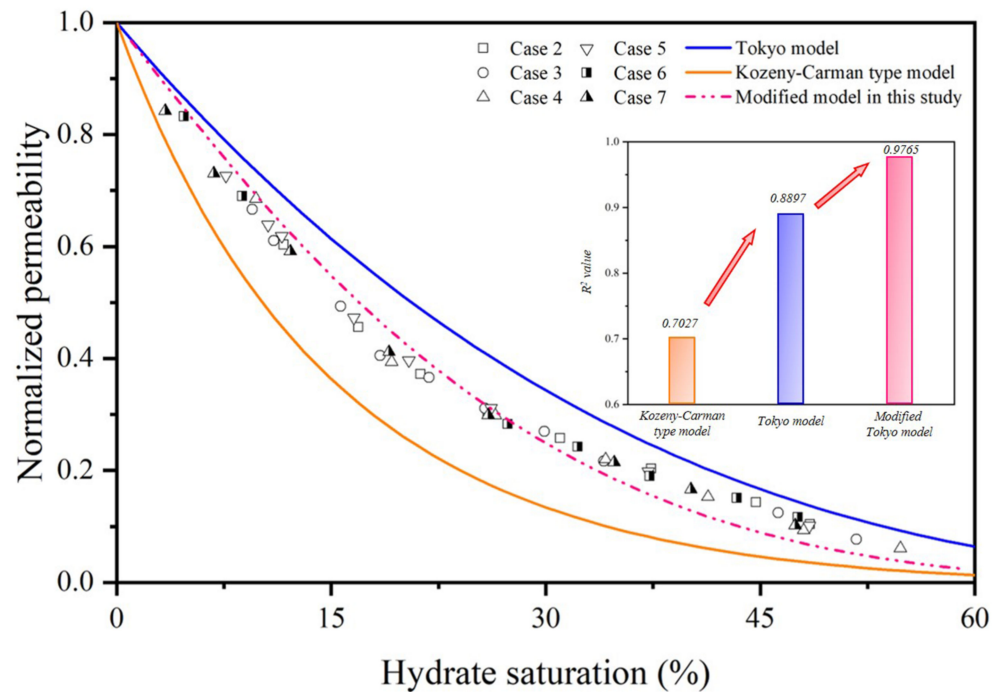


Figure 41. Comparison of normalized permeability between experimental results and permeability model predictions (The R^2 values for different models are shown in the inset) reprinted from [69] with permission from Elsevier.

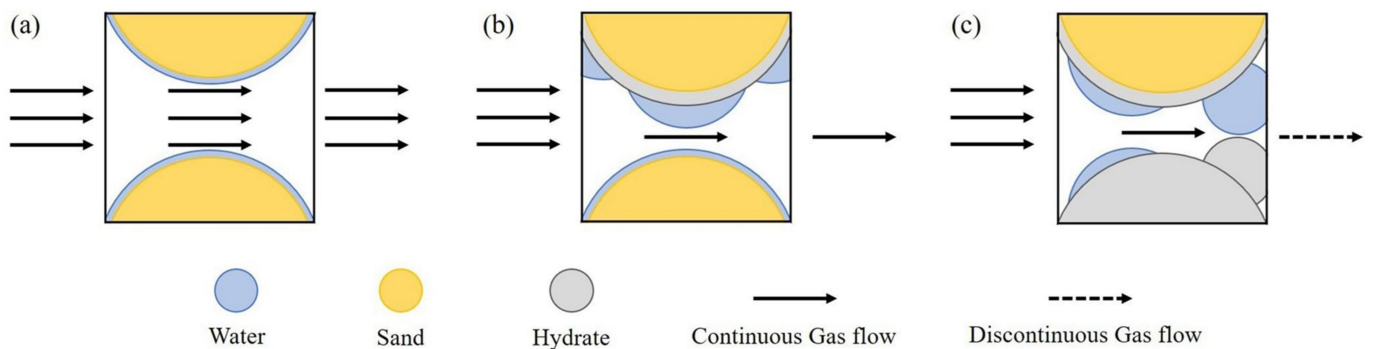


Figure 42. Schematic diagrams of the coupled influence mechanism of hydrate pore habits and wettability evolution on flow behavior in hydrate-bearing mix system reprinted from [69] with permission from Elsevier. (a) Initial stage; (b) medium S_h condition; (c) high S_h condition.

5.13. Summary

- (1) New SDR model adds one parameter to model the effect of hydrate-related interface evolution during the hydrate dissociation process on the NMR transverse surface relaxivity for closer to the actual situation and better used in engineering applications.
- (2) The established fractal theory-based permeability prediction models of HBSs that consider the interaction between hydrate formation/dissociation and pore structure in the host sediment enable one to well establish a quantitative relationship between pore-scale structure parameters and permeability. The most important aspect of using these models to predict HBS permeability is that microscale structure information

- (e.g., the maximal pore diameter and related fractal dimensions) in the porous media can be properly and precisely characterized. However, these models are all complex and many parameters cannot be accurately obtained by experiments.
- (3) The modified Corey models are proposed to capture the permeability variation behaviors with hydrate of HBSs using multiplying a linear Corey model with an exponential function of hydrate saturation or describing the index in a simple Corey model by a function with hydrate saturation as an independent variable. These types of models show good predictive performance due to the variability of fitting parameters. However, the fitting parameters do not have a clear physical meaning.
 - (4) Some permeability reduction models with novel mathematic forms and physical parameters proposed by some researchers consider the pore-scale effect of hydrates on the width and tortuosity of fluid seepage channels and the size of pore space available for fluid flow. Furthermore, these models take into different hydrate pore habits within pores account and the parameters in these models have definite physical meaning and are easy to be determined. However, there are still some assumptions and simplifications in the derivation of these models. Innovatively, the permeability theoretical model that is commonly used in coalbed methane reservoirs is introduced into the gas hydrate reservoir considering the pore space characteristics and the hydrate pore morphology, which are completely different from those assumed by PCTM and KGM.
 - (5) The hybrid permeability model based on the weighted combination of existing permeability models considers the evolution of hydrate pore habits with hydrate saturation and the dominance of hydrate pore habits within pores on the permeability change. In addition, this type of model offers an elegant expression that can be easily implemented in reservoir simulators for a more accurate estimation of gas production from hydrate reservoirs.
 - (6) The stress-dependent permeability models of HBSs capture the permeability evolution controlled by the pore structure of inner space and geomechanical behavior of hydrate reservoirs under stress conditions. However, existing models do not comprehensively consider the influence of different hydrate pore habits (e.g., grain-cementing, load-bearing hydrate, and patchy hydrates), the combined effect of particle crushing, and water-rock interactions on permeability, which are difficult to address in numerical modeling and analysis. The influence of the geomechanical behavior (considering the effects of the hydrate saturation, stress state, and hydrate pore habits) and chemical reaction between sediment and pore fluid on the permeability of fined-grained HBSs will be a new research hotspot for the permeability model of HBSs.
 - (7) The prediction accuracy of the modified Tokyo model considering the effect of wettability is better than reported permeability prediction models without consideration of the effect of the wettability and its evolution on the seepage characteristics. The evolution of wettability is crucial to impacting the gas–water two-phase flow in HBSs. In addition, the coupled influence mechanism of hydrate pore habits and wettability evolution on flow behavior at the pore scale in HBSs will be a new research hotspot and direction for the permeability model of HBSs.
 - (8) The research methods, the advantages and limitations, the using parameters and their physical meaning of various novel permeability models, and the factors that models consider are also provided. Table 7 lists the methods, advantages, and limitations of these novel permeability models of HBSs, while Table 8 summarizes the characteristics of these novel permeability models that used other theories and methods for permeability prediction of HBSs.

Table 7. Research methods, advantages, and limitations of novel permeability models for permeability prediction of HBSs.

Model	Research Methods	Advantages and Limitations
New SDR model [64]	Derived based on Kenyon relationship and NMR experiment data	Simple form and generally known, and considering the effect of hydrate-related interface evolution but needing NMR experiment data
Daigle [60]	Derived based on the pore-solid-fractal geometry with the critical path analysis method	Generally known and considering pore system properties but containing parameters that are difficult to simultaneously determine and only be suitable for disseminated hydrate within pores
Zhang et al. [61]	Derived based on fractal theory and experimental results	Simple form and containing parameters that quantify the evolution of pore space extracted from experimental results but containing a series of simplifications and empirical parameters, and only be suitable for coarse-grained HBSs
Du et al. [62]	Derived based on fractal theory and modified Hagen–Poiseuille equation	A power exponential function of structural parameters of porous media with specific physical meaning but complicated form with parameters that are difficult to determine
Chen et al. [65]	Modified Corey model based on fitting by LBM simulation	Simple form and generally known, an exponential function with only one fitting parameter with clear physical meaning
Liu et al. [66]	Modified Corey model based on fitting by LBM simulation	A simple and modified functional form effectively enhances the applicability of the simple Corey model but containing the fitting parameter without definite physical meaning and the uncertain functional relation between exponent N and hydrate saturation
Hou et al. [63]	Modified permeability-porosity relationship based on LBM simulation and geometrical analysis	Simple form and generally known, and considering the evolution of the control seepage channel with hydrate saturation, and containing fitting parameters related to physical phenomenon but containing empirical fitting parameters without definite physical meaning and may be restricted to two-dimensional porous media
Guo et al. [58]	Derived based on Poiseuille’s law and three-dimension hydraulic radius	Simple form and considering the evolution of pore size with hydrate saturation, and containing only one embedded parameter with clear physical meaning, but the accuracy may be slightly lower due to the embedded parameter assumed to be a constant parameter

Table 7. Cont.

Model	Research Methods	Advantages and Limitations
Lei et al. [72]	Derived based on the cubic fracture-permeability model commonly used in coalbed methane reservoir	Considering the novel type assumed pore space characteristics and hydrate pore morphology but piecewise function with complicated form and relatively rough prediction accuracy
Delli and Grozic [24,67]	A hybrid model based on the weighted combination of the KG model with two different pore habits in sediment	Generally known and considering hybrid hydrates pore habits but containing empirical parameters and complicated calculations
Wang et al. [68]	A pore-morphology-weighted model based on a two-parameter logistic function and grain-coating and pore-filling PCT model	Theoretical and elegant expression with two fitting parameters with clear physical meaning, considering coexisting hydrate pore habits and their evolution with ensued hydrate crystallization but containing complicated calculations
Lei et al. [71]	Derived by solving the steady-state Navier–Stokes equations in a fractal capillary tube with hydrate under stress condition	Comprehensively considering the effect of radial stress and coexisting hydrate pore habits on the permeability evolution in HBSs under different hydrate saturations, but complex form with empirical parameters, and neglecting the thickness of retained water film and deformation of hydrates
Zhang et al. [20]	Modified KC model based on step-by-step stress loading and water permeability tests and curve fitting method	Considering the combined influence of effective stress and hydrate saturation on hydraulic properties and porosity of fined-grained HBSs but complex form and containing empirical parameters
Lv et al. [69]	Modified Tokyo model coupled with wettability term based on NMR measurement	Simple form and considering the influence mechanism of wettability evolution on flow behavior but containing fitting parameters and neglecting coexisting hydrate pore habits

Table 8. Characteristics of novel permeability models for permeability prediction of HBSs.

Model	Parameters	Physical Meaning	Influencing Factors
New SDR model [64]	ρ_2^*	✓	Hydrate saturation and interface evolution; the effect weight and surface proportion of quartzitic sand phase
	T_{2LM}	✓	
Daigle [60]	β	✓	Hydrate saturation, pore disseminated hydrates; pore structure fractal characteristics, and percolation threshold
	ϕ_0	✓	
	p_c	✓	
	D	✓	
	S_x	✓	
	S_w	✓	

Table 8. Cont.

Model	Parameters	Physical Meaning	Influencing Factors
Zhang et al. [61]	$D_{T,0}$	✓	Hydrate saturation; pore structure fractal characteristics and maximal pore diameter
	$\lambda_{\max 2}^*$	✓	
	a	×	
	b	×	
	ϕ_0	✓	
Du et al. [62]	ϕ	✓	Hydrate saturation and coexistence of pore-filling and grain-coating hydrate; pore structure fractal characteristics, maximal pore diameter, and porosity of sediment without and with hydrates
	$D_{t,h}$	✓	
	D_t	✓	
	$D_{f,h}$	✓	
	D_f	✓	
	D_E	✓	
	$\lambda_{\max,0}$	✓	
	$\lambda_{\min,0}$	✓	
Chen et al. [65]	C	✓	Hydrate saturation; the degree of crystal coarsening and patch size in a multiphase system
Liu et al. [66]	a	×	Hydrate saturation
Hou et al. [63]	b	×	Hydrate saturation, pore habits, and morphology; the intrinsic porosity of sediment and the size and tortuosity of the control seepage channel
	d	×	
Guo et al. [58]	e_t	✓	Hydrate saturation and pore habits; the change in pore volumes of sediment
Lei et al. [72]	ϕ_0	✓	Hydrate saturation, pore habits, and morphology; the pore structure and intrinsic porosity of sediment
Delli and Grozic [24,67]	N	×	Hydrate saturation and coexisting pore habits
	M	×	
Wang et al. [68]	α	✓	Hydrate saturation and coexisting pore habits; hydrate formation conditions and sediments types
	β	✓	
Lei et al. [71]	ν	✓	Hydrate saturation and single or coexisting pore habits; retained water, effective stress, deformation of grains, and pore structure of sediment
	E	✓	
	P_{effr}	✓	
	β	✓	
Zhang et al. [20]	ϕ_0	✓	Hydrate saturation; effective stress, porosity, and host sediment types
	σ_e	✓	
	α_0	✓	
	n	×	
	m	×	
Lv et al. [69]	a	×	Hydrate saturation; hydrophilicity of HBSs
	NH	✓	
	b	×	

6. Conclusions

This paper presents the various permeability models of HBSs and summarizes the characteristics of various models in detail. The conclusions are briefly reviewed below:

- (1) The SDR model can be used for engineering applications to evaluate the permeability field data of NGH reservoirs in the presence of NMR data. PCTM and KGM were introduced into the research of HBS permeability and implemented for numerical simulations of gas production and provided a theoretical fundamental basis for

other permeability models because of their simplicity and capability of capturing the main pore structure characteristic in sediments and two typical hydrate pore habits. They can well describe the general reduction trend of the permeability with increased hydrate saturation. However, the analytical expressions of PCTM and KGM are oversimplified, which is too idealistic and far from actual HBSs due to the idealized inner structure of pore space and growth habits and morphology of hydrate.

- (2) The reservoir simulator used models took hydrate saturation into account but cannot capture the effect of hydrate pore habits on permeability. In addition, the determination of empirical parameters lacks a sound physical basis, and their values vary with the properties of HBSs. The inherent power law fitting characteristic of the Tokyo model makes good fitness by adjusting the value of parameter N . The Tokyo model is widely used in numerical modeling of gas production from hydrate reservoirs. The influence of pore structure characteristics and hydrate heterogeneous distribution on the value of the exponent N will be a new research hotspot.
- (3) The modified permeability models of HBSs based on the KC equation were mainly established in two ways: adding the fitting parameter or the polynomial, which comprehensively considers the relationship between hydrate saturation and pore structure properties based on numerical simulation results, or by strict mathematical deduction of new expressions of S_h and the ratio of internal surface area $A_0/A(S_h)$ based on series assumptions about sediment particles packing patterns. Some modified permeability models consisted of parameters with specific physical meaning to better explain the effect of hydrate on the characteristic of pore structure and the variation of permeability. The influences of hydrates (considering the effect factors such as the hydrate saturation, pore habits, and inhomogeneous distribution) on the pore structure characteristics (e.g., porosity, pore-throat size, tortuosity, pore connectivity) of hydrate sediments will be a new research hotspot.
- (4) Many novel permeability models of HBSs have been developed based on new theories and research methods investigating the effect of other hydrate- or sediment-related factors on the fluid flow and the permeability evolution. The fractal theory-based permeability model of HBSs considering the interaction between hydrate pore habits and pore structure in the host sediment enables to well establish a quantitative relationship between microstructure parameters and permeability. The modified Corey models show good predictive performance due to the variability of fitting parameters, but the fitting parameters do not have a definite physical meaning. Some permeability models with novel mathematic forms and novel physical concepts proposed by some researchers consider the effect of hydrates on the evolution of the main seepage channel and pore space size. The hybrid permeability model of HBSs considers the evolution of hydrate pore habits with hydrate saturation and the dominance of hydrate pore habits within pores on the permeability evolution.
- (5) The stress-dependent permeability models of HBSs capture the permeability evolution induced by the pore structure change of hydrate reservoirs under stress conditions. The influence of the geomechanical behavior and chemical reaction between sediment and pore fluid on the permeability of fined-grained HBSs will be a new research hotspot. In addition, wettability is crucial to influencing the multiphase flow in hydrate sediments. The coupled influence mechanism of hydrate pore habits and wettability evolution on seepage characteristics at the pore scale in HBSs will be a new research hotspot and direction.

7. Challenges and Suggestions of Future Research Directions

There are still many challenges and limitations in these models for elaborating the mechanisms of influencing factors on HBS permeability because of some idealized assumptions.

These idealized models assume [10]: (1) hydrates are evenly distributed in the pores with one or two pore habits, (2) hydrates are with isotropic surface tension, (3) the contact angles between hydrate and pore surfaces are 0° or 180° , that is, grain-coating or tube-

wall coating hydrate pore habit implicitly assumes that the grain or tube wall surface is completely hydrate-philic, while the pore-filling pore habit assumes that surface is completely hydrate-phobic, as shown in Figure 1, and (4) the pore size distribution (PSD) in sediment is uniform.

However, the following characteristics exist in natural hydrate sediments: (1) hydrate distribution in pores is heterogeneous, (2) hydrate with anisotropic surface tension, and (3) the contact angle between hydrate and the pore surface varies between 0° and 180° depending on the pressure-temperature condition, hydrate former and contacting phase as liquid or gas, and (4) pore size distribution (PSD) in sediment is non-uniform.

In addition, there are four main challenges in existing permeability models:

- (1) At present, most of the research on seepage theory in hydrate-bearing porous media still uses Darcy's law for reference. Most of the existing permeability models contain fitting parameters or make ideal assumptions in terms of sediment pore structure and hydrate pore habits, which have great limitations in practical applications. However, there is still no universally accepted general form to reflect the permeability reduction trend in HBSs even ignoring more complex aspects (e.g., heterogeneity, actual hydrate morphology, and so on). In addition, the exponent N of the widely used Tokyo model has a large variation range and still lacks a sound physical basis, and cannot be estimated based on easily measured parameters in HBSs [44].
- (2) Most of the empirical parameters used in the widely used permeability models are mainly derived from experimental data fitting in the limited hydrate saturation range. These fitting parameters are only applicable to specific conditions and the permeability prediction results are usually not universally representative of their participation. Moreover, due to the lack of enough experimental data, an appropriate selection of empirical constant values in some permeability models is not available for HBSs [126].
- (3) The existing permeability models almost ignore the analysis of some pore-scale influencing factors such as pore geometries, heterogeneous distribution of hydrates and sediment particles, capillarity, wettability, and so on [53,60,63], leading to inevitable discrepancies between hypotheses in theoretical models and reality in actual sediments.
- (4) None of these permeability models capture the common existing issue that permeability decreases to 0 before hydrate saturation reaches 100% [60]. This is inconsistent with the concepts of percolation threshold or irreducible saturation in natural porous media. Therefore, a physically realistic permeability model should be proposed for HBSs. With the above-mentioned issue, existing models for permeability prediction could not capture the intrinsic fluid flow and transport process in the pore of the natural host sediment.

Natural gas hydrates, as a promising strategic resource, need further exploitation and development [127]. To bridge the gap between hypothesis and reality and make the theoretical model closer to the actual situation, future research should start from the following aspects: anisotropy and heterogeneity of HBSs, hydrate pore habits and morphology, pore characteristics of sediments, fine-grained HBSs, embedded parameter in the model and multi-field coupling seepage characteristics.

7.1. Anisotropy and Heterogeneity of HBSs

The anisotropy and heterogeneity of HBSs are common characteristics in gas hydrate reservoirs [34]. The complicated pore structures of actual sediments make inherent flow characteristics complex and elusive. The nucleation and growth of gas hydrates in the pore show great randomness [32,34], leading to the uniform distribution of hydrates within pore space, as shown in Figure 43. The intrinsic anisotropy and heterogeneity exist in the distribution of hydrate in natural sediments, such as patchy in aged coarse-grained HBSs, or lenses/chunks in fine-grained HBSs [10,40]. It has been neglected for a long time that the distribution characteristics of hydrate in the pore may have more influence on the permeability evolution than its pore habit. Both inhomogeneously distributed sediment

particles and hydrate particles could result in scattered permeability measurements and unexpected predictions [39]. For example, this anisotropy and heterogeneity can result in a very large discrepancy in measured permeability, which can even reach several orders of magnitude [10,27], as shown in Figure 44. This indicates that multiple permeability models are needed to describe permeability evolution over the entire hydrate saturation range.

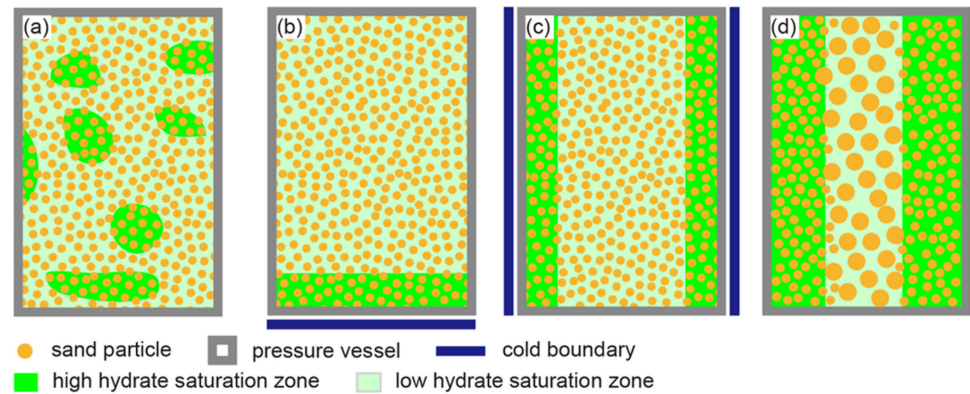


Figure 43. Several potential cases of heterogeneous hydrate distribution during upscaling process reprinted from [39] with permission from Elsevier. (a) Typical patchy distribution; (b,c) heterogeneous hydrate distribution due to water migration towards the cold boundary during hydrate formation; (d) heterogeneous hydrate distribution in layered systems.

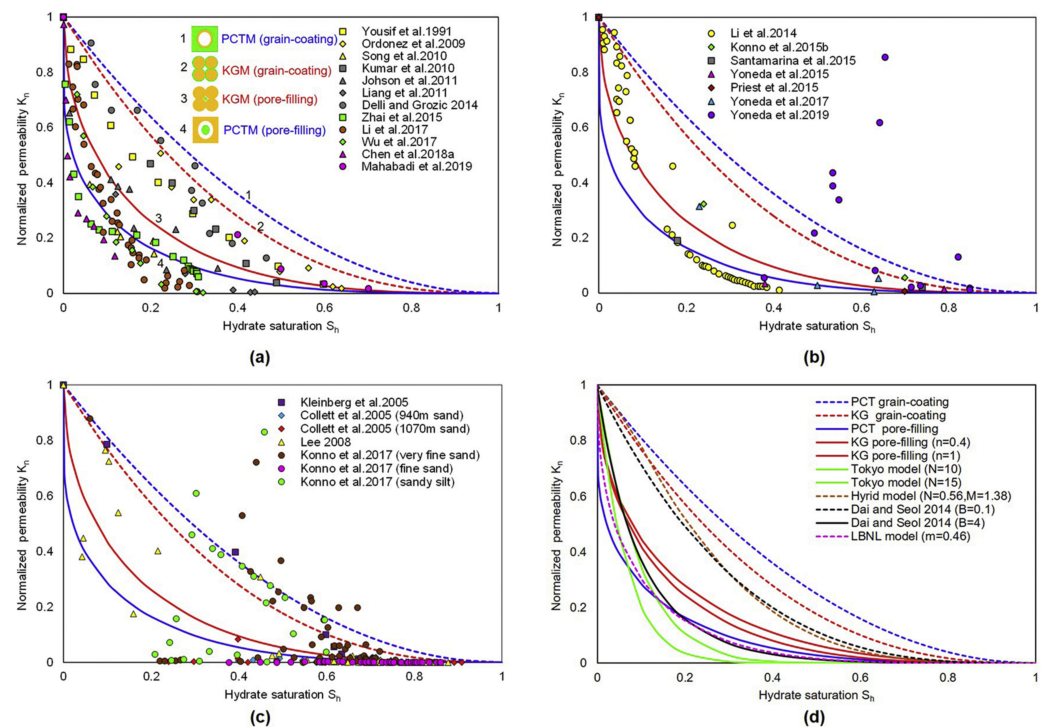


Figure 44. The relationship between normalized permeability and hydrate saturation reprinted from [10] with permission from Elsevier. (a) Data from laboratory synthesized specimens [24,27,55,82,89,95,111,112,128–131]; (b) data from pressure-core samples [97,114,132–136]; (c) data obtained from well log analysis [11,90,94,137]; (d) data obtained from existing widely used models in the literatures [23,24,40,42,48].

Recently, existing research has adopted homogenous assumptions of porous media in the flow tests and microscale numerical simulations [25,29,123,138]. In addition, most of the existing permeability models, especially the simplified theoretical models [23], assume

a homogeneous distribution of sediment particles and hydrates in pore space, which is different from the actual microstructure of gas hydrate reservoirs, and further adopt the parallel capillary theory, Kozeny–Carman equation and Darcy’s law to facilitate the theoretical derivation of the analytical expression of permeability. As Dai and Seol [40] suggested, although these models are easy to implement for numerical simulators of gas production from NGH reservoirs, they fail to capture the anisotropy and heterogeneity of natural HBSs since the distribution of sediment particles and hydrates is assumed to be homogeneous. Also, the previous discussion in the study by Pan et al. [39] suggested that pore connectivity controlled by overall hydrate distribution in pore space would be crucial for permeability evolution compared to the hydrate pore habits. They also discussed the distribution of permeability results in different hydrate saturation-normalized permeability zones (Figure 45) with respect to the inhomogeneous hydrates distribution (Figure 43) during the scaling process.

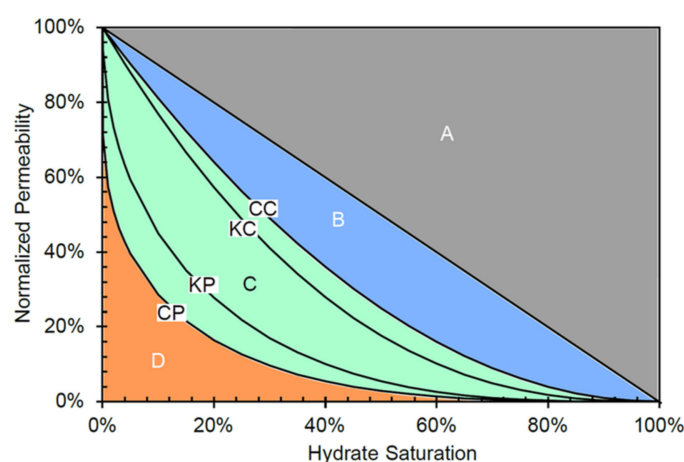


Figure 45. Several zones in the hydrate saturation-normalized permeability space reprinted from [39] with permission from Elsevier.

The complicated pore structures of sediment make inherent seepage characteristics elusive. In view of the vital role of anisotropy and heterogeneity in sediments, the microscopic pore structures and multi-scale hydrate distribution characteristics should be considered in permeability models to improve the prediction accuracy. Therefore, CT and NMR technology are necessary to visualize and measure the pore structures of hydrate reservoirs. Moreover, CT imaging can help capture 3D distributions of hydrate in pore space, and PNM enable to consider anisotropy of pore structure in porous media, more efforts should be made to use these two methods or their combination to study the effects of anisotropy and heterogeneity of HBSs on permeability evolution (some attempts have been made by Yang et al. [32] and Hu et al. [139]). The findings from these investigations will aid in a basic understanding of gas and water flow in hydrate-bearing sediments at the micro, meso, and macro scales, and in effectively evaluating how natural anisotropy and heterogeneity characteristics of hydrate reservoirs can affect gas production behavior. However, more efforts are still needed to modify existing widely used permeability models to add terms that consider anisotropy and heterogeneity, or to establish a new form of a theoretical model to better apply to field-scale gas production simulations.

7.2. Pore Habits and Morphology of Hydrate

It is known that the grain-coating and pore-filling hydrate are two typical pore habits that are usually considered in existing permeability models. On the one hand, natural HBSs include but are not limited to these two pore habits [10,103], as shown in Figure 46. Although grain-coating and pore-filling are two typical and valuable pore habits in the permeability study of hydrate sediments, it does not mean the existence of hydrates with other pore habits in natural sediments can be ignored. On the other hand, the

permeability model of HBSs suitable for different hydrate formation conditions needs careful consideration. Meanwhile, the difference between the idealized conceptual model of hydrate morphology and the actual shape of hydrates in natural HBSs may cause discrepancies in predictions and measurements. Actual and natural hydrate morphology presents some level of variability, such as lenses, nodules, chunks, veins, etc. [140]. Different shapes represent different roughness and specific surface area, which may affect wettability and capillarity, further influencing the flow characteristics at the pore scale. Additionally, the single hydrate pore habit exists only in a few extreme cases while the coexisting hydrate habits prevail in most cases [67,68], as shown in Figure 34. Hence, it is necessary to develop more physically reliable conceptual models to accurately describe the single or co-existing pore habits, morphology evolution, and distribution characteristics of hydrates in sediment pores, and to use these models to establish advanced permeability models and accurately predict gas production.

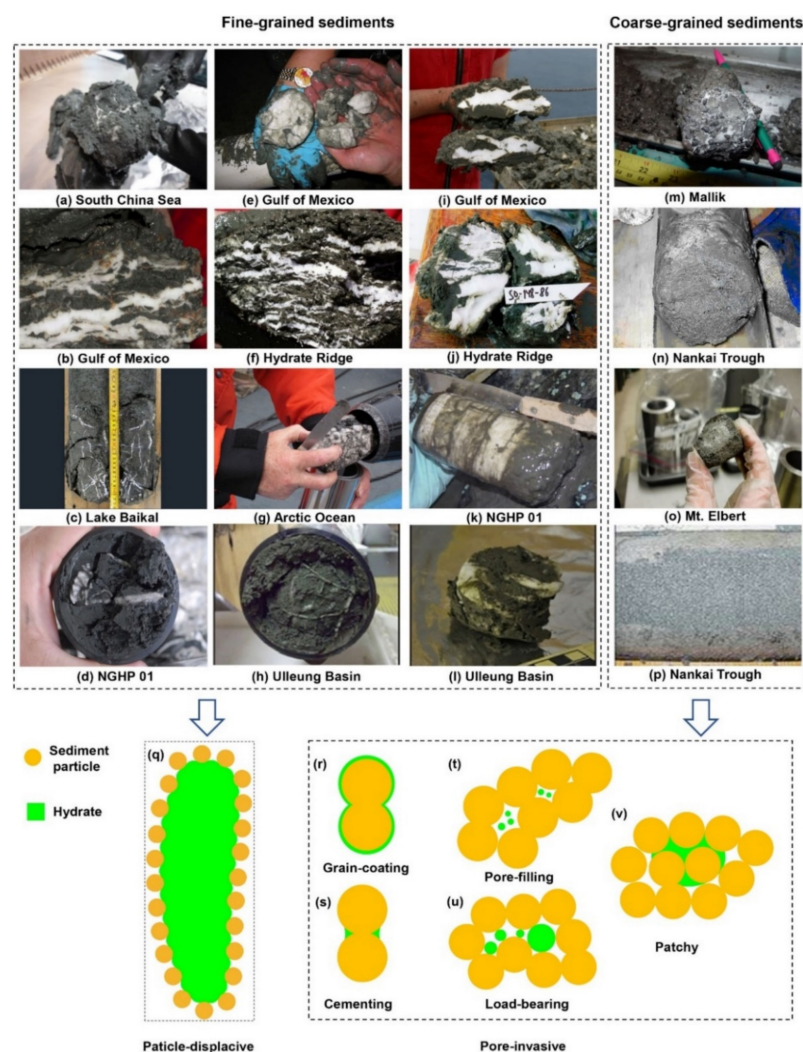


Figure 46. Core-scale hydrate morphology in hydrate samples from different geological settings and conceptual pore habits reprinted from [10] with permission from Elsevier. (a–l) Particle-displacive hydrate in fine-grained sediments (in white) shown as veins, lenses, and nodules; (m–p) coarse-grained sediments where hydrate is distributed in pores therefore not readily visible; (q) the formation of hydrate displaces surrounding sediment particles; (r–u) conceptual pore habits for hydrate in coarse-grained sediments: grain-coating, pore-filling, cementing and load-bearing; (v) hydrate distribution in the pore network may not be homogeneous but is likely to be locally concentrated and form patches.

7.3. Pore Characteristics of Sediments

It is well known that pore characteristics (e.g., pore-throat size, pore geometry, pore connectivity) play a significant role in the permeability of porous media. Since flow tests cannot capture the pore characteristics, it is necessary to combine the flow tests with other pore-scale visualization techniques such as CT [39,103,116] to study the effect of hydrate growth and/or dissociation on pore characteristics, and then on the permeability evolution of HBSs. Most of the existing models for permeability prediction lack quantitative descriptions of the evolution of pore space for fluid flow with varying hydrate saturation. More specific pore space characteristics need to be fully measured by indirect imaging techniques or direct methods, providing complete microstructure information to study seepage characteristics in HBSs. In addition, the sediment particles were assumed to be round or idealized in the most theoretical permeability models [10,23,26,54–56,58,72], though the natural sediment grains exhibit varying shapes. The category and shape of particles also determine their hydrophilicity and hydrophobicity [125]. The idealized shape simplifies the simulation and calculation process and ignores its effect on the permeability of HBSs, as well as a wide variety of measured permeability results [27,39].

7.4. Fine-Grained Sediments

Coarse-grained HBSs are more suitable for potential and commercial gas production due to relatively high hydrate saturation, high permeability, non-displacive pore habit, and small skeleton volume shrinkage during hydrate dissociation [55,141,142]. Therefore, existing investigations have mainly focused on coarse-grained sediments. However, over 90% of the sediments worldwide are fine-grained sediment [143] and exhibit particle-displacive pore habits [10], as shown in Figure 46.

In recent times, most laboratory flow tests have been performed on coarse-grained sediments, but only very few flow tests have been conducted for the fine-grained host sediments [30,31,144–146]. Therefore, due to the lack of reliable experimental permeability data, it is difficult to determine whether the existing permeability prediction models in the literature are suitable for fine-grained sediments or not. It should be noted that at a theoretical level, there is no difference in the derivation process of the permeability model for both coarse- and fine-grained sediments [58]. However, the variation trend of permeability may be different from that of coarse-grained sediments, because of the difference in lithology (argillaceous siltstone, silty mudstone), smaller pore sizes, and stronger capillary actions, and other unique characteristics of fine-grained sediments [10]. For instance, in the process of hydrate dissociation in fine-grained sediments, clay swelling caused by the bound water will lead to a reduction of permeability, which is contrary to the changing trend of permeability in coarse-grained sediments [31]. Moreover, the permeability increased during hydrate formation probably due to the influence of blockage of hydrates and the increase of pores in interaggregate zones [20].

In addition, due to the different mechanical strengths of different porous media skeletons, the strong stress sensitivity of formed fine-grained hydrate-bearing samples in the laboratory should be different. The effective stress generated during the hydrate phase transition will cause the change of pore structure (such as pore radius) of fine-grained HBSs and then affect the permeability. At present, there are few studies on the relationship between permeability and effective stress of HBSs [20,146]. It is urgent to establish a comprehensive permeability-stress model of HBSs to guide subsequent research.

Field evidence shows that hydrate displaces grains in fine-grained sediments and forms segregated lenses, veins, and nodules as particle-displacive type [10,147]. Additionally, previous laboratory studies have shown that hydrates can form in fractures in fine-grained sediments, where they inherit the morphology of fractures [141]. The latest micro-CT experimental study [148] showed that the occurrence patterns of hydrate in fractured hydrate reservoirs consist of contiguous-sheet, clustered, and isolated, which are slightly different from those of porous hydrate reservoirs (i.e., coarse-grained sediments). Moreover, the contiguous-sheet hydrate is the main morphology that determines

the seepage characteristics of fractured hydrate-bearing sediments. The distribution of fracture-filling hydrate at the pore scale is of great significance [10,141,147], which provides a theoretical basis for investigating the seepage capacity and permeability variation of fine-grained hydrate-bearing sediments by experiment [148] or numerical simulation [149].

In summary, there is still an inadequate understanding of the permeability characteristics of fine-grained HBSs. Therefore, to establish a permeability model suitable for fine-grained sediments, future studies need more laboratory experiments and numerical modeling to provide mechanism understanding.

7.5. Embedded Parameters in the Model

Reported theoretical models in previous studies that relate permeability to hydrate saturation are usually embedded with parameters whose physical meaning is not clear or difficult to determine, as well as the complicated analytical expression forms, which limits their application in numerical simulations and practices. Permeability of HBSs depends on several parameters: hydrate saturation, hydrate morphology, hydrate pore habits, hydrate reformation and dissociation during flow tests, lithology (e.g., mineral, sediments particle size), anisotropy, and heterogeneity of HBSs, effective stress, pore characteristics (e.g., pore/throat size, pore size distribution), wettability, interfacial tension and so on [10,140,147]. Although each of the factors mentioned above has been studied to a greater or less extent, the sensitivity of all the factors to the HBS permeability has not been analyzed yet. A theoretical model that predicts permeability with a simple form and physically sound parameters needs to be developed urgently based on the sensitivity analysis for the degree of effect of the above factors on permeability evolution.

As known, the Tokyo model [42,43], with a parameter of reduction exponent N , is widely used in numerical investigations. This model is simple, has only one parameter, and is easy to conduct fitting of permeability data. However, the value of N varies greatly with the nature of HBSs, such as sediments types and pore habits [10,40]. Determining the value of exponent N remains a challenge due to the lack of a reliable physical basis and estimation equations [40]. Three probable ways of dealing with this challenge are suggested [10]: (1) Theoretical analysis. Mathematical models should be derived based on the seepage theory of porous media to lay a good physical foundation for the study of N ; (2) Laboratory experiments. The effecting factors of N should be studied, and N should be estimated with easily measured parameters in HBSs; (3) Data statistical analysis. An alternative approach is to obtain and compile a large number of relevant data sets to discuss the clear physical meaning of the value of N based on big data and machine learning techniques.

In summary, classical permeability models were usually divided into different forms because of hydrate pore habits. Some general or modified forms were also proposed to cover different situations. However, there exist limitations, some embedded parameters in models lack a sound physical foundation and relationship with other easily measured parameters of HBSs. In addition, some new models were proposed based on new theories and assumptions. However, none of them underwent extensive and comprehensive verifications by further experiments and field tests.

7.6. Multi-Field Coupling Seepage Characteristics

No matter which exploitation method is adopted, the hydrate production process involves four coupling physical processes: heat transfer (T), multiphase seepage (H), formation deformation (M), and hydrate phase transformation (C) [7–10]. The seepage characteristics of hydrate reservoirs are the key to hydrate development research. However, the fluid seepage in hydrate sediments, influenced by many factors such as phase transition, heat transfer, and reservoir stability, is a complex multi-field coupled process. The effects of the thermal-mechanical-chemical (TMC) multi-field coupling process on seepage characteristics during the exploitation of natural gas hydrate are as follows:

- (1) Due to the decomposition of solid hydrate into liquid water and methane gas, the pore structure available for fluid flow in the sediment changes, which affects the porosity, fluid flow behavior, and permeability of the seepage field.
- (2) The decrease in temperature will even lead to the reformation of hydrate or the formation of ice, which will block the pores and greatly affect the seepage capacity of the reservoir.
- (3) The formation/decomposition of hydrate increases/decreases the cementation and support effect of hydrate on sediments, and sand migration and even formation deformation may occur, which affects the mechanical properties of the reservoir and leads to changes in pressure, porosity, and permeability of the seepage field.

Thus, hydrate exploitation is a very complex multi-field coupling fluid seepage process.

Advanced permeability models are very important for the dynamic prediction and analysis of long-term gas production simulation in hydrate reservoirs. However, the permeability models proposed recently do not comprehensively consider the effects of heat and mass transfer, and sediment deformation during the hydrate decomposition process, and only focus on the dynamic permeability change of the single-phase flow of the seepage field. Therefore, in the HBS permeability study, experiments or numerical simulations should be used to further explore the influence mechanism of the TMC process on fluid flow and permeability changes in hydrate-bearing sediments, and to establish a more advanced and comprehensive permeability model for macroscopic gas production modeling.

This paper provides guidance and constructive suggestions for the construction of new permeability models and the numerical simulation of the gas production from hydrate reservoirs during hydrate exploitation, and it will be a useful tool for researchers and practitioners to simulate and evaluate the physical properties of HBSs both on the laboratory and field scales.

Author Contributions: Writing—review and editing, J.X.; writing—original draft preparation, Z.B.; supervision, H.L.; formal analysis, X.W. and S.L.; funding acquisition, H.L. All authors have read and agreed to the published version of the manuscript.

Funding: This work was funded by the National Natural Science Foundation of China (51991365).

Institutional Review Board Statement: Not applicable.

Informed Consent Statement: Not applicable.

Data Availability Statement: Not applicable.

Conflicts of Interest: The authors declare no conflict of interest. The funders had no role in the design of the study; in the collection, analyses, or interpretation of data; in the writing of the manuscript, or in the decision to publish the results.

References

1. Sloan, E.D. Fundamental principles and applications of natural gas hydrates. *Nature* **2003**, *426*, 353–359. [[CrossRef](#)] [[PubMed](#)]
2. Song, Y.; Cheng, C.; Zhao, J.; Zhu, Z.; Liu, W.; Yang, M.; Xue, K. Evaluation of gas production from methane hydrates using depressurization, thermal stimulation and combined methods. *Appl. Energy* **2015**, *145*, 265–277. [[CrossRef](#)]
3. Kvenvolden, K.A. Gas hydrates—geological perspective and global change. *Rev. Geophys.* **1993**, *31*, 173–187. [[CrossRef](#)]
4. Yin, Z.; Linga, P. Methane hydrates: A future clean energy resource. *Chin. J. Chem. Eng.* **2019**, *27*, 2026–2036. [[CrossRef](#)]
5. Makogon, Y.F.; Holditch, S.; Makogon, T.Y. Natural gas-hydrates—A potential energy source for the 21st Century. *J. Pet. Sci. Eng.* **2007**, *56*, 14–31. [[CrossRef](#)]
6. Boswell, R.; Collett, T.S. Current perspectives on gas hydrate resources. *Energy Environ. Sci.* **2011**, *4*, 1206–1215. [[CrossRef](#)]
7. Liu, L.; Zhang, Z.; Li, C.; Ning, F.; Liu, C.; Wu, N.; Cai, J. Hydrate growth in quartzitic sands and implication of pore fractal characteristics to hydraulic, mechanical, and electrical properties of hydrate-bearing sediments. *J. Nat. Gas Sci. Eng.* **2020**, *75*, 103109. [[CrossRef](#)]
8. Wu, P.; Li, Y.; Liu, W.; Liu, Y.; Wang, D.; Song, Y. Microstructure evolution of hydrate-bearing sands during thermal dissociation and ensued impacts on the mechanical and seepage characteristics. *J. Geophys. Res. Solid Earth* **2020**, *125*, e2019JB019103. [[CrossRef](#)]
9. Wang, L.; Zhao, J.; Sun, X.; Wu, P.; Shen, S.; Liu, T.; Li, Y. Comprehensive review of geomechanical constitutive models of gas hydrate-bearing sediments. *J. Nat. Gas Sci. Eng.* **2021**, *88*, 103755. [[CrossRef](#)]
10. Ren, X.; Guo, Z.; Ning, F.; Ma, S. Permeability of hydrate-bearing sediments. *Earth Sci. Rev.* **2020**, *202*, 103100. [[CrossRef](#)]

11. Konno, Y.; Fujii, T.; Sato, A.; Akamine, K.; Naiki, M.; Masuda, Y.; Yamamoto, K.; Nagao, J. Key findings of the world's first offshore methane hydrate production test off the coast of Japan: Toward future commercial production. *Energy Fuels* **2017**, *31*, 2607–2616. [[CrossRef](#)]
12. Yamamoto, K.; Wang, X.-X.; Tamaki, M.; Suzuki, K. The second offshore production of methane hydrate in the Nankai Trough and gas production behavior from a heterogeneous methane hydrate reservoir. *RSC Adv.* **2019**, *9*, 25987–26013. [[CrossRef](#)] [[PubMed](#)]
13. Chen, L.; Feng, Y.; Okajima, J.; Komiya, A.; Maruyama, S. Production behavior and numerical analysis for 2017 methane hydrate extraction test of Shenhu, South China Sea. *J. Nat. Gas Sci. Eng.* **2018**, *53*, 55–66. [[CrossRef](#)]
14. Anderson, B.J.; Kurihara, M.; White, M.D.; Moridis, G.J.; Wilson, S.J.; Pooladi-Darvish, M.; Gaddipati, M.; Masuda, Y.; Collett, T.S.; Hunter, R.B. Regional long-term production modeling from a single well test, Mount Elbert gas hydrate stratigraphic test well, Alaska North slope. *Mar. Pet. Geol.* **2011**, *28*, 493–501. [[CrossRef](#)]
15. Yin, Z.; Wan, Q.-C.; Gao, Q.; Linga, P. Effect of pressure drawdown rate on the fluid production behaviour from methane hydrate-bearing sediments. *Appl. Energy* **2020**, *271*, 115195. [[CrossRef](#)]
16. Li, S.; Zheng, R.; Xu, X.; Hou, J. Energy efficiency analysis of hydrate dissociation by thermal stimulation. *J. Nat. Gas Sci. Eng.* **2016**, *30*, 148–155. [[CrossRef](#)]
17. Yin, Z.; Moridis, G.; Tan, H.K.; Linga, P. Numerical analysis of experimental studies of methane hydrate formation in a sandy porous medium. *Appl. Energy* **2018**, *220*, 681–704. [[CrossRef](#)]
18. Yin, Z.; Moridis, G.; Chong, Z.R.; Tan, H.K.; Linga, P. Numerical analysis of experimental studies of methane hydrate dissociation induced by depressurization in a sandy porous medium. *Appl. Energy* **2018**, *230*, 444–459. [[CrossRef](#)]
19. Li, S.; Wu, D.; Wang, X.; Hao, Y. Enhanced gas production from marine hydrate reservoirs by hydraulic fracturing assisted with sealing burdens. *Energy* **2021**, *232*, 120889. [[CrossRef](#)]
20. Zhang, Z.; Liu, L.; Ning, F.; Liu, Z.; Sun, J.; Li, X.; Sun, J.; Hyodo, M.; Liu, C. Effect of stress on permeability of clay silty cores recovered from the Shenhu hydrate area of the South China Sea. *J. Nat. Gas Sci. Eng.* **2022**, *99*, 104421. [[CrossRef](#)]
21. Hu, C.; Liu, X.; Jia, Y.; Duan, Z. Permeability anisotropy of methane hydrate-bearing sands: Insights from CT scanning and pore network modelling. *Comput. Geotech.* **2020**, *123*, 103568. [[CrossRef](#)]
22. Boswell, R. Is gas hydrate energy within reach? *Science* **2009**, *325*, 957–958. [[CrossRef](#)]
23. Kleinberg, R.; Flaum, C.; Griffin, D.; Brewer, P.; Malby, G.; Peltzer, E.; Yesinowski, J. Deep sea NMR: Methane hydrate growth habit in porous media and its relationship to hydraulic permeability, deposit accumulation, and submarine slope stability. *J. Geophys. Res. Solid Earth* **2003**, *108*, B10. [[CrossRef](#)]
24. Delli, M.L.; Grozic, J.L. Experimental determination of permeability of porous media in the presence of gas hydrates. *J. Pet. Sci. Eng.* **2014**, *120*, 1–9. [[CrossRef](#)]
25. Xu, J.; Bu, Z.; Li, H.; Li, S.; Sun, B. Pore-scale flow simulation on the permeability in hydrate-bearing sediments. *Fuel* **2022**, *312*, 122681. [[CrossRef](#)]
26. Li, G.; Li, X.-S.; Lv, Q.-N.; Zhang, Y. Permeability measurements of quartz sands with methane hydrate. *Chem. Eng. Sci.* **2019**, *193*, 1–5. [[CrossRef](#)]
27. Mahabadi, N.; Dai, S.; Seol, Y.; Jang, J. Impact of hydrate saturation on water permeability in hydrate-bearing sediments. *J. Pet. Sci. Eng.* **2019**, *174*, 696–703. [[CrossRef](#)]
28. Wang, J.; Zhao, J.; Zhang, Y.; Wang, D.; Li, Y.; Song, Y. Analysis of the effect of particle size on permeability in hydrate-bearing porous media using pore network models combined with CT. *Fuel* **2016**, *163*, 34–40. [[CrossRef](#)]
29. Zhang, J.; Liu, X.; Chen, D.; Yin, Z. An investigation on the permeability of hydrate-bearing sediments based on pore-scale CFD simulation. *Int. J. Heat Mass Transf.* **2022**, *192*, 122901. [[CrossRef](#)]
30. Liu, W.; Wu, Z.; Li, Y.; Song, Y.; Ling, Z.; Zhao, J.; Lv, Q. Experimental study on the gas phase permeability of methane hydrate-bearing clayey sediments. *J. Nat. Gas Sci. Eng.* **2016**, *36*, 378–384. [[CrossRef](#)]
31. Wu, Z.; Yang, S.; Zhang, L.; Liu, W.; Li, Y. Stress dependence of the gas permeability of montmorillonite sediments in the presence of methane hydrate. *J. Pet. Sci. Eng.* **2022**, *208*, 109697. [[CrossRef](#)]
32. Yang, L.; Ai, L.; Xue, K.; Ling, Z.; Li, Y. Analyzing the effects of inhomogeneity on the permeability of porous media containing methane hydrates through pore network models combined with CT observation. *Energy* **2018**, *163*, 27–37. [[CrossRef](#)]
33. Wang, J.; Zhang, L.; Ge, K.; Zhao, J.; Song, Y. Characterizing anisotropy changes in the permeability of hydrate sediment. *Energy* **2020**, *205*, 117997. [[CrossRef](#)]
34. Kou, X.; Li, X.-S.; Wang, Y.; Liu, J.-W.; Chen, Z.-Y. Heterogeneity of hydrate-bearing sediments: Definition and effects on fluid flow properties. *Energy* **2021**, *229*, 120736. [[CrossRef](#)]
35. Wu, Z.; Liu, W.; Zheng, J.; Li, Y. Effect of methane hydrate dissociation and reformation on the permeability of clayey sediments. *Appl. Energy* **2020**, *261*, 114479. [[CrossRef](#)]
36. Wang, Z.; Liu, S.; Li, H.; Li, S.; Xu, J.; Wang, X. A numerical simulation study of methane hydrate reformation during the dissociation process induced by depressurization. *Fuel* **2022**, *313*, 122983. [[CrossRef](#)]
37. Wang, J.; Zhao, J.; Zhang, Y.; Wang, D.; Li, Y.; Song, Y. Analysis of the influence of wettability on permeability in hydrate-bearing porous media using pore network models combined with computed tomography. *J. Nat. Gas Sci. Eng.* **2015**, *26*, 1372–1379. [[CrossRef](#)]
38. Wang, J.; Zhang, L.; Zhao, J.; Ai, L.; Yang, L. Variations in permeability along with interfacial tension in hydrate-bearing porous media. *J. Nat. Gas Sci. Eng.* **2018**, *51*, 141–146. [[CrossRef](#)]

39. Pan, L.; Lei, L.; Seol, Y. Pore-scale influence of methane hydrate on permeability of porous media. *J. Nat. Gas Sci. Eng.* **2021**, *87*, 103758. [[CrossRef](#)]
40. Dai, S.; Seol, Y. Water permeability in hydrate-bearing sediments: A pore-scale study. *Geophys. Res. Lett.* **2014**, *41*, 4176–4184. [[CrossRef](#)]
41. Wang, Z.; Wang, Q.; Fan, Z.; Wei, W.; Li, M.; Wang, Y.; Huang, X.; Song, Y.; Wang, D. Equivalency and Replaceability between Different Permeability Models of Hydrate-Bearing Porous Media When Applied to Numerical Modeling of Hydrate Dissociation: Implications for Model Selection and Parameter Assignment. *Energy Fuels* **2021**, *35*, 6090–6100. [[CrossRef](#)]
42. Masuda, Y.; Naganawa, S.; Ando, S.; Sato, K. Numerical calculation of gas-production performance from reservoirs containing natural gas hydrates. *SPE J.* **1997**, *29*, 201–210.
43. Masuda, Y. Modeling and experimental studies on dissociation of methane gas hydrates in Berea sandstone cores. In Proceedings of the Third International Gas Hydrate Conference, Salt Lake City, UT, USA, 18–22 July 1999.
44. Minagawa, H.; Ohmura, R.; Kamata, Y.; Nagao, J.; Ebinuma, T.; Narita, H.; Masuda, Y. Water permeability of porous media containing methane hydrate as controlled by the methane-hydrate growth process. *AAPG Mem.* **2009**, *89*, 734–739.
45. Van Genuchten, M.T. A closed-form equation for predicting the hydraulic conductivity of unsaturated soils. *Soil Sci. Soc. Am. J.* **1980**, *44*, 892–898. [[CrossRef](#)]
46. Giraldo, C.; Klump, J.; Clarke, M.; Schicks, J.M. Sensitivity analysis of parameters governing the recovery of methane from natural gas hydrate reservoirs. *Energies* **2014**, *7*, 2148–2176. [[CrossRef](#)]
47. Civan, F. Scale effect on porosity and permeability: Kinetics, model, and correlation. *AIChE J.* **2001**, *47*, 271–287. [[CrossRef](#)]
48. Moridis, G. EOSHYDR: A TOUGH2 module for CH₄-hydrate release and flow in the subsurface. In Proceedings of the Methane Hydrates, Chiba City, Japan, 20–22 October 1998.
49. Moridis, G.J. Numerical studies of gas production from methane hydrates. *SPE J.* **2003**, *8*, 359–370. [[CrossRef](#)]
50. Sakamoto, Y.; Komai, T.; Miyazaki, K.; Tenma, N.; Yamaguchi, T.; Zvyoloski, G. Laboratory-scale experiments of the methane hydrate dissociation process in a porous media and numerical study for the estimation of permeability in methane hydrate reservoir. *J. Thermodyn.* **2010**, *2010*, 9879–9884. [[CrossRef](#)]
51. Kozeny, J. Über kapillare leitung der wasser in boden. *R. Acad. Sci. Vienna Proc. Class I* **1927**, *136*, 271–306.
52. Carman, P.C. Fluid flow through granular beds. *Trans. Inst. Chem. Eng.* **1937**, *15*, 150–166. [[CrossRef](#)]
53. Kang, D.H.; Yun, T.S.; Kim, K.Y.; Jang, J. Effect of hydrate nucleation mechanisms and capillarity on permeability reduction in granular media. *Geophys. Res. Lett.* **2016**, *43*, 9018–9025. [[CrossRef](#)]
54. Katagiri, J.; Konno, Y.; Yoneda, J.; Tenma, N. Pore-scale modeling of flow in particle packs containing grain-coating and pore-filling hydrates: Verification of a Kozeny–Carman-based permeability reduction model. *J. Nat. Gas Sci. Eng.* **2017**, *45*, 537–551. [[CrossRef](#)]
55. Li, G.; Wu, D.-M.; Li, X.-S.; Lv, Q.-N.; Li, C.; Zhang, Y. Experimental measurement and mathematical model of permeability with methane hydrate in quartz sands. *Appl. Energy* **2017**, *202*, 282–292. [[CrossRef](#)]
56. Shen, P.; Li, G.; Li, B.; Li, X.; Liang, Y.; Lv, Q. Permeability measurement and discovery of dissociation process of hydrate sediments. *J. Nat. Gas Sci. Eng.* **2020**, *75*, 103155. [[CrossRef](#)]
57. Xiao, C.; Li, X.; Lv, Q.; Yu, Y.; Yu, J.; Li, G.; Shen, P. Experimental measurement and clustered equal diameter particle model of permeability with methane hydrate in glass beads. *Fuel* **2022**, *320*, 123924. [[CrossRef](#)]
58. Guo, Z.; Fang, Q.; Nong, M.; Ren, X. A novel Kozeny–Carman-based permeability model for hydrate-bearing sediments. *Energy* **2021**, *234*, 121203. [[CrossRef](#)]
59. Cai, J.; Xia, Y.; Lu, C.; Bian, H.; Zou, S. Creeping microstructure and fractal permeability model of natural gas hydrate reservoir. *Mar. Pet. Geol.* **2020**, *115*, 104282. [[CrossRef](#)]
60. Daigle, H. Relative permeability to water or gas in the presence of hydrates in porous media from critical path analysis. *J. Pet. Sci. Eng.* **2016**, *146*, 526–535. [[CrossRef](#)]
61. Zhang, Z.; Li, C.; Ning, F.; Liu, L.; Cai, J.; Liu, C.; Wu, N.; Wang, D. Pore fractal characteristics of hydrate-bearing sands and implications to the saturated water permeability. *J. Geophys. Res. Solid Earth* **2020**, *125*, e2019JB018721. [[CrossRef](#)]
62. Du, P.; Zhao, C.; Peng, P.; Gao, T.; Huang, T. Fractal characterization of permeability prediction model in hydrate-bearing porous media. *Chem. Eng. Sci.* **2020**, *218*, 115576. [[CrossRef](#)]
63. Hou, J.; Ji, Y.; Zhou, K.; Liu, Y.; Wei, B. Effect of hydrate on permeability in porous media: Pore-scale micro-simulation. *Int. J. Heat Mass Transf.* **2018**, *126*, 416–424. [[CrossRef](#)]
64. Zhang, Y.; Liu, L.; Wang, D.; Zhang, Z.; Li, C.; Meng, Q.; Liu, C. The interface evolution during methane hydrate dissociation within quartz sands and its implications to the permeability prediction based on NMR data. *Mar. Pet. Geol.* **2021**, *129*, 105065. [[CrossRef](#)]
65. Chen, X.; Verma, R.; Espinoza, D.N.; Prodanović, M. Pore-scale determination of gas relative permeability in hydrate-bearing sediments using X-ray computed micro-tomography and lattice Boltzmann method. *Water Resour. Res.* **2018**, *54*, 600–608. [[CrossRef](#)]
66. Liu, X.; Dong, H.; Yan, W.; Arif, M.; Zhang, Y.; Golsanami, N. Influence of gas hydrate saturation and pore habits on gas relative permeability in gas hydrate-bearing sediments: Theory, experiment and case study. *J. Nat. Gas Sci. Eng.* **2021**, *95*, 104171. [[CrossRef](#)]

67. Delli, M.L.; Grozic, J.L. Prediction performance of permeability models in gas-hydrate-bearing sands. *SPE J.* **2013**, *18*, 274–284. [[CrossRef](#)]
68. Wang, Q.; Chen, X.; Zhang, L.; Wang, Z.; Wang, D.; Dai, S. An analytical model for the permeability in hydrate-bearing sediments considering the dynamic evolution of hydrate saturation and pore morphology. *Geophys. Res. Lett.* **2021**, *48*, e2021GL093397. [[CrossRef](#)]
69. Lv, J.; Xue, K.; Cheng, Z.; Wang, S.; Liu, Y.; Mu, H. New insights into gas production behavior and seepage-wettability evolution during methane hydrate dissociation in sand matrix by NMR investigation. *Fuel* **2022**, *316*, 123344. [[CrossRef](#)]
70. Dai, S.; Kim, J.; Xu, Y.; Waite, W.F.; Jang, J.; Yoneda, J.; Collett, T.S.; Kumar, P. Permeability anisotropy and relative permeability in sediments from the National Gas Hydrate Program Expedition 02, offshore India. *Mar. Pet. Geol.* **2019**, *108*, 705–713. [[CrossRef](#)]
71. Lei, G.; Liao, Q.; Zhang, D.; Patil, S. A mechanistic model for permeability in deformable gas hydrate-bearing sediments. *J. Nat. Gas Sci. Eng.* **2020**, *83*, 103554. [[CrossRef](#)]
72. Lei, X.; Yao, Y.; Luo, W.; Wen, Z. Permeability change in hydrate bearing sediments as a function of hydrate saturation: A theoretical and experimental study. *J. Pet. Sci. Eng.* **2022**, *208*, 109449. [[CrossRef](#)]
73. Gray, I. Reservoir engineering in coal seams: Part 1-The physical process of gas storage and movement in coal seams. *SPE Reserv. Eng.* **1987**, *2*, 28–34. [[CrossRef](#)]
74. Kenyon, W. Nuclear magnetic resonance as a petrophysical measurement. *Nucl. Geophys.* **1992**, *6*, 153–171.
75. Scheidegger, A.E. The physics of flow through porous media. In *The Physics of Flow through Porous Media*, 3rd ed.; University of Toronto Press: Toronto, ON, Canada, 2020.
76. Rödinger, M.; Ma, Z.; Torquato, S. Predicting permeability via statistical learning on higher-order microstructural information. *Sci. Rep.* **2020**, *10*, 15239. [[CrossRef](#)] [[PubMed](#)]
77. Hearst, J.R.; Nelson, P.H. *Well Logging for Physical Properties*; John Wiley & Sons, Ltd.: New York, NY, USA, 1985.
78. Hearst, J.; Nelson, P.; Paillet, F. *Well Logging for Physical Properties*; McGraw-Hill, Ltd.: New York, NY, USA, 2000; Volume Chapter 15.
79. Spangenberg, E. Modeling of the influence of gas hydrate content on the electrical properties of porous sediments. *J. Geophys. Res. Solid Earth* **2001**, *106*, 6535–6548. [[CrossRef](#)]
80. Ruan, X.; Li, X.-S.; Xu, C.-G. A review of numerical research on gas production from natural gas hydrates in China. *J. Nat. Gas Sci. Eng.* **2021**, *85*, 103713. [[CrossRef](#)]
81. Minagawa, H.; Ohmura, R.; Kamata, Y.; Ebinuma, T.; Narita, H.; Masuda, Y. Water permeability measurements of gas hydrate-bearing sediments. In Proceedings of the 5th International Conference on Gas Hydrates, Trondheim, Norway, 12–16 June 2005.
82. Kumar, A.; Maini, B.; Bishnoi, P.; Clarke, M.; Zatsepina, O.; Srinivasan, S. Experimental determination of permeability in the presence of hydrates and its effect on the dissociation characteristics of gas hydrates in porous media. *J. Pet. Sci. Eng.* **2010**, *70*, 114–122. [[CrossRef](#)]
83. Konno, Y.; Oyama, H.; Nagao, J.; Masuda, Y.; Kurihara, M. Numerical analysis of the dissociation experiment of naturally occurring gas hydrate in sediment cores obtained at the Eastern Nankai Trough, Japan. *Energy Fuels* **2010**, *24*, 6353–6358. [[CrossRef](#)]
84. Konno, Y.; Jin, Y.; Uchiumi, T.; Nagao, J. Multiple-pressure-tapped core holder combined with X-ray computed tomography scanning for gas–water permeability measurements of methane-hydrate-bearing sediments. *Rev. Sci. Instrum.* **2013**, *84*, 064501. [[CrossRef](#)]
85. Mualem, Y. A new model for predicting the hydraulic conductivity of unsaturated porous media. *Water Resour. Res.* **1976**, *12*, 513–522. [[CrossRef](#)]
86. Parker, J.; Lenhard, R.; Koppusamy, T. A parametric model for constitutive properties governing multiphase flow in porous media. *Water Resour. Res.* **1987**, *23*, 618–624. [[CrossRef](#)]
87. Phirani, J.; Pitchumani, R.; Mohanty, K.K. Transport Properties of Hydrate Bearing Formations from Pore-Scale Modeling. In Proceedings of the SPE Annual Technical Conference and Exhibition, New Orleans, LA, USA, 4–7 October 2009; OnePetro: Richardson, TX, USA, 2009.
88. Helba, A.; Sahimi, M.; Scriven, L.; Davis, H. Percolation theory of two-phase relative permeability. *SPE Reserv. Eng.* **1992**, *7*, 123–132.
89. Johnson, A.; Patil, S.; Dandekar, A. Experimental investigation of gas-water relative permeability for gas-hydrate-bearing sediments from the Mount Elbert Gas Hydrate Stratigraphic Test Well, Alaska North Slope. *Mar. Pet. Geol.* **2011**, *28*, 419–426. [[CrossRef](#)]
90. Kleinberg, R.; Flaum, C.; Collett, T. Magnetic resonance log of JAPEX/JNOC/GSC et al. Mallik 5L-38 gas hydrate production research well: Gas hydrate saturation, growth habit, and relative permeability. *Bull.-Geol. Surv. Can.* **2005**, *585*, 114.
91. Liang, H.; Song, Y.; Liu, Y.; Yang, M.; Huang, X. Study of the permeability characteristics of porous media with methane hydrate by pore network model. *J. Nat. Gas Chem.* **2010**, *19*, 255–260. [[CrossRef](#)]
92. Kleinberg, R.; Griffin, D. NMR measurements of permafrost: Unfrozen water assay, pore-scale distribution of ice, and hydraulic permeability of sediments. *Cold Reg. Sci. Technol.* **2005**, *42*, 63–77. [[CrossRef](#)]
93. Sakamoto, Y.; Komai, T.; Kawamura, T.; Minagawa, H.; Tenma, N.; Yamaguchi, T. Laboratory-scale experiment of methane hydrate dissociation by hot-water injection and numerical analysis for permeability estimation in reservoir: Part 1-Numerical study for estimation of permeability in methane hydrate reservoir. *Int. J. Offshore Polar Eng.* **2007**, *17*, ISOPE-07-17-1-047.

94. Lee, M. *Models for Gas Hydrate-Bearing Sediments Inferred from Hydraulic Permeability and Elastic Velocitie*; Scientific Investigations Report 2008-5219; US Geological Survey: Reston, VA, USA, 2008; 14p.
95. Liang, H.; Song, Y.; Chen, Y.; Liu, Y. The measurement of permeability of porous media with methane hydrate. *Pet. Sci. Technol.* **2011**, *29*, 79–87. [[CrossRef](#)]
96. Minagawa, H.; Egawa, K.; Sakamoto, Y.; Komai, T.; Tenma, N.; Narita, H. Characterization of Hydraulic Permeability of Methane-Hydrate-Bearing Sediment Estimated by T2-Distribution of Proton NMR. In Proceedings of the Twenty-Second International Offshore and Polar Engineering Conference, Rhodes, Greece, 17–22 June 2012; OnePetro: Richardson, TX, USA, 2012.
97. Li, C.-H.; Zhao, Q.; Xu, H.-J.; Feng, K.; Liu, X.-W. Relation between relative permeability and hydrate saturation in Shenhu area, South China Sea. *Appl. Geophys.* **2014**, *11*, 207–214. [[CrossRef](#)]
98. Wang, J.-Q.; Zhao, J.-F.; Yang, M.-J.; Li, Y.-H.; Liu, W.-G.; Song, Y.-C. Permeability of laboratory-formed porous media containing methane hydrate: Observations using X-ray computed tomography and simulations with pore network models. *Fuel* **2015**, *145*, 170–179. [[CrossRef](#)]
99. Sakamoto, Y.; Komai, T.; Kawabe, Y.; Tenma, N.; Yamaguchi, T. Formation and Dissociation Behavior of Methane Hydrate in Porous Media. *J. MMIJ* **2004**, *120*, 85–90. [[CrossRef](#)]
100. Shen, P.; Li, G.; Li, B.; Li, X. Coupling effect of porosity and hydrate saturation on the permeability of methane hydrate-bearing sediments. *Fuel* **2020**, *269*, 117425. [[CrossRef](#)]
101. Shen, P.; Li, X.; Li, Z.; Li, G. Permeability determination of hydrate sediments and a new reduction model considering hydrate growth habit. *Fuel* **2020**, *279*, 118297. [[CrossRef](#)]
102. Clarke, M.; Bishnoi, P.R. Determination of the activation energy and intrinsic rate constant of methane gas hydrate decomposition. *Can. J. Chem. Eng.* **2001**, *79*, 143–147. [[CrossRef](#)]
103. Kou, X.; Li, X.-S.; Wang, Y.; Wan, K.; Chen, Z.-Y. Pore-scale analysis of relations between seepage characteristics and gas hydrate growth habit in porous sediments. *Energy* **2021**, *218*, 119503. [[CrossRef](#)]
104. Kleinberg, R.L. 9. Nuclear magnetic resonance. *Exp. Methods Phys. Sci.* **1999**, *35*, 337–385.
105. Kvamme, B.; Graue, A.; Aspenes, E.; Kuznetsova, T.; Gránásy, L.; Tóth, G.; Pusztai, T.; Tegze, G. Towards understanding the kinetics of hydrate formation: Phase field theory of hydrate nucleation and magnetic resonance imaging. *Phys. Chem. Chem. Phys.* **2004**, *6*, 2327–2334. [[CrossRef](#)]
106. Ge, X.; Liu, J.; Fan, Y.; Xing, D.; Deng, S.; Cai, J. Laboratory investigation into the formation and dissociation process of gas hydrate by low-field NMR technique. *J. Geophys. Res. Solid Earth* **2018**, *123*, 3339–3346. [[CrossRef](#)]
107. Minagawa, H.; Egawa, K.; Sakamoto, Y.; Komai, T.; Tenma, N.; Narita, H. Characterization of hydraulic permeability and pore-size distribution of methane hydrate-bearing sediment using proton nuclear magnetic resonance measurement. *Int. J. Offshore Polar Eng.* **2012**, *22*, ISOPE-12-22-4-306.
108. Zhang, Y.; Liu, L.; Wang, D.; Chen, P.; Zhang, Z.; Meng, Q.; Liu, C. Application of low-field nuclear magnetic resonance (LFNMR) in characterizing the dissociation of gas hydrate in a porous media. *Energy Fuels* **2021**, *35*, 2174–2182. [[CrossRef](#)]
109. Liu, L.; Dai, S.; Ning, F.; Cai, J.; Liu, C.; Wu, N. Fractal characteristics of unsaturated sands—Implications to relative permeability in hydrate-bearing sediments. *J. Nat. Gas Sci. Eng.* **2019**, *66*, 11–17. [[CrossRef](#)]
110. Ning, F.; Li, C.; Cai, J.; Zhang, Z.; Wang, D.; Liu, Z.; Sun, J. Study on the relative permeability of hydrate-bearing sediments by a fractal parallel capillary model. In Proceedings of the 9th International Conference on Gas Hydrates, Denver, CO, USA, 25–30 June 2017.
111. Yousif, M.; Abass, H.; Selim, M.; Sloan, E. Experimental and theoretical investigation of methane-gas-hydrate dissociation in porous media. *SPE Reserv. Eng.* **1991**, *6*, 69–76.
112. Ordonez, C.; Grozic, J.; Chen, W. Permeability of Ottawa sand specimens containing R-11 gas hydrates. In Proceedings of the 62nd Canadian Geotechnical Conference, Halifax, NS, Canada, 21–23 September 2009; ETDEWB. BiTech: Richmond, BC, Canada, 2009.
113. Kneafsey, T.J.; Seol, Y.; Gupta, A.; Tomutsa, L. Permeability of laboratory-formed methane-hydrate-bearing sand: Measurements and observations using X-ray computed tomography. *SPE J.* **2011**, *16*, 1678–1694. [[CrossRef](#)]
114. Konno, Y.; Yoneda, J.; Egawa, K.; Ito, T.; Jin, Y.; Kida, M.; Suzuki, K.; Fujii, T.; Nagao, J. Permeability of sediment cores from methane hydrate deposit in the Eastern Nankai Trough. *Mar. Pet. Geol.* **2015**, *66*, 487–495. [[CrossRef](#)]
115. Chen, X.; Espinoza, D.N. Ostwald ripening changes the pore habit and spatial variability of clathrate hydrate. *Fuel* **2018**, *214*, 614–622. [[CrossRef](#)]
116. Lei, L.; Seol, Y.; Choi, J.-H.; Kneafsey, T.J. Pore habit of methane hydrate and its evolution in sediment matrix—Laboratory visualization with phase-contrast micro-CT. *Mar. Pet. Geol.* **2019**, *104*, 451–467. [[CrossRef](#)]
117. Tohidi, B.; Anderson, R.; Clennell, M.B.; Burgass, R.W.; Biderkab, A.B. Visual observation of gas-hydrate formation and dissociation in synthetic porous media by means of glass micromodels. *Geology* **2001**, *29*, 867–870. [[CrossRef](#)]
118. O’Connell, M.; Belanger, B.; Haaland, P. Calibration and assay development using the four-parameter logistic model. *Chemom. Intell. Lab. Syst.* **1993**, *20*, 97–114. [[CrossRef](#)]
119. Semenova, V.; Schiffer, J.; Steward-Clark, E.; Soroka, S.; Schmidt, D.; Brawner, M.; Lyde, F.; Thompson, R.; Brown, N.; Foster, L.; et al. Validation and long term performance characteristics of a quantitative enzyme linked immunosorbent assay (ELISA) for human anti-PA IgG. *J. Immunol. Methods* **2012**, *376*, 97–107. [[CrossRef](#)]
120. Singh, H.; Myshakin, E.M.; Seol, Y. A nonempirical relative permeability model for hydrate-bearing sediments. *SPE J.* **2019**, *24*, 547–562. [[CrossRef](#)]

121. Cao, S.C.; Jang, J.; Jung, J.; Waite, W.F.; Collett, T.S.; Kumar, P. 2D micromodel study of clogging behavior of fine-grained particles associated with gas hydrate production in NGHP-02 gas hydrate reservoir sediments. *Mar. Pet. Geol.* **2019**, *108*, 714–730. [[CrossRef](#)]
122. Weber, D.; Mitchell, J.; McGregor, J.; Gladden, L.F. Comparing strengths of surface interactions for reactants and solvents in porous catalysts using two-dimensional NMR relaxation correlations. *J. Phys. Chem. C* **2009**, *113*, 6610–6615. [[CrossRef](#)]
123. Lv, J.; Xue, K.; Zhang, Z.; Cheng, Z.; Liu, Y.; Mu, H. Pore-scale investigation of hydrate morphology evolution and seepage characteristics in hydrate bearing microfluidic chip. *J. Nat. Gas Sci. Eng.* **2021**, *88*, 103881. [[CrossRef](#)]
124. Lv, J.; Cheng, Z.; Xue, K.; Liu, Y.; Mu, H. Pore-scale morphology and wettability characteristics of xenon hydrate in sand matrix-Laboratory visualization with micro-CT. *Mar. Pet. Geol.* **2020**, *120*, 104525. [[CrossRef](#)]
125. Jańczuk, B.; Chibowski, E.; Białopiotrowicz, T. Interpretation of the contact angle in quartz/organic liquid film-water system. *J. Colloid Interface Sci.* **1984**, *102*, 533–538. [[CrossRef](#)]
126. Mahabadi, N.; Dai, S.; Seol, Y.; Sup Yun, T.; Jang, J. The water retention curve and relative permeability for gas production from hydrate-bearing sediments: Pore-network model simulation. *Geochem. Geophys. Geosyst.* **2016**, *17*, 3099–3110. [[CrossRef](#)]
127. Gaidukova, O.; Misyura, S.; Strizhak, P. Key Areas of Gas Hydrates Study. *Energies* **2022**, *15*, 1799. [[CrossRef](#)]
128. Song, Y.; Huang, X.; Liu, Y.; Yang, M. Experimental study of permeability of porous medium containing methane hydrate. *J. Therm. Sci. Technol.* **2010**, *9*, 51–57.
129. Zhai, C.; Sun, K.; Xin, L.; Tian, S. Experimental study of permeability of sand soil bearing sediments containing methane hydrates. *J. Wuhan Univ. Technol.* **2015**, *37*, 78–82.
130. Wu, D.; Li, G.; Li, X.; Lv, X. Experimental investigation of permeability characteristics under different hydrate saturation. *Chem. Ind. Eng. Prog.* **2017**, *36*, 2916–2923.
131. Chen, B.; Yang, M.; Zheng, J.-n.; Wang, D.; Song, Y. Measurement of water phase permeability in the methane hydrate dissociation process using a new method. *Int. J. Heat Mass Transf.* **2018**, *118*, 1316–1324. [[CrossRef](#)]
132. Santamarina, J.C.; Dai, S.; Terzariol, M.; Jang, J.; Waite, W.F.; Winters, W.J.; Nagao, J.; Yoneda, J.; Konno, Y.; Fujii, T.; et al. Hydro-bio-geomechanical properties of hydrate-bearing sediments from Nankai Trough. *Mar. Pet. Geol.* **2015**, *66*, 434–450. [[CrossRef](#)]
133. Yoneda, J.; Masui, A.; Konno, Y.; Jin, Y.; Egawa, K.; Kida, M.; Ito, T.; Nagao, J.; Tenma, N. Mechanical properties of hydrate-bearing turbidite reservoir in the first gas production test site of the Eastern Nankai Trough. *Mar. Pet. Geol.* **2015**, *66*, 471–486. [[CrossRef](#)]
134. Priest, J.A.; Druce, M.; Roberts, J.; Schultheiss, P.; Nakatsuka, Y.; Suzuki, K. PCATS Triaxial: A new geotechnical apparatus for characterizing pressure cores from the Nankai Trough, Japan. *Mar. Pet. Geol.* **2015**, *66*, 460–470. [[CrossRef](#)]
135. Yoneda, J.; Masui, A.; Konno, Y.; Jin, Y.; Kida, M.; Katagiri, J.; Nagao, J.; Tenma, N. Pressure-core-based reservoir characterization for geomechanics: Insights from gas hydrate drilling during 2012–2013 at the eastern Nankai Trough. *Mar. Pet. Geol.* **2017**, *86*, 1–16. [[CrossRef](#)]
136. Yoneda, J.; Oshima, M.; Kida, M.; Kato, A.; Konno, Y.; Jin, Y.; Jang, J.; Waite, W.F.; Kumar, P.; Tenma, N. Permeability variation and anisotropy of gas hydrate-bearing pressure-core sediments recovered from the Krishna–Godavari Basin, offshore India. *Mar. Pet. Geol.* **2019**, *108*, 524–536. [[CrossRef](#)]
137. Collett, T.S.; Lee, M.W.; Zyrianova, M.V.; Mrozewski, S.A.; Guerin, G.; Cook, A.E.; Goldberg, D.S. Gulf of Mexico Gas Hydrate Joint Industry Project Leg II log-ging-while-drilling data acquisition and analysis. *Mar. Pet. Geol.* **2012**, *34*, 41–61. [[CrossRef](#)]
138. Muraoka, M.; Yamamoto, Y.; Tenma, N. Simultaneous measurement of water permeability and methane hydrate pore habit using a two-dimensional glass micromodel. *J. Nat. Gas Sci. Eng.* **2020**, *77*, 103279. [[CrossRef](#)]
139. Hu, C.; Jia, Y.; Duan, Z. The influence of inhomogeneous hydrate formation on permeability anisotropy of porous media. *Geo-Mar. Lett.* **2021**, *41*, 10. [[CrossRef](#)]
140. Waite, W.F.; Santamarina, J.C.; Cortes, D.D.; Dugan, B.; Espinoza, D.; Germaine, J.; Jang, J.; Jung, J.; Kneafsey, T.J.; Shin, H. Physical properties of hydrate-bearing sediments. *Rev Geophys* **2009**, *47*, 4. [[CrossRef](#)]
141. Lei, L.; Santamarina, J. Laboratory strategies for hydrate formation in fine-grained sediments. *J. Geophys. Res. Solid Earth* **2018**, *123*, 2583–2596. [[CrossRef](#)]
142. Moridis, G.; Collett, T.S.; Pooladi-Darvish, M.; Hancock, S.; Santamarina, C.; Boswell, R.; Kneafsey, T.; Rutqvist, J.; Kowalsky, M.B.; Reagan, M.T. Challenges, uncertainties, and issues facing gas production from gas-hydrate deposits. *SPE Reserv. Eval. Eng.* **2011**, *14*, 76–112. [[CrossRef](#)]
143. Boswell, R.; Collett, T. The gas hydrates resource pyramid. *Nat. Gas Oil* **2006**, *304*, 285–4541.
144. Wu, Z.; Li, Y.; Sun, X.; Wu, P.; Zheng, J. Experimental study on the effect of methane hydrate decomposition on gas phase permeability of clayey sediments. *Appl. Energy* **2018**, *230*, 1304–1310. [[CrossRef](#)]
145. Wu, Z.; Yang, S.; Liu, W.; Xu, H.; Li, G.; Li, Y. Experimental Study on the Difference of Fluid Flow between Methane Hydrate-Bearing Sand and Clay Sediments. *Energy Fuels* **2022**, *36*, 2739–2750. [[CrossRef](#)]
146. Wu, Z.; Yang, S.; Liu, W.; Li, Y. Permeability analysis of gas hydrate-bearing sand/clay mixed sediments using effective stress laws. *J. Nat. Gas Sci. Eng.* **2022**, *97*, 104376. [[CrossRef](#)]
147. Dai, S.; Santamarina, J.C.; Waite, W.F.; Kneafsey, T.J. Hydrate morphology: Physical properties of sands with patchy hydrate saturation. *J. Geophys. Res. Solid Earth* **2012**, *117*, B11. [[CrossRef](#)]

-
148. Bian, H.; Qin, X.; Luo, W.; Ma, C.; Zhu, J.; Lu, C.; Zhou, Y. Evolution of hydrate habit and formation properties evolution during hydrate phase transition in fractured-porous medium. *Fuel* **2022**, *324*, 124436. [[CrossRef](#)]
 149. Jia, B.; Xian, C.-G. Permeability measurement of the fracture-matrix system with 3D embedded discrete fracture model. *Pet. Sci.* **2022**. [[CrossRef](#)]